NOTE TO USERS

This reproduction is the best copy available.

uOttawa

L'Université canadienne
Canada's university

FACULTÉ DES ÉTUDES SUPÉRIEURES ET POSTOCTORALES

uOttawa

L'Université canadienne
Canada's university

FACULTY OF GRADUATE AND POSDOCTORAL STUDIES

Kunal Bhanot

AUTEUR DE LA THÈSE / AUTHOR OF THESIS

M.Sc. (Neuroscience)

GRADE / DEGREE

Department of Neuroscience

FACULTÉ, ÉCOLE, DÉPARTEMENT / FACULTY, SCHOOL, DEPARTMENT

New Roles for and old Giant : Novel Interactions of the Dystonin Protein

TITRE DE LA THÈSE / TITLE OF THESIS

R. Kothary

DIRECTEUR (DIRECTRICE) DE LA THÈSE / THESIS SUPERVISOR

CO-DIRECTEUR (CO-DIRECTRICE) DE LA THÈSE / THESIS CO-SUPERVISOR

David Picketts

Chris Kennedy

Gary W. Slater

Le Doyen de la Faculté des études supérieures et postdoctorales / Dean of the Faculty of Graduate and Postdoctoral Studies

New roles for an old giant: Novel interactions of the dystonin protein

by
Kunal Bhanot

Thesis presented as a partial
requirement for the
Master's of Science (M.Sc.) in Neuroscience

Department of Cellular and Molecular Medicine
University of Ottawa
Ottawa, Ontario, Canada

Your file Votre référence
ISBN: 978-0-494-65518-4
Our file Notre référence
ISBN: 978-0-494-65518-4

Abstract

Dystonin/Bpag1 is a large cytoskeletal plakin protein that contributes to the integrity and subcellular structure of various cell types. Loss of dystonin in mice results in neuromuscular dysfunction and early death in a mouse mutant called *dystonia musculorum*. The phenotype in these mice is a result of sensory neuropathy causing abnormal posturing, uncoordinated muscle movements and poor muscle tone. The multi-domain structure of dystonin isoforms allows for their participation in numerous cell-specific interactions. Previous characterization of the non-epithelial dystonin proteins has focused on the alternatively spliced N-terminal actin-binding domain and the C-terminal microtubule-binding domain. Interactions of the family-defining plakin domain, however, have not been explored in detail. We therefore hypothesised that the plakin domain of neuronal dystonin (dystonin-a) interacts with a number of cytoplasmic and nuclear proteins and ultimately determines the function of these molecules in a cell-type specific manner. To this end, a pull-down interaction approach was utilized and several candidate interacting partners were identified. The candidate partners were validated through co-immunoprecipitation, co-immunofluorescence and proximity ligation assays. Through these efforts CRMP2 and myosin IIb were identified as potential binding partners of neuronal dystonin. Additionally, MAP1B, a microtubule stabilizing protein, and clathrin heavy chain, the major component of the clathrin triskelion were also identified as strong interaction partners for dystonin-a. The current study proposes new avenues of exploration that may elucidate the functional role of this versatile cross-linker and highlight its involvement in the cytoskeletal and endo-exocytic pathways of the cell. We

hope this will further facilitate our understanding of how cytoskeletal proteins affect and regulate various neurodegenerative disorders.

Table of contents

List of tables

List of figures

List of abbreviations

AChE; Acetylcholinesterase
bp; Base pairs
Bpag1; Bullous pemphigoid antigen 1
CRMP; Collapsin response mediating protein
Daxx; Flag-tagged death associated protein
di-cAMP; dibutyryl cyclic adenosine monophosphate
DRG; dorsal root ganglia
dt; Dystonia musculorum
ECL; Enhanced chemiluminescent
GFPNes3α; Green-fluorescent-protein-tagged Nesprin 3a
GFPNes3β; Green-fluorescent-protein-tagged Nesprin 3β
GST-Plakin; GST-tagged N-terminal plakin domain
GST; glutathione-s-transferase
HDAC; Histone deacetylase
his-desmin; C-terminal and N-termnal 6X his-tagged desmin
his-plakin; C-terminal and N-termnal 6X his-tagged plakin
IF; Intermediate filament
IFBD; Intermediate filament binding domain
IFBD2; Intermediate filament binding domain of the muscle isoform (dystonin-b)
IPTG; isopropyl β-D-1thiogalactopyranoside
kD; Kilodalton
LB; Luria-Bertani broth
MACF; Microtubule actin cross-linking factor
MAP; Microtubule associated protein
MT; Microtubule
MTBD; Microtubule binding domain
N2myc; Myc-tagged dystonin isoform 2 unique N-terminal region
Ntermlong; Flag-tagged N-terminal dystonin-a with plakin domain
PAGE; Polyacrylamide gel electrophoresis
PBS; Phosphate-buffered saline
PFA; Paraformaldehyde
Plakin; Flag-tagged plakin domain
PlakinCH1; Flag-tagged dystonin plakin domain with one calponin repeat
PLA; Proximity ligation assay
RT-PCR; Reverse transcription- polymerase chain reaction
Sc; Slow component
SDS; Sodium dodecyl sulfate
SH3; Src-homology 3
YFP-mini-a2; C-terminus yellow fluorescent protein-tagged mini-dystonin isoform-a2

Acknowledgements

I would first like to extend my sincere gratitude to my supervisor and mentor, Dr. Rashmi Kothary, for all his support and guidance. I consider myself extremely fortunate to have been given the opportunity to work with and learn from such a kind and generous person. I would also like to thank Dr. Kevin Young for his advice, guidance, and technical expertise throughout the project. Additionally, I would like to acknowledge my lab members both past and present for their helpful thoughts and frutiful discussion. I would like to thank Mr. Yves De Repentigny for his technical assistance and animal care work. I also thank my committee members, Dr. Hsiao-Huei Chen and Dr. David Picketts, for their valuable insight and constructive comments. Finally, I would like to thank my family and friends for their support and encouragement during these past years.

Introduction

Diversity, morphology, and size are just a few of the properties attributed to the proper regulation of cytoskeletal and nucleoskeletal structures in a cell. An understanding of the framework provided by these structures is essential for the development of therapies targeting treatment of the pathological conditions arising from abnormalities in cytoskeletal organization. Loss of essential structural organization in the cells of the body is often fatal; however, compensatory redundancy amongst cellular organization structures may allow for the survival of the organism - albeit with severe disabilities at times.

These essential cytoskeletal structures are dependent upon the appropriate modulation of simple filaments in the cell. In eukaryotic cells, three basic filaments exist, namely actin microfilaments, intermediate filaments (IFs), and microtubules (MTs) (Janmey, 1991; Strelkov et al., 2003). Disruptions in the proper functioning of these components result in several debilitating conditions in humans (Table I).

The cytoskeleton

Actin microfilaments

The smallest of the three basic filaments, actin microfilaments, possess a diameter of 6 nm and are assembled from globular-actin monomers which when polymerized form filaments with a double-helix shape (Alberts, 2002). Although actin filaments exist in several structurally similar forms which have been classified as α, β, and γ, no known redundancy in function has been reported (Shimada et al., 1997; Khaitlina, 2001). These small filamentous structures provide support and rigidity to the cell; they are also involved in critical cell functioning activities such as division and movement. In a

constant state of change, actin filaments rapidly assemble and disassemble, allowing them to cater to the ever-varying needs of the cell and thus enabling it to perform its essential functions. A role for actin microfilaments in chromatin remodelling and nuclear lamina formation has also been proposed (Percipalle and Visa, 2006).

Intermediate filaments

IFs possess a general diameter of 10 nm and are composed of 2 sets of coiled-coil monomers which bind to form a tetramer (Alberts, 2002). Several IFs have been identified, namely nuclear, vimentin-like, epithelial, and axonal (Alberts, 2002). IFs impart structural integrity by way of intracellular mechanical strength. The high-tensile strength provided by these filaments helps to reinforce the structural integrity of the cell. These filaments are found abundantly in tissue facing large mechanical insults such as skin. Nucleoskeletal structural support is also believed to be an important function of IFs (Schulze et al., 2005). Interestingly, IF knockout models demonstrate little or no phenotypic alterations, indicating that the role of these filaments may be compensated for by other cytoskeletal components, or in fact may not be essential for survival (Capetanaki et al., 1997; Zhu et al., 1997; Zhu et al., 1998; Levavasseur et al., 1999; Reichelt et al., 2001). Nevertheless, neuronal IF aggregation has been associated with several neuronal pathologies, and several human conditions have been linked to abnormal intermediate filament functioning (Table I).

Table I. An overview of mutant structural proteins involved in pathologies

Disease	Phenotypic traits	Affected protein(s)	Cytoskeletal role*
Epidermolysis bullosa simplex with muscular dystrophy	skin blistering and muscle weakness	plectin	multifunctional crosslinker interacting with IFs, MFs, and adhesion proteins
Limb girdle muscular dystrophy type 1A	weakness and atrophy of shoulder and hip muscles	myotilin	actin MF bundling in muscle sarcomere
Nemaline myopathy	muscle weakness	nebulin	regulation of MF length
		muscle α-skeletal actin	muscle MF component
Duchenne/Becker muscular dystophies	muscle weakness and atrophy; cardiomyopathy	dystrophin	tethering MFs to muscle sarcolemma
Desmin myopathy	muscle weakness; cardiomyopathy	desmin	muscle IF component
Amyotrophic lateral sclerosis	progressive neuropathy affecting motor neurons	neurofilament heavy	neuronal IF component
		tau	neuronal MT stabilization
Charcot-Marie-Tooth disease types 1 and 2	neuropathy affecting motor and sensory neurons with muscle atrophy	neurofilament light	neuronal IF component
Alexander disease	early childhood spasticity and dementia	glial fibrillary acidic protein	glial IF component
Focal segmental glomerulosclerosis	kidney dysfunction	α-actinin-4	MF organization
Spherocytosis	red blood cell fragility leading to anemia	α-spectrin	cortical MF organization
Inflammatory bowel disease	inflammation of the intestines	keratin 8	epithelial IF component
mutliple skin disorders	skin blistering and fragility	various keratin proteins	epidermal IF components

*IF = intermediate filament; MF = actin microfilament; MT = microtubule

(Young, unpublished)

Microtubules

The third type of filamentous structure in eukaryotic cells is the MT. They are approximately 23 nm in diameter and hence the largest among the basic filaments described here (Alberts, 2002). MTs are composed of α- and β-tubulin subunits which heterodimerize continually, allowing them to demonstrate a dynamic 'tread-milling' effect throughout the cell (Alberts, 2002). In addition to being involved with overall cellular organization through the regulation of organelle positioning, MTs are also involved in neurite growth and chromosome alignment (Buck and Zheng, 2002; Mitchison et al., 2005). Despite the rigidity demonstrated by these structures, they are capable of continually modifying their arrangement and possess the ability to withstand large compressive loads. Deficiencies in these cytoskeletal filaments and their interacting proteins have been implicated in neuromuscular dysfunction (Cairns et al., 2004) (Table I).

The essential role of cytoskeletal linkers

Plakins

Despite the defined characteristics and functions of the simple structural filaments described above, significant plasticity occurs in the cytoskeleton as a result of the diversity of cytoskeletal organizing and manipulating proteins. Various arrangements and assortments of these cytoskeletal structures provide for unique cellular functions and morphologies (Ruhrberg and Watt, 1997; Roper et al., 2002). These proteins act as the 'nails' that keep the cyto-architecture of the cell intact. A particularly interesting family of cyto-linker proteins referred to as the plakin family has been identified. Members of this family of proteins play an important role in maintaining the function and integrity of

tissues undergoing mechanical stress, such as skin and muscle (Sonnenberg and Liem, 2007; Young and Kothary, 2007). It should be noted, however, that they also play a significant role in neuronal tissues as well (Fuchs and Karakesisoglou, 2001).

Members of the plakin family of proteins are depicted in Figure 1. The family receives its name from the plakin domain found to be common amongst most of its members. The domain, the functions of which are still poorly understood, is composed of six antiparallel segments arranged in a α-helical fashion (Jefferson et al., 2007). Some members of this family also possess plectin repeats, which have been shown to bind IFs (Sonnenberg and Liem, 2007). Some plakins also possess an actin binding domain (ABD) as well as a microtubule-binding domain (MTBD) (Fuchs and Karakesisoglou, 2001; Leung et al., 2002; Jefferson et al., 2004; Sonnenberg and Liem, 2007).

Spectraplakins as cytoskeletal linkers

A subset of the plakin family of proteins, including bullous pemphigoid antigen 1 (Bpag1)/dystonin and microtubule actin cross-linking factor 1 (MACF1)/Acf7, have been classified as spectraplakins (Roper et al., 2002; Jefferson et al., 2007). In addition to possessing characteristics of the plakin family, members of this subset also demonstrate attributes associated with the spectrin protein superfamily. For example, dystonin possesses both a plakin domain and a spectrin repeat region (Jefferson et al., 2007). Spectrin repeats are composed of repeating tri-helix bundles, which give rise to very large domains which are believed to play a spacer role in proteins such as dystrophin and α-actinin (Djinovic-Carugo et al., 2002). Dystonin is a particularly interesting cytoskeletal plakin protein family member. Loss of the dystonin protein, which arises from the *Dystonin/Bpag1* (*Dst*) gene in mice, results in an observable phenotype that is

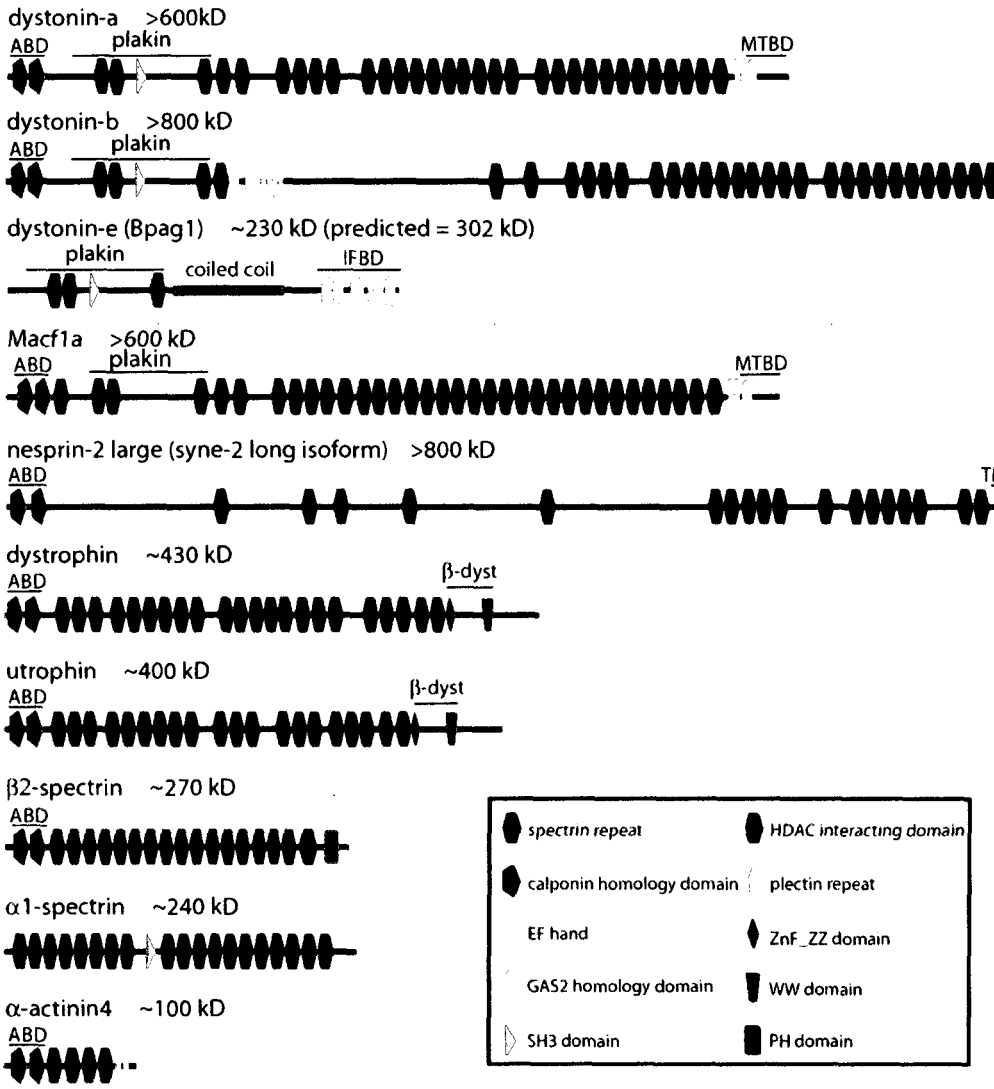

Figure 1. Dystonin isoforms and other spectrin superfamily members
(Young and Kothary, 2008). The figure illustrates SMART (Simple Modular Architecture Research Tool) (http://smart.embl.de/) analysis of the dystonin protein and compares the different members of the spectrin superfamily. These proteins are generally composed of an N-terminal actin binding domain (ABD) made up of tandem calponin homology domains, a spectrin repeat containing central coiled region and varying functional domain at the C-terminal end. The neuronal and muscle isoforms of dystonin, dystonin-1a and dystonin-1b, possess EF hand motifs in addition to a microtubule-binding domain (MTBD) at the C-terminal end (Leung, 2001). Dystonin-1e however comprises of an intermediate filament binding domain (IFBD) composed of multiple plectin repeats at its C-terminus. Src-homology 3 (SH3) and putative histone deacetylase (HDAC) domains are believed to exist in the common plakin domain of the dystonin isoforms. MACF1a (shown) and MACF1b (not shown) have similar structures to the corresponding dystonin isoforms. The identified domains are derived from SMART analysis of the respective mouse protein sequences. Based on the amino acid residues, each protein has been drawn to scale.

characteristically similar to human dystonia (Brown et al., 1995b; Brown et al., 1995a; Leung et al., 2001).

Dystonin/Bpag1 isoforms and functions

The dystonin/Bpag1 gene has been mapped to chromosome 6p12-p11 in humans (Li et al., 1992) and chromosome 1 in the mouse (Copeland et al., 1993). The gene itself is very large, spanning 400 kb in the mouse and 500 kb in humans, with over 100 exons in each (Leung et al., 2001; Pool et al., 2005). Dystonin is known to have at least three alternative isoforms with varying tissue distribution (Figure 1). Dystonin-e (230 kDa) is referred to as the epithelial isoform. It is comprised of a globular N-terminal end containing a conserved plakin domain, central coiled-coil region, and a C-terminal intermediate filament-binding domain (IFBD) (Figure 1) (Sawamura et al., 1991). Dystonin-e is the antigenic factor in the auto-antigenic severe skin blistering disorder referred to as bullous pemphigoid. Dystonin-b (~800 kDa) is the largest of the three isoforms and is referred to as the muscle isoform as it is primarily expressed in muscle tissue. The muscle isoform is composed of an N-terminal ABD and a plakin domain(Leung et al., 2001). In addition, it possesses a putative IFBD, a rod domain containing a large number of spectrin repeats, and a MTBD at the C-terminus (Leung et al., 2001). The structure of the dystonin-a isoform (~600 kDa), which is primarily found is neuronal tissues, is similar to the dystonin-b isoform with the exception that it does not possess a putative IFBD region (Leung et al., 2001).

Alternative splicing at the N-terminal end just upstream from the ABD results in the generation of four isoforms (Brown et al., 1995a; Leung et al., 2001). In addition to

dystonin-e, three isoforms are observed in both dystonin-a and dystonin-b proteins. These isoforms are referred to as dystonin-a1, dystonin-a2, and dystonin-a3 for the dystonin-a protein and dystonin-b1, dystonin-b2, and dystonin-b3 for the dystonin-b protein (Leung et al., 2001). The existence of multiple N-terminal variants has raised the possibility of alternate sub-cellular localizations for each isoform. Several studies have been conducted to explore the possible alternate localization patterns of the various isoforms and, to this effect, the generation of several antibodies has been attempted (Young et al., 2003; Jefferson et al., 2006; Young et al., 2006; Young and Kothary, 2008). Additionally, fusion protein constructs have been generated and their over-expression patterns observed in cultured cells (Young et al., 2003; Young et al., 2006; Young and Kothary, 2008). Dystonin isoform 2 has been shown to localize to the perinuclear region in both muscle and neuronal cells (Young et al., 2003; Young et al., 2006). Young et al. (2003) demonstrated the co-localization of dystonin-a/b isoform 2 with the central, but not the peripheral, stress fibres in myoblasts. However, the dystonin antibody used in this study did not stain focal adhesion junctions and the staining pattern was unaltered in nocodazole treated cells. Dystonin N-terminal isoform 2 fusion constructs expressed in myogenic and Cos-1 cells demonstrated co-alignment with a typical actin cytoskeletal network, in addition to the actin stress fibre bundling (Young et al., 2003; Jefferson et al., 2006).

Dystonin and disease

Human pathology of dystonin dysfunction

In humans, conditions arising from the disruption of the *DST* locus affecting the neuronal and muscle isoforms are rarely reported. It may be that mutations in this gene result in embryonic lethality in most cases. However, a patient with reciprocal (6;15) translocation mutation with oesophageal atresia, mental retardation, delayed visual acuity and non-progressive encephalopathy has been reported (Giorda et al., 2004). The patient showed progressive delay in motor and cognitive abilities from birth to the age of 4. The patient did not present with skin blistering as the sequence for the epithelial isoform was intact. As very few human cases depicting alteration in dystonin-a/b expression have been reported, mouse models have been extensively used to understand to complexity of this diverse protein and its influence on disease manifestation.

Dystonin and dystonia musculorum

Mutant alleles of the *Dst* gene result in the occurrence of *dystonia musculorum (dt)* mice which are characterised by a severe movement disorder (Duchen et al., 1963; Duchen and Strich, 1964; Brown et al., 1995b; Guo et al., 1995). *dt* mice were first described over 40 years ago arising from an autosomal recessive disorder resulting in severe sensory neuropathy (Duchen and Strich, 1964). The phenotypic properties of *dt* mice have provided an excellent candidate model for human dystonia. It should be noted, however, that *dt* mice exhibit a pronounced decrease in life expectancy and are generally not able to survive past weaning, which is not typical of human dystonia (Duchen and Strich, 1964). It has been suggested that this decrease in life expectancy may be attributed to the inability of the incapacitated mice to compete for survival in a large litter (De Repentigny

and Kothary, unpublished). However, *dt* mice have been observed to live well into sexual maturity in some cases (De Repentigny and Kothary, unpublished). It is thus believed that although the *dt* mutation itself may not be lethal, the ensuing movement disorder results in a significantly incapacitating condition making unassisted survival a challenge. The large size of the *Dst* gene leaves it prone to mutation; as such 16 lines of mice with mutated *dt* alleles have been reported (Mouse Genome Informatics website). These lines include dt^{24J}, dt^{27J}, dt^{Alb}, dt^{Frk}, and dt^{Tg4}. Southern blot analysis of genomic DNA from dt^{24J}, dt^{27J}, and dt^{Frk} revealed that these mice did not have any major deletions or rearrangements in the *Dst* locus (Pool et al., 2005). The dt^{Alb} line however was shown to have a large central deletion between exon 12 and exon 46 (Pool et al., 2005). The dt^{Tg4} line was unexpectedly generated when researchers introduced a *Lac Z* hybrid gene in mice under the hsp68 promoter, in an effort to study the gene regulation of heat-shock proteins (Kothary et al., 1988). A quarter of the offspring from this line exhibited a phenotype similar to that of the *dt* phenotype described by Duchen and Strich (1964). Further analysis of this line through breeding with the *dt* line from Jackson laboratories revealed the Tg4 mutation to be allelic to *dt*. Copies (15.5) of the heat-shock promoter-reporter construct had been incorporated into the genome as a single head to tail concatamer. The transgene was inserted into the *Dst* locus (Brown et al., 1994). The alteration in these mice is a result of a 70 kB insertion accompanied by a 45 kB genomic DNA deletion (Kothary et al., 1988). Alignment of the altered sequence to the genomic sequence reveals that the deletion removes the exon encoding alternate N-terminus 1 and N-terminus 2. It is therefore apparent that this deletion causes the loss of dystonin-a/b isoform 1 and 2 expression in the dt^{Tg4} line (Young and Kothary, 2007).

A dystonin knockout mouse model generated in an effort to study skin blistering also developed the neurological phenotype characteristic of the *dt* mice (Guo et al., 1995). This work further substantiated the results demonstrated by Brown et al. (1994, 1995a) and confirmed the location of the *Dst* locus. Reverse-transcription polymerase chain reaction (RT-PCR) assays of dystonin levels in the dt^{24J}, dt^{27J}, dt^{Alb}, and dt^{Tg4} lines revealed, as expected, a pronounced decrease in transcript levels. Interestingly, the dt^{Frk} line was shown to have only a minor reduction in the transcript levels of dystonin (Pool et al., 2005). Despite differences in the transcript levels and thus gene expression in the mice carrying *Dst* muted alleles, they all exhibit a similar neuropathology.

Pathology of the dt condition

dt mice suffer from neuronal abnormalities. The gradual loss of nerve fibres in the peripheral and central regions of the sensory pathways along with focal swellings along the affected fibres is characteristic of this condition (Duchen and Strich, 1964). Degeneration occurs within the sensory root of the spinal cord ganglia and the cranial nerves of *dt* mice as a result of neurofilament and MT aggregation (Duchen and Strich, 1964; Sotelo and Guenet, 1988; al-Ali and al-Zuhair, 1989; Bernier and Kothary, 1998). Nuclear eccentricities, in which the nucleus is found positioned close to the cell membrane, are noted in addition to the dispersion of the rough endoplasmic reticulum from around the nucleus (Young and Kothary, 2008). Interestingly, nerve fibre swellings are seen in the youngest subjects, and have been suggested to be the primary abnormality associated with *dt* mice (Bernier and Kothary, 1998). The other observed characteristics of the condition could possibly arise as a result of the swellings and thus may be considered to be secondary etiologies for the condition. A possible mechanism by which

the secondary characteristics may arise is referred to as 'dying back', where axonal abnormalities in the sensory and spinocerebellar neurons may eventually spread back to the cell body and cause disruptions in functioning throughout the neuron (Sotelo and Guenet, 1988).

As neurofilament aggregation has been found in *dt* mice at the focal swellings (Janota, 1972), it has been suggested that disruptions in axonal transport and aberrant cytoskeletal architecture may also be a primary cause of the neuropathy observed (De Repentigny et al., 2003). De Repentigny et al. (2003) demonstrated axonal transportation defects in the dt^{27J} line by monitoring acetylcholinesterase (AChE) activity at the site of nerve ligature. The study suggests both anterograde and retrograde transport is affected, as no accumulation of AChE was observed either proximal or distal to the site of ligature in the mutant mice. Dystonin-a has also been implicated in vesicular transportation in sensory neurons through its association with retrolinkan, a member of the dynactin complex of proteins (Liu et al., 2003; Liu et al., 2007). It was initially thought that vesicle transportation defects in dystonic mice were a result of a disorganized MT cytoskeleton (Dalpé et al., 1998; Yang et al., 1999). However, the MT cytoskeleton in cultured sensory neurons from *dt* mice are in fact intact and thus allow for normal steady-state vesicle distribution throughout the cell (Pool et al., 2006). Thus, the true etiology behind the axonal transportation defects observed in *dt* mice remains to be fully understood.

Dystonin has also been implicated in the functioning of the cytoskeleton of Schwann cells (Bernier et al., 1998). Schwann cells are necessary for myelinating axon tracts in the peripheral nervous system. Dystonin deficient Schwann cells, maintained in cell culture, have been shown to demonstrate a perturbed cytoskeleton and abnormal

morphology (Bernier et al., 1998). Additionally, peripheral nerves of the dt^{27J} and dt^{Tg4} mice demonstrate both hypo-myelination as well as amyelination (Bernier et al., 1998). In the central nervous system myelination is performed by oligodendrocytes. In *dt* mice, the optic nerve, which is part of the central nervous system, possesses higher proportions of amyelinated fibers with reduced axonal density when compared to wild type controls (Saulnier et al., 2002).

As *dt* mice demonstrate significant impairment in posturing and gait, it is surprising that evidence of degeneration in motor neurons has not been reported, despite the presence of dystonin in wild-type motor neurons (Dalpé et al., 1998). Axon density however is lower in *dt* mice in comparison to wild-type controls (De Repentigny and Kothary, unpublished). It has been postulated that the severe motor dysfunction observed may be partly a result of poor proprioceptive input from abnormal muscle spindles (Duchen, 1976; Kothary et al., 1988; Yang et al., 1996; Dowling et al., 1997).

MACF1 and dystonin

As plakin family members share several common domains and demonstrate similarities at both the transcript and protein levels, it may seem likely that a compensatory mechanism exists within this family. Interestingly, Leung et al. (2001) have observed dystonin transcripts in MACF1 knockout mice up to pre-natal day 17. However, despite being homologous to MACF1, dystonin is unable to compensate for its loss in these mice as this condition is embryonic lethal. It has been postulated that MACF1 is necessary for establishing the initial structural integrity within tissues while dystonin maintains this integrity once it has been established (Sonnenberg and Liem, 2007). In *dt* mice exhibiting the characteristic phenotype, it has been demonstrated that MACF1 mRNA levels in the

spinal cord of both mutant and wild-type mice are the same (Bernier et al., 2000). It is therefore unlikely that MACF1 is compensating for the loss of all dystonin isoforms in these mice. It should be noted, however, that the specific isoform responsible for the *dt* phenotype has not yet been identified. Although, it is believed that loss of the dystonin-a2 isoform is responsible for the manifestation of *dt* in mice, as this isoform possesses a unique N-terminal trans-membrane domain not observed in any of its homologues. Thus, even if other members of the plakin family such as plectin or MACF1 do possess strong homology with dystonin and are able to compensate for the loss of some dystonin isoforms, they seem unable to compensate for the loss of dystonin-a2 in *dt* mice (Young and Kothary, 2007). Additionally, the reduced transcript levels of MACF1 in the sensory root ganglia of *dt* mice further substantiate the theory that MACF1 is unable to compensate for the loss of dystonin in these mutant mice (Sonnenberg and Liem, 2007).

Known roles for dystonin-a/b

The diversity due to the alternative N-terminal ends of the dystonin isoforms is believed to be responsible for their varying roles in different tissue types (Brown et al., 1995a). Localization of the dystonin- a/b isoform 1 to actin stress fibres and the nucleus has been demonstrated using an N-terminal fusion protein composed primarily of the N-terminal ABD and plakin domain (Young et al., 2003). It was further shown that a nuclear localization signal was responsible for the observed affinity of the fusion protein to the nucleus (Young et al., 2003; Young and Kothary, 2005). Interestingly, N-terminal fusion proteins of differing N-terminal isoforms interacted differently with the actin cytoskeleton, and also displayed varying localization to the nucleus (Young et al., 2003).

This evidence suggests that dystonin-a/b is quite likely present in the nucleus and thus is not simply a cytoplasmic or membrane protein.

Evidence suggesting that dystonin is a candidate to be involved in several protein interactions has been advanced. Nesprin 3α, actin, and MTs are just a few of the already identified interactors of dystonin (Young et al., 2003; Young et al., 2006; Young and Kothary, 2008). However, based on its modular structure, it is likely that dystonin is involved in other interactions and possibly plays a significant role in cytoskeletal integrity pathways. As mentioned, localization of dystonin outside of the nucleus has been observed (Young and Kothary, 2008). In addition, strong intranuclear staining has also been noted (Young and Kothary, 2005). The role of dystonin within the nucleus has not yet been understood; however, its presence there raises the question of its participation in nuclear interactions.

Thus, in order to gauge a better understanding of the functions of this diverse protein, we performed interaction analyses aimed at identifying and characterizing proteins that may have a relationship with the dystonin protein. For the purposes of this study, the focus of the analyses was on the dystonin-a isoform. Studies have shown that this isoform is primarily neuronal and significantly present in the sensory ganglia (Bernier et al., 1995). It is believed that loss of this isoform results in the overt *dt* phenotype (Young and Kothary, 2007), and identifying its novel interaction partners may help provide a better understanding of the functional role of this protein in the cell.

As a result of the large size of the dystonin proteins, interaction studies were performed using a specific domain of the protein as bait. The region of dystonin-a chosen for this study was the plakin domain. Extensive interaction analyses of the plakin domain

in epithelial plakins have been performed. The plakin domain of desmoplakin, for example, interacts with several desmosome associated proteins such as plakophilin-1, plakophilin-2, desmosomal cadherins, and plakoglobin (Getsios et al., 2004). Additionally, the plakin domains of plectin and dystonin-e interact with proteins that associate with hemidesmosomes such as β4 integrin (Koster et al., 2003). An interaction analysis of the plakin domain of dystonin-a, however, has not yet been reported.

Electron microscopy studies of the plakin domain of plectin and dystonin-e have predicted it to be globular and α-helical (Foisner and Wiche, 1987; Tang et al., 1996). Crystal structure analysis of the protease-resistant fragment of the dystonin plakin domain reveals an overall fold structure made up of a triple helical bundle which is characteristic of spectrin repeats (Jefferson et al., 2007). Jefferson et al. (2007) propose that the plakin domain of dystonin is composed of two pairs of spectrin repeats separated by a Src-homology 3 (SH3) domain. The SH3 domain is a conserved region which is comprised of 60 amino acid residues. The domain possesses a characteristic β-barrel fold consisting of β-strands which are tightly packed into anti-parallel β-sheets. This domain is generally found in proteins which mediate interactions and complex formations with other proteins by binding to proline-rich peptide sequences. This region is central to the interaction ability of other spectrin superfamily members such as α1-spectrin (Figure 1), which is known to dimerize with β-spectrin (Figure 1) (Woods and Lazarides, 1986). Therefore, we believe that the SH3 domain of dystonin is an important interacting region. Work done on the MACF1 protein, which is structurally similar to dystonin, further substantiates this belief. The SH3 region of MACF1 may be an essential interacting region as it has been shown to interact with β-catenin and other canonical Wnt-signalling

pathway members (Chen et al., 2006). It was therefore a logical avenue to examine the interaction potential of the SH3 region of dystonin-a. Additionally, the conserved plakin domain region of the dystonin protein contains a putative histone deacetylase (HDAC) binding region (Fig. 1). HDAC proteins are known to be essential for gene regulation through histone interactions (Hisahara et al., 2005). By exploring the interaction potential of the plakin domain that contains a predicted HDAC interacting region, we hoped to further our understanding of the role of dystonin in the nucleus. We believed that the applied approach would help identify novel interacting partners of the dystonin-a protein through its plakin domain.

Hypothesis and Objectives

We hypothesize that dystonin proteins interact with a number of cytoplasmic and nuclear proteins that ultimately determine their functions in a cell type specific manner. The objective of this thesis is to identify and validate dystonin interacting proteins. To explore the validity of our hypothesis we have the following specific aims.

1) To identify interaction partners of dystonin-a. We will use pull down assays of neuronal tissue lysates with recombinant fusion proteins. Interacting proteins will be identified by mass spectrometry analysis.

2) To validate the interaction of dystonin-a and the novel proteins identified by mass spectrometry. The putative interactors of our dystonin-a fusion will be validated through several biochemical procedures including co-immunoprecipitation, co-immunofluorescence, and proximity ligation assay.

Materials and Methods

Constructs

Bacterial expression

A his-tagged plakin (his-plakin) plasmid was kindly provided by Dr. Kevin Young and was used for pull-down analysis. The plasmid was generated using the pET30c(+) vector (Novagen) and encoded the plakin domain of dystonin-a (bp 1512-bp 4644 GenBank Accession NM133833.2). The pET30c(+) vector has his-tags at both the N-terminal and C-terminal ends. Protein expression of the plakin coding region incorporated into the multiple cloning region of the vector along with the his-tags was driven by the T7 promoter. His-tagged desmin (his-desmin) was generated by incorporating the desmin coding sequence (bp 66-bp 787 GenBank Accession NM010043.1) into the pET30c(+) vector. A glutathione-s-transferase (GST)-tagged N-terminal plakin domain (GST-Plakin) plasmid was generated by cloning the N-terminal region of the plakin domain (bp 1022-bp 2959 GenBank Accession NM133833.2) into the pGex4t1 vector (GE Healthcare) (Figure 2).

Mammalian expression

Flag-tagged fusion plasmids were used to perform co-immunoprecipitation reactions as part of interaction validation experiments. A flag-tagged fusion plasmid expressing the N-terminal domain of dystonin in addition to the entire plakin domain (Ntermlong) was used (Young et al., 2003). Two smaller flag-tagged fusion plasmids were generated from the Ntermlong plasmid to identify the region of dystonin participating in any identified interactions. 'PlakinCH1' contained the plakin domain along with the second calponin homology repeat and 'Plakin' encoded the complete plakin domain. Flag-tagged death

associated protein (Daxx), a kind gift provided by Dr. David Picketts, was used as a negative control for the co-immunoprecipitation validation experiments. For co-immunofluorescence analysis, a C-terminus Yellow Fluorescent Protein-tagged mini-dystonin isoform-a2 (YFP-mini-a2) mammalian expression construct generated by Dr. Young (unpublished) was used. The YFP-mini-a2 construct possesses all of the structural characteristics of the dystonin-a2 protein; however, it has a shortened spectrin repeat region (Figure 2).

Protein expression - Bacterial

BL-21 E.coli were transformed with the appropriate fusion construct and streaked on a Luria-Bertani broth (LB 1% bacto-tryptone, 1% NaCl, 0.5% bacto-yeast) plate containing antibiotics for selection. Plates were incubated at 37°C overnight. Colonies were picked the next day and grown in culture tubes containing LB and the appropriate antibiotic overnight at 37°C in a shaking incubator. The overnight culture (0.5 ml) was then added to a 250 ml Erlenmeyer flask containing 50 ml of LB with antibiotics and incubated at 37°C for 3 hours while agitated. To induce protein expression isopropyl β-D-1thiogalactopyranoside (IPTG) was added to the culture flask, which was incubated at 32°C for 4 hours. The bacterial culture was then centrifuged at 9000 RPM for 10 minutes at 4°C. The supernatant was removed and the pellet was resuspended in STE buffer (0.1 M NaCl, 10 mM Tris-HCl, 1mM EDTA) containing 1.5% sarkosyl. Resuspended pellets were sonicated (Sonics and Materials Inc., Connecticut) for 2 minutes at 35% amplitude

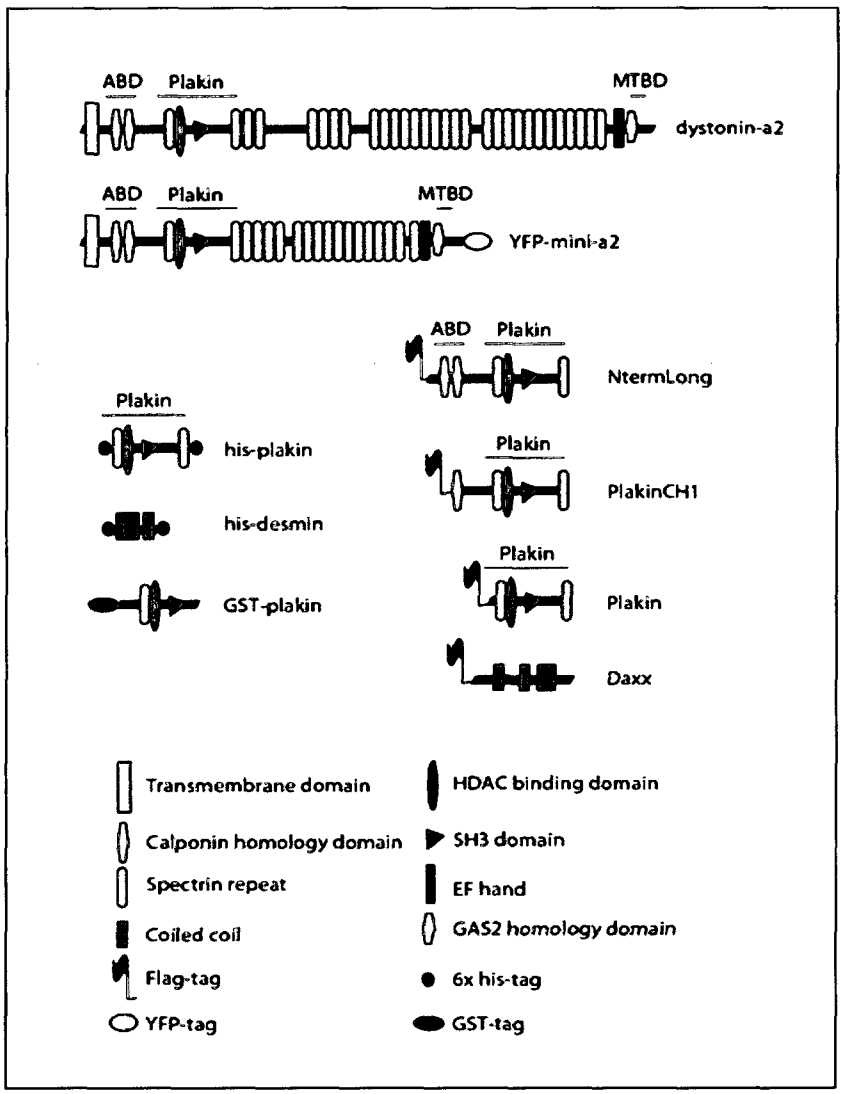

Figure 2. Schematics of plasmids used for interaction analysis.
Dystonin-a2 provides an overview of the neuronal dystonin isoform 2 protein (dystonin-a). This protein is composed of an N-terminal actin binding domain (ABD) made up of tandem calponin homology domains, a spectrin repeat containing central coiled region and a growth arrest specific 2 (GAS2) homology domain which binds MTs (MTBD) at the C-terminal end. Dystonin-a also possesses EF hand motifs at the C-terminal end (Leung et al., 2001). Src homology 3 (SH3) and putative histone deacetylase (HDAC) domains are believed to exist in the plakin domain of dystonin-a. A YFP-tagged mini dystonin-a2 (YFP-mini-a2) construct generated by Dr. Kevin Young encoding the structural components of the full-length dystonin-a2 with the spectrin repeat region shortened and YFP-tagged at the C-terminal was used for immunofluorescence analysis. For bacterial expression and interaction analysis, double his-tagged plakin domain (his-plakin) and GST-tagged N-terminal plakin domain (GST-plakin) were used. N-terminal dystonin with the plakin domain flag-tagged at the N-terminus (NtermLong) was used in co-immunoprecipitation experiments. Smaller N-terminal flag-tagged plakin domain constructs, PlakinCH1, comprised of the plakin domain with one calponin repeat, and Plakin, with just the plakin domain were also used for co-immunoprecipitation validation experiments. His-tagged desmin (his-desmin) and flag-tagged death associated protein (Daxx) were used as control plasmids for the bacterial and mammalian expression interaction studies respectively.

with a 1 second on/off pulse while kept on ice. 0.1% triton X-100 was added to the sonicated lysate which was then centrifuged at 13000 RPM for 5 minutes at 4°C. Soluble (supernatant) and insoluble (pellet) fractions were separated and either used immediately or stored at -80°C for further analysis.

Protein purification – Bacterial expression

The his-epitope was used to purify the fusion protein from the soluble fraction of the bacterial culture. For his-tagged constructs, a his-bind kit (Novagen) was used according to the manufacture's protocol. A total of 500 μg of bacterially expressed fusion protein was purified using his-bind beads (60 μl bed volume). The his-tagged protein bound to the his-bind beads was washed in accordance with the manufacturer's recommended protocol; however, the purified protein was not eluted off of the beads.

For GST tagged constructs, GST-sepharose 4B beads (GE Healthcare) were used for purification. The purification was performed in accordance with the manufacturer's recommended protocol. As with the his-bind purification, the GST-purification was also performed up until the step just prior to elution from the beads.

Whole brain lysate cytosolic fraction isolation

The cytosolic fraction from whole brain lysate used for the pull-down analysis was a kind gift from Mr. Shaun Beug, a Ph.D. candidate in Dr. Valerie Wallace's laboratory. Whole brains were dissected from rat pups in accordance with the University of Ottawa animal care facility guidelines. Dissected whole brains were washed in 1X PBS (Phosphate buffered saline; 137 mM NaCl, 2.7 mM KCl, 4.3 mM Na_2HPO_4, 1.47 mM KH_2PO_4) solution before washing with sucrose solution (5 mM imidazole, 250 mM sucrose, 1 mM $MgCl_2$). The whole brains were then minced using a razor blade and suspended in twice

the volume of sucrose solution. The minced brain in sucrose solution was then homogenized on ice using a mini-homogenizing apparatus. Homogenized samples were left on ice for 15 minutes following which they were centrifuged at 10,000 g for 30 minutes. The centrifugation step was repeated if a distinct pellet was not formed. The pellet obtained from this step was used for the generation of nuclear protein extract. The supernatant was collected and centrifuged at 100,000 g for 60 minutes. The supernatant collected from this high-speed centrifugation was the cytosolic fraction of the whole brain lysate. The cytosolic fraction collected was dialysed in HEPES buffer (20 mM HEPES-KOH pH7.4, 150 mM NaCl, 1 mM $MgCl_2$) for 6 hours. The volume of the dialysed solution was adjusted to 10% glycerol and 1 ml aliquots (5 mg total protein per 1 ml aliquot) were snap-frozen using liquid nitrogen and stored for later use at -80°C. The aliquots were subsequently thawed on ice and used for the pull-down analysis.

Whole brain lysate nuclear fraction isolation

Pellet collected during the cytosolic fraction collection was used to isolate nuclear protein. The pellet was resuspended in buffer A (10 mM Tris pH 8, 1.5 mM $MgCl_2$, 5 mM KCl, 1 mM PMSF, 0.5% NP-40) and left to incubate at room temperature for 15 minutes. Resuspended solutions were centrifuged at 1000 RPM for 5 minutes at 4°C. Supernatant was discarded and pellet was resuspended in buffer A with DNAse I (100 U/ml) and incubated for 15 minutes on ice. Suspensions were then centrifuged at 1000 RPM for 5 minutes at 4°C and the supernatant was discarded. The remaining pellet was resuspended in buffer B (20 mM Tris pH 8, 25% glyceol, 1.5 mM $MgCl_2$, 400 mM KCl, 0.2 mM EDTA, 1 mM PMSF, 100 U/ml DNAse I). Samples were incubated on ice for 20 minutes following which centrifugation was performed at 13000 RPM for 5 minutes at

4°C. The final supernatant collected was the nuclear fraction, which was used immediately or stored at -80°C for subsequent pull-down analysis.

Protein concentration determination

Protein sample concentrations were determined using the Bradford method (Bio-Rad) (Bradford, 1976). Diluted protein samples (1:8) were added to 1 ml of dye in duplicate and readings were collected at a wavelength of 595 nm with a calibrated spectrophotometer.

Pull-down protocol

The purified fusion constructs still bound to the purification beads as previously described, were incubated with the cytosolic fraction of whole brain rat pup lysate (600 μg) for 4 hours at 4°C with gentle agitation. The purification beads bound to the fusion protein along with any potential plakin binding partners were centrifuged at 2,000 RPM for 3 minutes at 4°C. For the his-plakin construct, the bead-plakin-partner complex was washed 5 times with 400 μl of 100 mM imidizole solution followed by centrifugation at 2,000 RPM for 1 minute between each wash. The his-plakin fusion protein along with any potential binding partners were then eluted off of the purification beads with 50 μl elution buffer (500 mM imidazole). The eluate was analyzed by sodium dodecyl sulfate-polyacrylamide gel electrophoresis (SDS-PAGE).

After the GST-tagged protein was incubated with the cytosolic fraction from brain lysate, the bead-plakin-partner complex was washed with 400 μl of 1X PBS 5 times with centrifugation (2000 RPM for 3 minutes) between each wash. Following the washes, the plakin fusion protein along with any potential interacting partners was eluted off the beads with GST-elution buffer (50 mM Tris-HCl, 20 mM reduced glutathione, pH 8.0).

The eluate was used for SDS-PAGE.

As negative controls, his-tagged desmin and the GST-tag by itself were expressed, purified and incubated with the cytosolic fraction in the same procedure as the experimental fusion proteins. SDS-PAGE of the eluates from the experimental and control pull-down experiments was performed to identify potential plakin binding partners. Figure 3 is a flowchart representation of the expression, purification and pull-down process.

Sodium Dodecyl Sulphate-Polyacrylamide Gel Electrophoresis

The mini-protein 3 system (Bio-Rad) was used according to the manufacturer's specifications. Eight percent separating gels (8% acrylamide mix (Protogel) 0.015 M Tris pH 8.8, 0.1% SDS, 0.1% ammonium persulfate and 0.04% TEMED) were allowed to set followed by a 5% stacking gel (5% acrylamide mix, 125 mM Tris pH 6.8, 0.05% SDS, 0.1% ammonium persulfate, 0.1% TEMED). Protein samples were mixed with loading buffer (60 mM Tris pH 6.8, 2% SDS, 10% glycerol, 5% β-mercaptoethanol, 0.1% bromophenol) and boiled for 5 minutes and then loaded (50 μg) into the gel along with the Precision Plus protein ladder (Bio-Rad). Gels were allowed to run at 100V in running buffer (25 mM Tris base, 250 mM glycine pH 8.3, 0.1% SDS) for as long as necessary dependent upon the application. The gel containing the separated proteins were either coomassie stained, silver stained, or transferred onto a PVDF membrane (Millipore, Billerica, Massachusetts).

For novel binding partner identification from the pull-down analysis, the acrylamide gels were carefully stained with either coomassie (sensitivity from 50-100 ng of protein) or silver (sensitivity from 5-10 ng of protein). Caution was taken to limit the

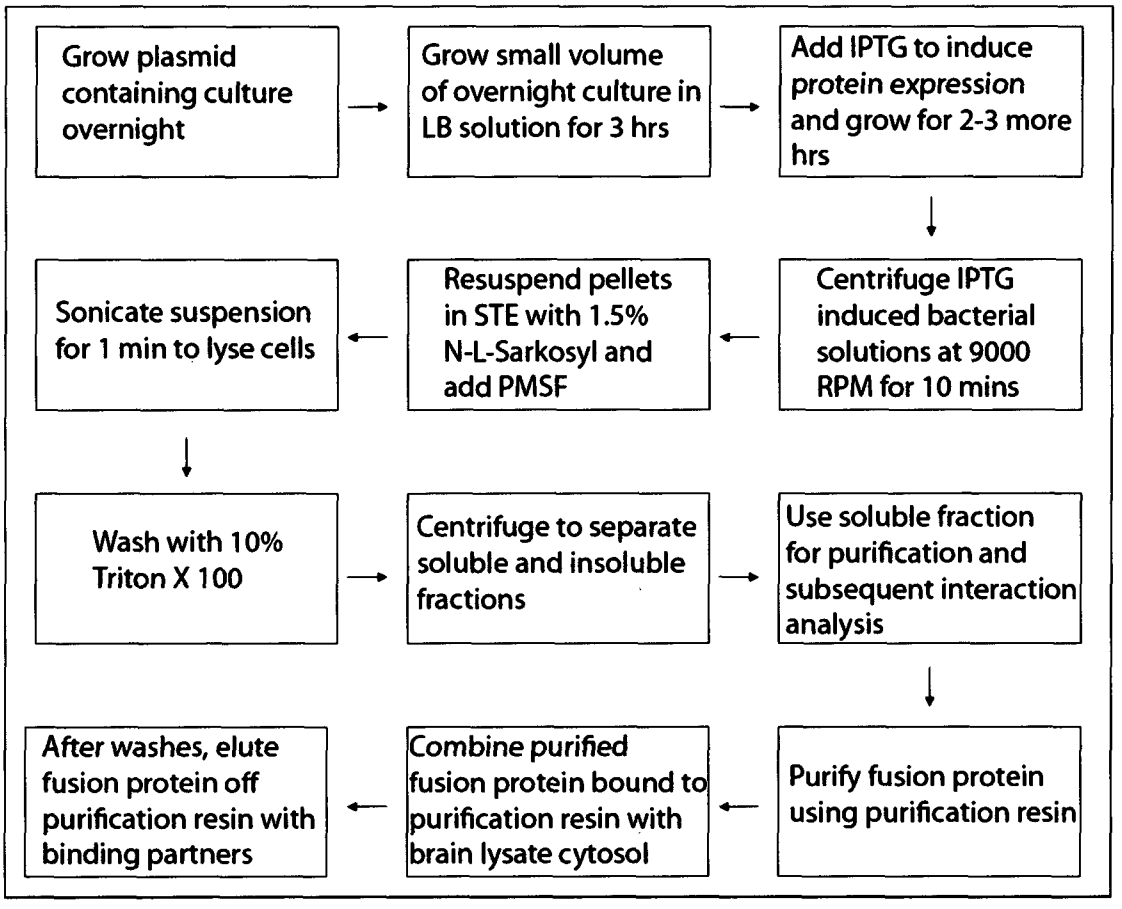

Figure 3. Flowchart of fusion protein expression, purification and pull-down. Construct containing E.coli. BL-21 host bacteria is cultured overnight. A volume unit of this overnight culture is then further grown in nutrient Luria's broth (LB) media with isopropyl β-D-1thiogalactopyranoside (IPTG) to induce protein expression. Subsequent to centrifuging the cultures, the cells are re-suspended in N-Lauryl Sarkosyl. Sonification is then performed to lyse the suspended cells and release the promoted protein. Triton X-100 is added to remove detergent residue. Centrifugation separates the soluble and insoluble fractions. The soluble fraction is purified using his-bind resin. Washes are performed using buffers containing increasing concentration of imidazole. Purified fusion proteins still bound to the purification resin is combined with cytosolic fraction of whole brain lysate. After mild buffer washes the fusion protein is eluted off the purification resin using high-imidazole buffer along with any binding partners.

handling of the gel to prevent contact contamination. Bands unique to the plakin with cytosol lanes were carefully excised using a sterile scalpel and used for mass spectrometry analysis. All staining and excision procedures were performed in a biological safety cabinet.

Coomassie blue staining

SDS-PAGE completed gels were placed in a tight-lid container with coomassie blue solution (Coomassie blue R350 dye, 20% methanol, 10% acetic acid) with gentle agitation at room temperature for 4 hours. The stain was removed and the gel was destained overnight using a destain solution (50% methanol in water with 10% acetic acid). Absorbent large KimWipes (Kimberly Clark) were placed in the destain solution along with the gel to facilitate the destaining process. The gels were then placed in storage/mild destain solution (10% methanol, 5% acetic acid) until band excision was performed or they were dried for analysis. All of the gel handling was performed in a biological safety cabinet to reduce contact contamination.

Silver Staining

Silver staining was used to detect unique binding partners of the his-plakin fusion construct with the cytosolic fraction from whole brain lysate. Once the SDS-PAGE gels had run to completion, they were carefully placed in a tight-lid container and all subsequent procedures were performed in a biological safety cabinet to prevent contamination in the mass spectrometry analysis. The gels were briefly rinsed in deionised water and fixed (50% ethanol, 5% acetic acid) for 30 minutes. Following fixation, the gels were washed using the washing solution (50% ethanol). The gels were then washed with deionised water twice for 10 minutes each time followed by immersion

into the sensitizer solution (0.02% sodium thiosulfate). Following two deionised water washes of 3 minutes each, the gels were stained with staining solution (0.1% silver nitrate) for 30 minutes. After the removal of the staining solution and following a deionised water wash for 1 minute, a 50:50 diluted developer solution (2% sodium Na_2CO_3, 0.12% formalin) was used for 10 seconds to begin the detection process. Concentrated developer solution was added and the gel container was gently agitated until bands were visualized. Deionised water was added to slow the reaction. When the desired stain strength was achieved, the reaction was arrested using the stopping solution (5% acetic acid).

Immunodetection

Once an SDS protein gel had run to completion it was transferred to a PVDF membrane using the Bio-Rad semi-dry transfer apparatus. A methanol activated PVDF membrane was sandwiched between the gel and Whatman blotting paper soaked in transfer buffer (200 mM glycine, 25 mM Tris base, 20% methanol). The gel apparatus was run at 250 mA for 90 mins. The membranes were then incubated in blocking solution (5% non-fat dried milk in 1XTBST (tris buffered saline with tween); 0.02 M Tris base, 0.1 M NaCl, 0.002 M KCl, 0.1% Tween) with gentle agitation for 1 hour at room temperature. Membranes were then incubated overnight at 4°C with appropriate primary antibodies diluted in 5 ml of blocking solution. The membranes were then washed in 1XTBST solution for 10 minutes for a total of 3 washes. Following these washes the membrane was incubated with an appropriate horse-raddish-peroxidase conjugated secondary antibody for 1 hour at room temperature with gentle agitation. Immunodetection was performed using an enhanced chemiluminescent (ECL) kit (Amersham Corp., Arlington

Heights, IL) according to the manufactures protocol. The reactive chemiluminescent membrane was then exposed to film (Kodak BioMax) for an appropriate length of time, following which the film was developed using a film processing system (Konica-Minolta).

Cell Culture

Cos-1 monkey kidney, C2C12 mouse myoblast, and F11 mouse neuroblastoma rat DRG hybrid cell lines were cultured in DMEM (Dulbecco's modified eagle media) (Wisent) with 10% fetal bovine serum (FBS) (Sigma) and 1% pen/strep/antimycotic (Invitrogen). Phaeochromocytoma derived PC-12 rat adrenal medulla cells were cultured in DMEM with 10% horse serum (Sigma), 5% FBS (Sigma), 1% pen/strep (Invitrogen) and 1% MEM non-essential amino acids (Invitrogen). Cells were cultured in 6-well and 10 cm plates (Corning) for protein extract collection when used for co-immunoprecipitation experiments. For immunofluorescence, the cells were cultured on coverslips in 12-well plates (Corning). PC-12 cells were cultured on plates that were coated with rat-tail collagen (Cultrex) overnight when used to collect protein extracts. For immunofluorescence these cells were cultured on coverslips that were coated with Poly-L-lysine (Sigma) overnight and laminin (Roche; 20 μg/ml) for 1 hour just prior to seeding. Cell transfections were performed using lipofectamine 2000 (Invitrogen) according to the manufacturer's protocol for each cell type. Transfected cells were cultured for at least 36 hours prior to performing any analyses. When necessary, F11 cells were differentiated using 0.5 mM dibutyryl cyclic adenosine monophosphate (di-cAMP) in DMEM for 48 hours post-transfection. PC-12 cells were differentiated in DMEM containing 1% FBS, 1% pen/strep, 1% MEM non-essential amino acids and 50 ng/ml

neural growth factor (Sigma) 2.5S.

Protein collection

Whole Tissue Lysate

Wild-type and *dt* animals were sacrificed by cervical dislocation. Protein extracts were obtained from brain and spinal cord tissue by homogenizing in chilled RIPA buffer containing a cocktail of protease and phosphatase inhibitors (50 mM TrisHCl pH 7.4, 150 mM NaCl, 2 mM EDTA, 1% NP-40, 0.1% SDS 1 μg/ml leupeptin, 1 μg/ml aprotinin, 5 μg/ml PMSF, 1 μg/ml pepstatin). The samples were then centrifuged at 13,000 RPM for 20 minutes at 4°C and the supernatant was either stored at -80°C or used immediately for further analysis.

Adherent cell cultures

Cell culture plates were washed twice quickly with PBS and incubated with lysis buffer contaning protease and phosphatase inhibitors (50 mM TrisHCl pH 7.4, 150 mM NaCl, 2 mM EDTA, 1% NP-40, 1 μg/ml leupeptin, 1 μg/ml aprotinin, 5 μg/ml PMSF, 1 μg/ml pepstatin) on ice for 5 minutes. Adherent cells were then scraped off the culture plates using a cell scraper (Fisher) and the lysate was placed in chilled centrifuge tubes. Lysate containing tubes were gently agitated for 30 minutes at 4°C. The tubes were then centrifuged for 15 minutes at 13,000 RPM and the soluble and insoluble fractions were either used immediately or stored at -80°C for further analysis.

Mass spectrometry

Mass spectrometry was performed by Mr. Julian Vasilescu at the Ottawa Institute of Systems Biology and Dr. Lawrence Puente at the Ottawa Hospital Research Institute Proteomics Core Facility. In-gel digestion was performed using trypsin as previously

described (Wilm et al., 1996). Sixteen hour digestions were performed using sequencing grade trypsin obtained from Promega (Madison, WI, USA). Peptides from gel bands were extracted and hydrated in 20 mL of 5% formic acid and analyzed by LC-MS/MS as follows. Peptides were loaded at a rate of 5 uL/min onto a 200 um x 50 mm precolumn packed with 5 um YMC ODS-A C_{18} beads (Waters, Milford, MA, USA) using an Agilent 1100 series HPLC system (Agilent Technologies, Palo Alto, CA, USA). Subsequent to the desalting step, the flow was split and peptides were eluted through a second 75 um x 50 mm column, packed with the same beads, at approximately 200 nL/min using a 5–80% gradient of acetonitrile with 0.1% formic acid for 1 hr. The LC effluent was electrosprayed into an LTQ linear ion-trap mass spectrometer (Thermo-Electron, USA). MS/MS spectra were acquired in a data-dependant acquisition mode that automatically selected and fragmented the four most intense peaks from each MS spectrum generated. Peptide and MS/MS mass tolerances were set at 6 2 and 0.8 Da, respectively. MS/MS data were then analyzed and matched to human protein sequences in the NCBI database (nrdb) using the MASCOT database search engine version: 2.2.04 (MatrixScience, UK). A minimum peptide ion score cut-off of 40 was employed. Scores of over 400 were deemed acceptable for subsequent analysis.

Co-immunoprecipitation

Protein isolated from transfected adherent cell cultures was used in co-immunoprecipitation analysis. Soluble lysate (300 µg) containing flag-tagged constructs was incubated with sepharose protein G beads (50 µl bed volume, GE healthcare) or dynal protein G magnetic beads (50 µl bed volume, Invitrogen) along with 5 µg of anti-flag M2 antibody (Sigma) in eppendorf tubes for 3 hours at 4°C on a rocking platform.

These tubes were then centrifuged or placed on a magnetic rack according to the manufacturer's specification and the supernatant was collected for later analysis. The beads were then washed twice with 1XPBS of 200 µl per tube followed by another two lysis buffer washes (50 mM TrisHCl pH 7.4, 150 mM NaCl, 2 mM EDTA, 1% NP-40) of the same volume. Two final 1XPBS washes of the same volume were performed and the beads were transferred to new eppendorf tubes. The flag-tagged proteins were eluted off of the beads using 30 µl of mild protein loading buffer (60 mM Tris pH 6.8, 2% SDS, 10% glycerol) and boiling for 5 minutes. PAGE was performed on the eluates and the protein was then transferred to a PVDF membrane which was probed for potential co-immunoprecipitation partners.

Immunofluorescence

Immunostaining was performed on tissue sections and cells cultured on coverslips. Slides with sections (8 µM) from dorsal root ganglia (DRG) and tibialis were placed on microscope slides (Premium slides, Fisher). Cells (Cos-1, PC-12, C2-C12 and F11) were grown on coverslips (ethanol washed, autoclaved and matrix coated when necessary) in appropriate cell culture media. Both tissue sections and cells were fixed with 4% (paraformaldehyde) PFA for 10 min followed by 3 1XPBS washes. Samples were then incubated at room temperature with blocking solution (1XPBS, 0.4% Triton X-100, 10% goat serum). Appropriate primary antibodies were diluted in the antibody solution (1XPBS, 0.4% Triton X-100, 0.05% bovine serum albumin) overnight at 4°C. The samples were then washed with 1XPBS for 10 minutes for a total of three times. Appropriate secondary antibodies were diluted in the same solution used for the primary antibody and incubated with the samples for 1 hour at room temperature. After

performing one 10 minute 1XPBS wash, the samples were incubated with DAPI nuclear stain (1 ng/ml) for 10 minutes at room temperature. Three 10-minute 1XPBS washes were performed and the stained tissue section slides had coverslips placed on them with mounting media (Dako). The cells grown on coverslips and stained were mounted onto microscope slides (Fisher premium frosted) using mounting media (Dako). Micrographs were obtained from the Zeiss Axiovert 200 inverted microscope and the Zeiss LSM 510 confocal microscope. Image analysis was performed using Abode Photoshop CS software.

Proximity ligation assay

The Duolink proximity ligation assay kit which includes an anti-rabbit proximity ligation assay (PLA) plus probe, an anti-mouse PLA minus probe, and the 613 detection kit was purchased from Olink Bioscience (Sweden). PFA fixed F11 cells grown on coverslips in a 12-well plate were blocked for 1 hour in 10% goat serum and incubated with MAP1B (mouse isotype) and dystonin isoform 2 (rabbit isotype) antibodies in antibody solution (1XPBS, 0.4% Triton X-100, 0.05% bovine serum albumin) overnight at 4°C. All subsequent reagent incubations were performed in a humidity chamber at 37°C. PLA probes were diluted in antibody solution (1:5) and all other duolink reagent dilutions were performed according to the manufacturer's specifications. Following a 110 minute incubation with the PLA probes, the cells were washed twice with TBST for 5 minutes. Subsequent to these washes the cells were incubated with the hybridization mixture for 15 minutes followed by a 15 minute incubation with the ligation mixture with a TBST wash for 2 minutes in between. Two 5 minute TBST washes were performed and the amplification mixture was added to the cells for 90 minutes. The detection mixture was

then added after 2 TBST washes of 5 minutes each were performed. The cells were then washed in 2X saline sodium citrate buffer (2XSSC; 0.3 M NaCl, 0.03 M Sodium Citrate (tri basic di hydrate)), 1X SSC, 0.2X SSC and 0.02X SSC for 2 minutes each and 70% ethanol for 1 minute. After air drying in a light-protected enclosure coverslips were mounted on slides using Olink mounting media containing DAPI nuclear stain. Detection of the PLA signal using the Ziess axiovert inverted microscope indicated that the proteins were within 40 nm of eachother within the cell.

Tissue sections

Tissue sections of tibialis and DRG from *dt* and wild-type mice were prepared by Mr. Yves de Repentigny and cardiac tissue sections were prepared by Mr. Justin Boyer. Animals were euthanized by cervical dislocation in accordance with University of Ottawa animal care facility guidelines. Tissues of interest were harvested placed in OCT compound (Tissue-Tek) and flash-frozen in liquid nitrogen. Samples were sectioned at 10 μM thickness using a Leica CM1850 cryostat. Prepared sections were either used immediately for immunofluorescence or stored at -80° C for future analysis.

Antibodies

The antibodies used in the present study have been listed in Table II.

Table II. Antibodies used in present study

Antibody	Manufacturer	Species	Immunofluorescence	Immunoblot	Immunprecipitation	Proximity Ligation Assay
Clathrin	Cell Signaling	Rabbit	1:350	1:750		
CRMP2	Cell Signaling	Rabbit	1:450	1:1000		
Dystonin-2	Generated	Mouse	1:400			1:400
Dystonin-b	Generated	Chicken	1:5000	1:20000		
Flag M2	Sigma	Mouse	1:2500	1:15000	5ug	
GM130	Abcam	Mouse	1:500			
His	Cell Signaling	Rabbit		1:1000		
MAP1B	Sigma	Mouse	1:1500	1:5000		1:1500
Myosin IIb	Cell Signaling	Rabbit	1:450	1:1000		
PDI	Abcam	Mouse	1:200			
Vimentin	Abcam	Mouse	1:250			

Results

The plakin protein family has been shown to stabilize the cytoskeleton in several cell types. Mutations in the plakin family member dystonin, have been associated with a neurodegenerative disease in mice called *dystonia musculorum*. The purpose of the present study was to identify novel binding partners of dystonin in an effort to elucidate the function of this complex protein. In particular, we narrowed our search for proteins that interacted with the dystonin-a plakin domain.

1. Identification of interacting partners through pull down analysis

Identification of interaction partners was pursued using a pull-down assay. Bacterially expressed dystonin-a plakin domain with his-tags at both the N and C-terminal ends was used for this purpose. Purified plakin protein was incubated with the cytosolic fraction of rat pup whole-brain lysate and unique binding partners were identified through mass spectrometry analysis.

Expression and purification of his-plakin protein

In an effort to conduct the pull-down interaction analysis it was necessary to express a soluble his-plakin. For this purpose the open reading frame coding for the plakin region of dystonin was inserted into a bacterial expression plasmid. Soluble his-plakin expression was successfully achieved through IPTG induction. IPTG induces the transcription of the *lac* operon which was replaced in the expression plasmid by the his-plakin sequence. Bacterial cultures expressing the his-plakin protein were separated into soluble and insoluble fractions through centrifugation. Figure 4 depicts the expression of his-plakin in the soluble and insoluble forms, with and without IPTG induction. His-plakin was found to be strongly expressed after IPTG induction and largely found in the

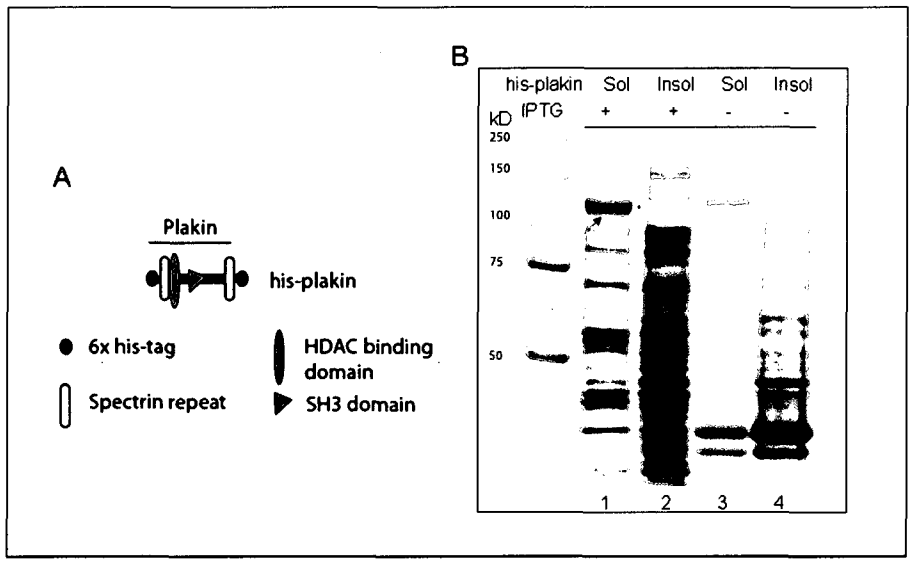

Figure 4. Protein extraction from bacterial culture.
A. Schematic representation of the plakin domain of dystonin-a/b his-tagged at both the N-terminal and C-terminal ends (his-plakin). **B.** Post transformation of the his-tagged plakin construct (his-plakin) into BL-21 E.coli bacteria, protein production was induced by IPTG. IPTG induced (lanes 1 and 2) and non-IPTG induced (lanes 3 and 4) bacterial lysates were collected. Soluble (Sol) and insoluble (Insol) fractions were separated for each condition. PAGE analysis followed by coomassie blue staining revealed that the desired his-plakin fusion protein was in the soluble fraction. The IPTG induced soluble fraction of the his-plakin construct produced an ~128kD protein (red arrow) as anticipated.

soluble fraction. This outcome of the expression procedure was ideal for the interaction pull-down analysis as a fusion protein in soluble form facilitated the incubation with the cytosolic fraction from rat pup whole-brain lysate.

Once the his-plakin fusion protein was successfully expressed in soluble form, purification of the expressed product was optimized. Purification was necessary to ensure that the novel potential interactors identified during the pull-down experiments were not a by-product of non-specific binding to background bacterial expression products. Efficient purification was achieved by varying the amounts of imidazole in the purification buffers (Figure 5). Imidazole out-competes the his-tag for binding affinity with the his-bind resin. As the levels of imidazole are increased, greater amounts of non-specific bacterial expression products are removed. The final elution step reveals a purified his-plakin fusion product (~128kD) with minimal bacterial background. Unexpectedly, two smaller bands were resistant to removal by the purification buffers. Subsequent mass spectrometry analysis revealed that these additional bands were actually cleavage products of the his-plakin protein. The resilience of these bands to removal by the purification buffers was most likely a result of having 6x his-tags at both the N-terminal and C-terminal ends of the fusion protein. As the fusion protein was cleaved, the his-tag at each end remained bound to the purification resin until the final elution was performed.

Identification of novel binding partners for dystonin-a

After successfully purifying the protein produced from the his-plakin fusion construct using a his-bind resin purification kit, the purified product still bound to the purification resin was incubated with the cytosolic fraction of rat pup whole-brain lysate. A comparison between the PAGE banding pattern of just his-plakin and his-plakin

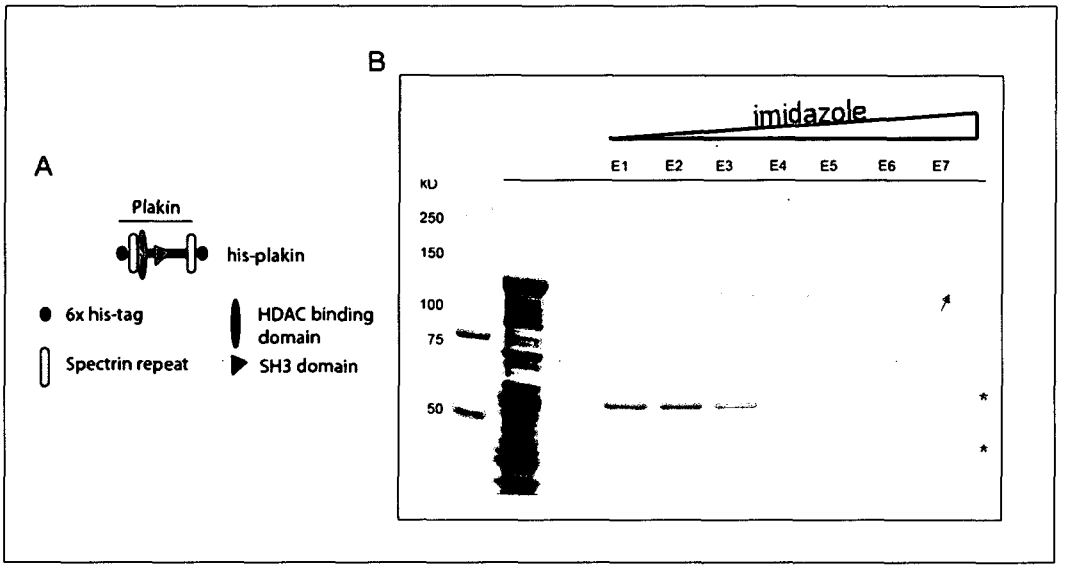

Figure 5. Purification of plakin domain of dystonin-a/b his-tagged at both the N-terminal and C-terminal ends (his-plakin).
A. Schematic representation of his-plakin **B.** Purification of the his-plakin construct. Purification of the protein produced from the IPTG induced soluble fraction of the his-plakin construct was performed using a his-bind purification resin. As previously demonstrated, the protein induction technique produced an ~128kD protein (his-plakin) shown in lane 1. The first wash was comprised of 1XPBS and 20 mM imidazole (lane 2). Imidazole out-competes the his-tag for binding affinity to the his-bind resin. As levels of imidazole are increased, the his-tagged fusion construct is eluted off the resin. Subsequently, PBS solutions containing linearly increasing amounts of imidazole were used to eliminate non-specific background. The eluates were collected and PAGE analysis was performed followed by coomassie blue staining. The elution buffers ranged from 100 mM to 500 mM of imidazole in PBS and have been labelled E1-E7. The purified product is indicated by the red arrow. The two lower bands (asterisks) observed in the final elution have been identified as cleavage products of the his-plakin fusion construct through mass spectrometry. The his-plakin construct is his-tagged at both the N-terminal and C-terminal ends. As a result, cleavage products of the full construct would also be expected to effectively bind to the his-bind resin used for its purification.

incubated with brain cytosol, visualized using coomassie blue, revealed potential novel partners. After these bands were excised from the PAGE gel, mass spectrometry analysis was performed to determine their composition. As dystonin-a is the predominant isoform of dystonin in neuronal tissue, the use of lysate from rat pup whole-brains was believed to be identifying novel binding partners of this isoform. The results of this analysis provided several strong candidates, based on MASCOT scores (over 150) and peptide match numbers (Table III), including collapsin response mediating protein (CRMP/Ulip3), tubulin and actin (Figure 6). The CRMP protein identified was an interesting candidate interacting partner and was selected for further analysis. CRMP exists in 5 isoforms, which are known to play a role in the developing nervous system (Stenmark et al., 2007). CRMP2 has been shown to play a significant role in cytoskeletal dynamics through the manipulation of the MT network at the axonal growth cone.

The pull-down experiment was repeated to identify additional potential interacting partners of the plakin domain of dystonin-a (Figure 7). In an effort to increase the sensitivity of the assay, the pull-down eluate PAGE gel was silver stained. His-desmin was produced and purified in the same manner as the his-plakin fusion protein and used as a control. Several unique partners were identified after this analysis was performed. Mass spectrometry analysis of an excised band at 270 kD was identified to be microtubule associated protein (MAP) -1B. MAP1B is a developmentally regulated MT associated phosphoprotein. It is generally expressed in the developing nervous system as well as in areas of neuronal plasticity and regeneration in adult nervous tissue (Noble et. al, 1989). It helps stabilize MTs; however, differential phosphorylation of MAP1B is believed to result in a weaker stabilizing effect on MTs than other MAPs.

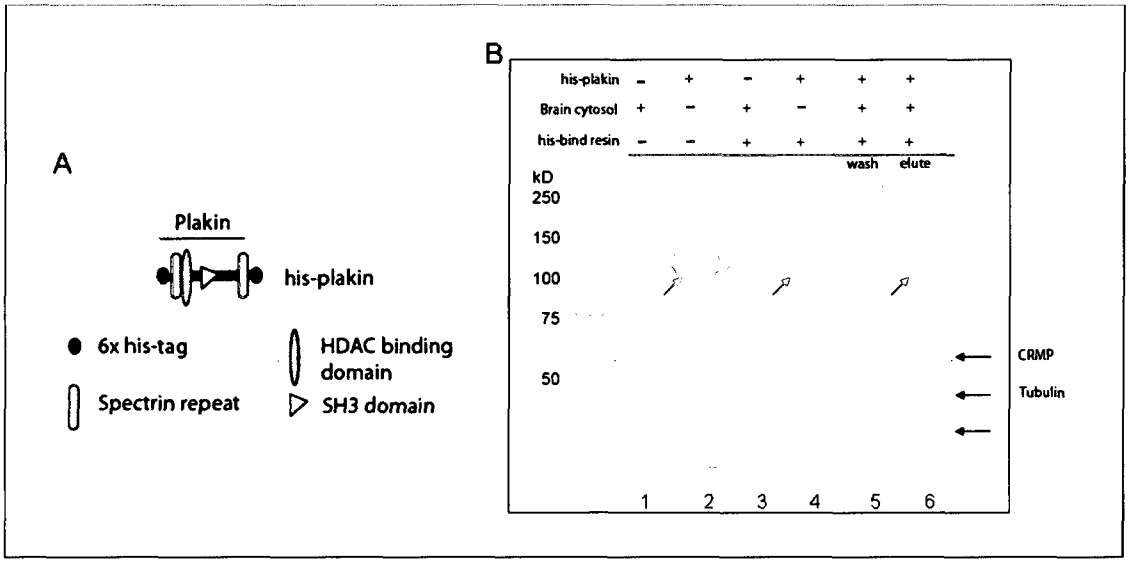

Figure 6. Pull-down of CRMP with his-plakin.
A. Schematic representation of the plakin domain of dystonin-a/b his-tagged at both the N-terminal and C-terminal ends (his-plakin) used for pull-down analysis. **B.** Coomassie blue stained PAGE gel reveals unique potential interactors which were identified when purified his-plakin was incubated with the cytosolic fraction of rat pup brain lysate (brain cytosol). The fusion protein was prepared as previously indicated producing an ~128kD soluble protein (red arrow lane 2). Purification of the fusion protein was performed using the his-bind resin. Lane 1 depicts the protein banding pattern of brain cytosol. Lane 2 demonstrates the successful bacterial expression of the his-plakin protein in the soluble fraction prior to purification with his-bind resin. Lane 3 demonstrates the absence of non-specific binding of the brain cytosol to the his-bind resin. Lane 4 illustrates the successful purification of the his-plakin protein. The his-plakin protein was purified, and just prior to elution from the his-bind resin was incubated with the cytosolic fraction of rat pup whole-brain lysate. After several stringent washes (flow-through illustrated in lane 5) the his-plakin protein was eluted from the his-bind resin along with any potential interacting partners, using high levels of imidazole. The bands present in lane 6 (blue arrows) and not in lane 4 were excised and prepared for mass spectrometry analysis. Collapsin response mediated protein (CRMP) at ~62 kD and tubulin at ~50 kD were identified in the mass spectrometry analysis.

Clathrin heavy chain (170 kD) is another potential interactor that was identified through mass spectrometry of an excised band unique to the his-plakin with brain cytosol pull-down. Clathrin is the most abundant protein in intracellular transport vesicles, which are necessary for endocytosis and membrane trafficking processes (Traub, 2005). Clathrin is generally formed of a basic assembly unit called a triskelion made up of three clathrin heavy and three light chains (Edeling et al., 2006).

The non-muscle myosin-IIb protein (230 kD) produced from the MYH10 gene was also identified through mass spectrometry of the pull-down experiment. This protein is an actin-based motor that is necessary for cell motility, division, migration and polarity, as well as adhesion. The main function of this protein and its isoforms, namely, myosin IIa and IIc, is to bind and contract actin microfilaments coupled to ATP hydrolysis. The results of the pull-down analysis have been depicted in Figure 7. It should be noted that CRMP was not identified in this analysis as excision of a ~62 kD band was not performed. However, closer examination of the silver stained PAGE gel revealed that indeed a unique band of ~60-65 kD in the his-plakin with brain cytosol lane, and this may be CRMP.

Dystonin plakin-domain potential interactor specificity

Immunoblot follow up experiments were performed to ensure that the identified potential interactors were unique to the his-plakin pull-down. Successful expression of both his-plakin (~128 kD) and his-desmin (~65 kD) was confirmed through the detection of the his-tag in both samples (Figure 8A). MAP1B, at 270 kD, was only detected in the his-plakin with brain cytosol lane (Figure 8B). Myosin IIb was only detected in the lane containing his-plakin with brain-cytosol as indicated by the band present at 230 kD, the

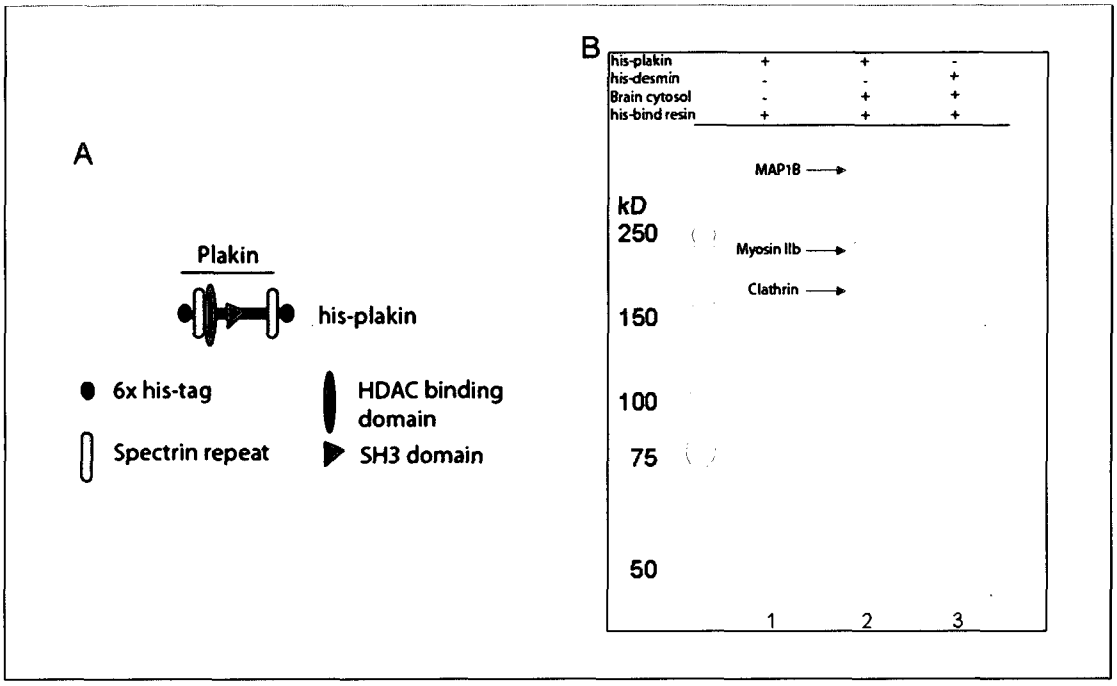

Figure 7. Pull-down of several novel his-plakin interactors.
Purified his-plakin and his-desmin proteins were incubated with the cytosolic fraction of rat pup whole-brain lysate (brain-cytosol). PAGE was performed on the eluates from the pull-down experiments followed by silver staining to visualize the proteins. **A.** Schematic representation of the plakin domain of dystonin-a/b his-tagged at both the N-terminal and C-terminal ends (his-plakin) used for pull-down analysis. **B.** The his-plakin fusion construct produced ~128 kD soluble protein (lane 1). Lane 1 depicts the successful purification of the his-plakin protein. After the purification of the fusion proteins and just prior to their elution from the his-bind resin, they were incubated with the cytosolic fraction of rat pup whole-brain lysate. Several stringent washes were performed to remove non-specific binding proteins. After elution and PAGE, several unique bands were observed in the his-plakin with brain-cytosol lane when the gel was silver stained. Lanes 2 and 3 illustrate the bands remaining in the his-plakin with brain-cytosol and his-desmin with brain-cytosol eluates respectively, after the stringent wash protocol was performed. Bands present in lane 2, but not present in lanes 1 and 3, were excised and prepared for mass spectrometry analysis. Mass spectrometry results from the excised bands indicated three significant potential binding partners, namely MAP1B, myosin IIb and clathrin heavy chain (Clathrin). These unique bands have been highlighted with arrows accordingly.

Table III. Summary of mass spectrometry analysis

	MAP1B	Clathrin Heavy Chain	Myosin IIb	CRMP2
Mascot Score	475	866	2163	161
Peptide Match	13	18	51	5

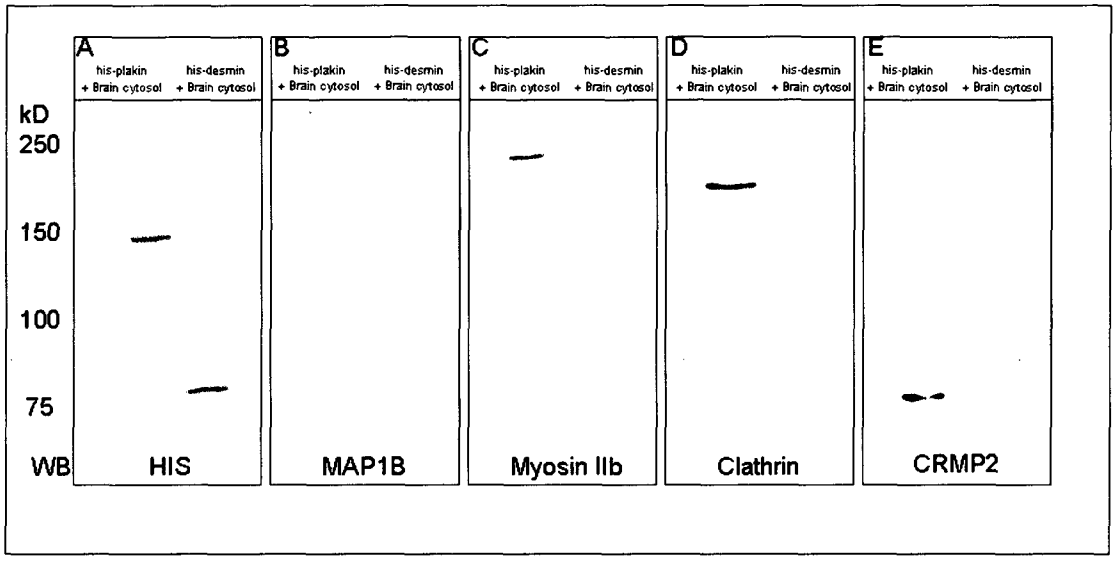

Figure 8. Plakin domain novel binding partner specificity.
Western blots were performed on eluates used for the pull-down analysis. **A.** Anti-his immunoblot detected expression of his-plakin (128 kD) and his-desmin (68 kD) in his-plakin with brain cytosol and his-desmin with brain cytosol lanes respectively. **B-E.** MAP1B, myosin IIb, clathrin and CRMP2 were detected only in the plakin with brain cytosol lane, indicating specificity in the pull-down analysis.

predicted size of the protein (Figure 8C). Similarly a band was detected at 170 kD indicating the presence of clathrin heavy chain in only the his-plakin with brain-cytosol lane (Figure 8D). As the CRMP family of proteins has been shown to demonstrate high homology amongst its members, and as CRMP2 has been implicated in cytoskeletal dynamics, we decided to pursue this member of the family. An immunoblot of CRMP2 on the samples used for the pull-down analysis indicated that this protein was only detected in the lane containing the his-plakin with brain cytosol (Figure 8E).

Follow up studies on MAP1B, myosin IIb and CRMP2 as potential interaction partners of dystonin were performed as these proteins play an integral part in cell cytoskeletal dynamics. Clathrin heavy chain was also deemed to be a relevant candidate to pursue for further analysis given its involvement in vesicular-cargo transportation and trafficking.

2. Validation of partners identified through pull-down analysis

A multi-faceted approach including co-immunofluorescence, co-immunoprecipitation and proximity ligation assay was undertaken to further explore and validate the potential interactors identified through the pull-down experiments of dystonin-a plakin domain with the cytosolic fraction from rat pup whole-brain lysate.

Validation of dystonin-a and MAP1B interaction

MAP1B co-immunoprecipitates with plakin domain of dystonin-a

Co-immunoprecipitation experiments using Ntermlong, PlakinCH1, and Plakin were conducted on transiently transfected and differentiated F11 cells. As fusion proteins expressing only the plakin domain have been shown to localize within the nucleus (Jefferson et al., 2006), the use of multiple constructs featuring the plakin domain along

with other dystonin components ensured localization of the constructs would be representative of the full-length protein. Daxx fusion (a kind gift from Dr. D. Picketts) was used as a negative control for the co-immunoprecipitation experiments to ensure that co-immunoprecipitation was not a result of non-specific binding to the flag epitope. MAP1B was co-immunoprecipitated with NtermLong, PlakinCH1 and Plakin from the lysate of transiently transfected and differentiated F11 cells. Minimal detection of MAP1B signal was observed in the Daxx immunoprecipitation lane, despite comparatively much higher levels of Daxx expression. This indicates that MAP1B's co-immunoprecipitation with the dystonin plakin domain constructs was not a result of non-specific or background interactions (Figure 9).

Immunoblot for the flag epitope of the Ntermlong, PlakinCH1, Plakin and Daxx constructs was observed in the lysate from the transiently transfected and differentiated F11 cells, verifying tag-expression and successful binding to the sepharose protein G beads used for the immunoprecipitation reaction (Figure 9C). This lysate, which was used as the input for the co-immunoprecipitation reaction, was also probed for the expression of endogenous MAP1B. A band at ~270 kD in all of the lanes indicates the successful expression and detection of MAP1B in the input lysate (Figure 9D). The results from this co-immunoprecipitation analysis indicate that the plakin domain of dystonin-a possesses the capability of interacting with MAP1B in this assay. The results demonstrated in this assay were found to be reproducible as the experiment was repeated several times.

Reciprocal co-immunoprecipitation experiments were attempted to determine if plakin domain containing fusion proteins could immunoprecipitate with MAP1B. Unfortunately, the MAP1B antibody used for this assay was not designed or verified for

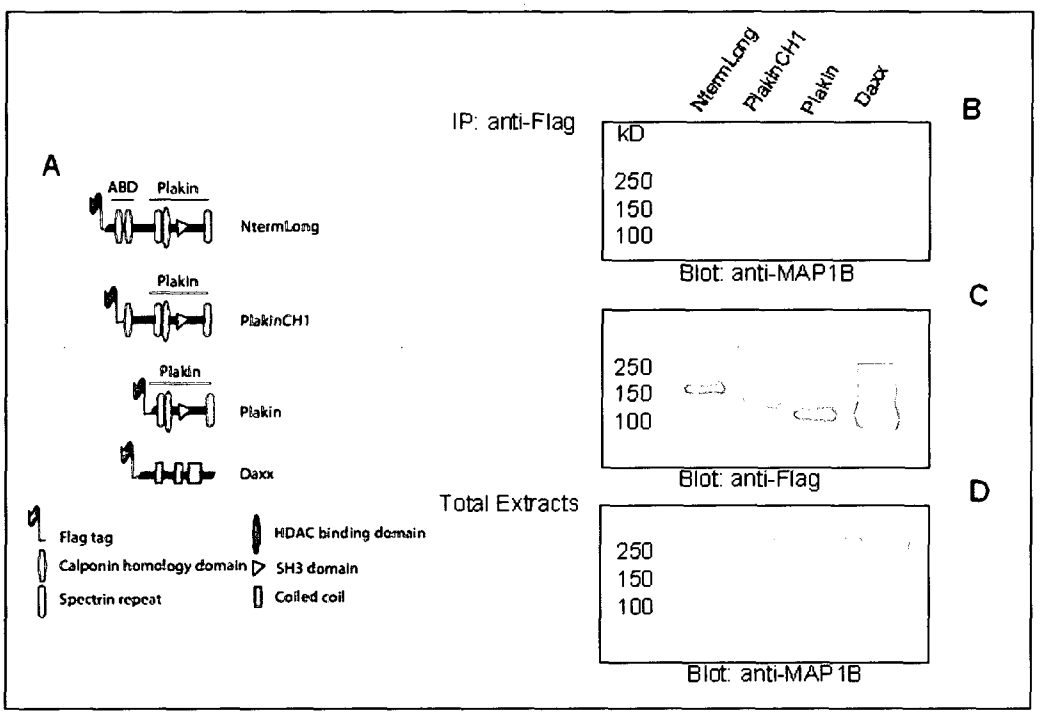

Figure 9. MAP1B interactions with plakin domain of dystonin.
Co-immunoprecipitation of endogenous MAP1B with flag epitope-tagged plakin fusion constructs from transiently transfected and differentiated F11 cells. **A.** Schematic diagram of flag-epitope fusion constructs used for immunoprecipitation reactions. Flag-tagged plakin domain with N-terminal region is referred to as NtermLong. Flag-tagged plakin domain with one calponin homology repeat is named PlakinCH1. A flag-tagged construct encoding the entire plakin domain was also generated and is referred to as Plakin. As a negative control for the immunoprecipitation assay, a flag-tagged death associated protein construct called Daxx was used. **B.** Immunoblot of MAP1B following PAGE on eluates from immunoprecipitation reactions using lysate expressing flag-fusion constructs and containing endogenous MAP1B from transiently transfected and differentiated F11 cells. MAP1B was successfully detected in lanes immunoprecipitated for flag from lysate containing NtermLong, PlakinCH1 and Plakin from transiently transfected and differentiated F11 cells. Minimal MAP1B was co-immunoprecipitated with Daxx. **C.** Anti-flag immunoblot of lysate from F11 cells transiently transfected with the flag-tagged mammalian expression constructs shown in panel A and differentiated for 48 hours post-transfection. Detection of flag indicates successful transfection and expression of the fusion constructs. NtermLong was detected at 171 kD, PlakinCH1 was detected at 144 kD, Plakin was detected at 120 kD and Daxx was blotted at 110 kD. **D.** Immunoblot of MAP1B in the input lysate from the transiently transfected and differentiated F11 cells used for the co-immunoprecipitation reactions described above.

this application. As such, despite multiple attempts, we were unable to successfully co-immunoprecipitate plakin fusion proteins with MAP1B. Interestingly, MAP1B was also not able to co-immunoprecipitate MAP1B itself, lending to the notion that the antibody employed was not suitable for this purpose.

MAP1B localizes with endogenous dystonin-a2

In an effort to further validate the potential interaction of the plakin domain of dystonin-a and MAP1B, immunofluorescence experiments were performed to determine the localization of the two proteins in the F11 cell line which is hybid of mouse neuroblastoma and rat DRG cells. Endogenous dystonin-a2 was found to co-localize with endogenous MAP1B in a perinuclear, slightly polarized pattern in differentiated F11 cells (Figure 10A-C). Over-exposure of the co-localization images indicated that dystonin-a2 and MAP1B co-aligned along the neurites as well (Figure 10D-F). The co-localization pattern observed in the differentiated F11 cells was representative of the majority of the cells observed. This experiment was repeated in triplicate with a cell plating density of ~35,000 cells per well in a 12-well plate.

MAP1B localizes with dystonin-a2 fusion protein

As F11 cells have very small cell bodies, structural localization assessments are difficult to make. We therefore explored the localization of MAP1B and dystonin-a2 in rat pheochromocytoma PC12 cells. Characterization of the dystonin-a2 antibody has not been performed in PC12 cells, we therefore resorted to transfecting and over-expressing a dystonin-a2 fusion protein. PC12 cells were transfected with a YFP-mini-a2 fusion and subsequently differentiated. The YFP-mini-a2 construct possesses all of the structural characteristics of the dystonin-a2 protein; however, it has a shortened spectrin repeat

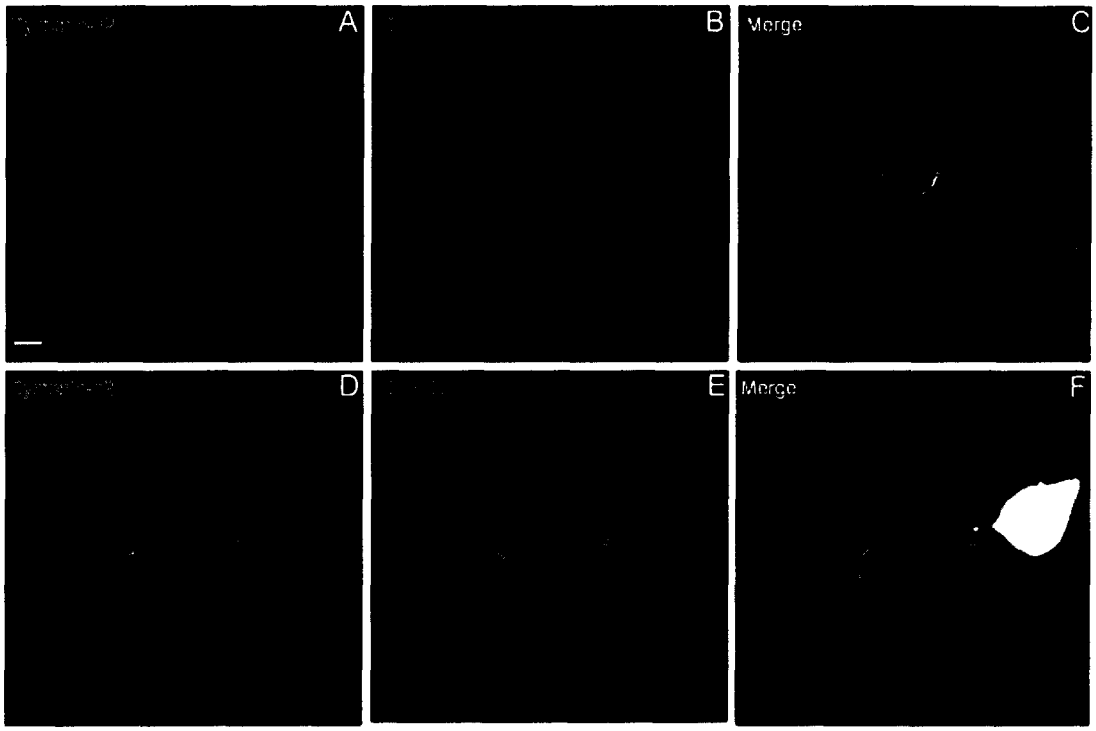

Figure 10. Endogenous MAP1B and endogenous dystonin-a isoform 2 (dystonin-a2) localization in F11 cells.
Endogenous dystonin isoform 2 was visualized in differentiated F11 cells using dystonin isoform 2 antibody (Young et al., 2003). A-C. Confocal micrographs showing strong co-localization of endogenous dystonin-a2 and endogenous MAP1B in the perinuclear region of differentiated F11 cells. A polarized staining pattern is observed along one side of the nucleus for both dystonin-a2 and MAP1B. D-F. High exposure confocal micrographs demonstrating co-localization of endogenous dystonin-a2 and endogenous MAP1B along the neurite of a differentiated F11 cell as indicated by the arrows. Scale bar: 5 uM scale bar indicated in panel A is applicable to panels B-F as well.

region. YFP signal was detected in 15% of the total cells observed (~50,000 cells per well in a 12-well plate). Strong perinuclear co-localization of the YFP-mini-a2 signal with endogenous MAP1B was observed. As endogenous MAP1B has been shown to strongly associate with MTs, the overlapping pattern of YFP-mini-a2 with MAP1B is believed to be along the MT network throughout the cell body of the transfected cell. This pattern of perinuclear and cytoplasmic localization was found to be representative of 40% of the transfected cells, while the remaining transfected cells exhibited very little endogenous MAP1B expression (Figure 11). These results were reproducible as the experiment was carried out in triplicate.

MAP1B associates with dystonin-a2 through proximity ligation assay

A proximity ligation assay was also used to determine whether dystonin-a2 and MAP1B associate with each other *in situ.* To determine the efficacy of this assay, it was performed on a myc-tagged dystonin isoform 2 unique N-terminal region (N2myc) construct and a green-fluorescent-protein-tagged Nesprin 3α (GFPNes3α) construct. Young and Kothary (2008) have characterized this interaction at the nuclear envelope in transiently transfected Cos-1 cells. Figure 12 (A-C) indicates signal detection in some of the GFPNes3α transiently transfected Cos-1 cells. This would be expected as not all of the GFPNes3α positive cells would be transfected with N2myc as well. Young and Kothary (2008) also found that green-fluorescent-protein-tagged Nesprin 3β (GFPNes3β) and N2myc were not associated partners. Supporting this notion, the proximity ligation assay did not detect any signal in these transiently transfected Cos-1 cells (Figure 12D and E). When the proximity ligation assay was performed on endogenous MAP1B and

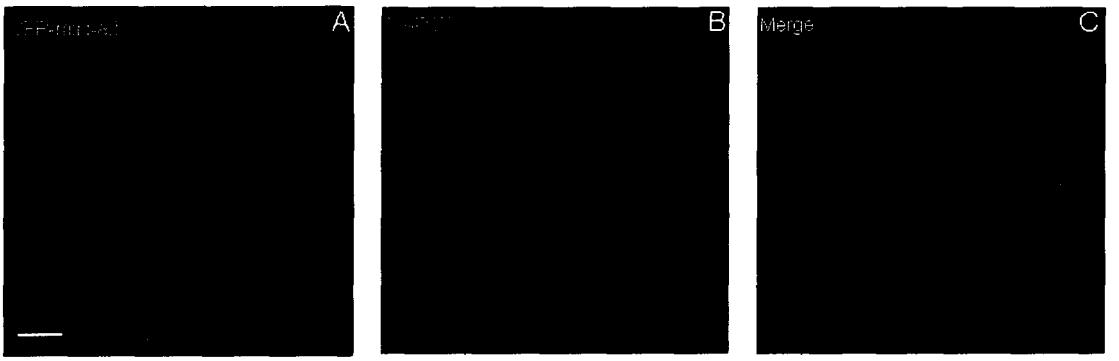

Figure 11. MAP1B and dystonin-a2 expression in PC12 cells.
YFP-tagged-mini-dystonin-a2 (YFP-mini-a2) construct generated by Dr. Kevin Young encoding the structural components of the full-length dystonin-a2 with the spectrin repeat region shortened and YFP-tagged at the C-terminal end was transfected into PC12 cells, which were differentiated for 72 hours. **A-C.** Confocal micrographs demonstrating the expression and co-localization of endogenous MAP1B and YFP-mini-a2 in transfected PC12 cells, which were differentiated for 72 hours post-transfection. The co-localization pattern occurred along the perinuclear region and extended along what appears to be the MT network throughout the cell body in 40% of the transfected cells. The remaining transfected cells demonstrated minimal endogenous MAP1B expression, most likely a result of the transfection itself. Nuclei have been marked with DAPI nuclear stain and are visualized in blue. Scale bar: 5 uM scale bar indicated in panel A is applicable to panels B and C as well.

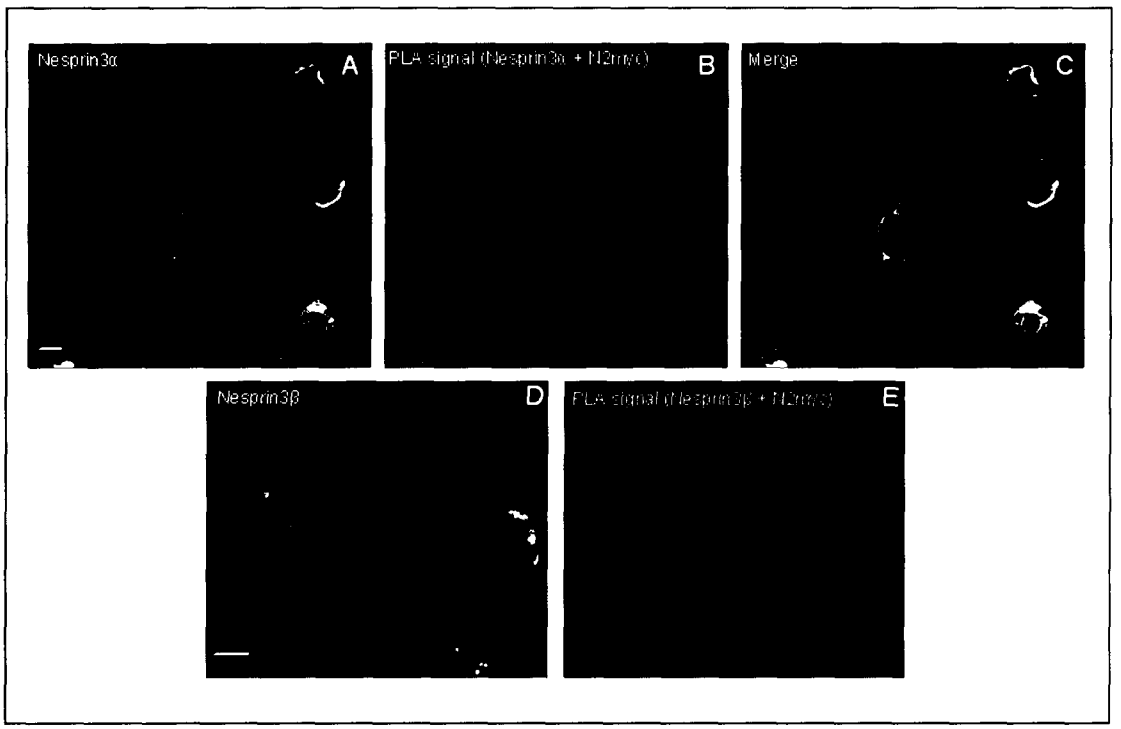

Figure 12. Proximity ligation assay control experiment.
A-C. Proximity ligation assay was performed on Cos-1 cells transfected with GFP epitope tagged Nesprin 3α (Nesprin3α) and Myc-epitope tagged dystonin N-terminal end (N2myc). N2myc and Nesprin3α have been previously shown to interact in transiently double-transfected Cos-1 cells (Young and Kothary, 2008) and therefore serve as a positive control for the proximity ligation assay (PLA) approach. GFP signal was detected in Nesprin3α transfected cells. PLA (Red) was detected in approximately 30% of the Nesprin3α transfected cells as only those Cos-1 cells that were successfully double-transfected with Nesprin3α and N2myc would produce a positive signal. **D and E.** PLA signal was not detected above background in Cos-1 cells transfected with both GFP epitope tagged Nesprin 3β (Nesprin3β) and N2myc. As Nesprin 3β and N2myc do not interact (Young and Kothary, 2008), this experiment serves as a negative control. Scale bars: 10 μm scale bar indicated in panel A is applicable to panels B and C as well. 10 μm scale bar indicated in panel D is applicable to panel E.

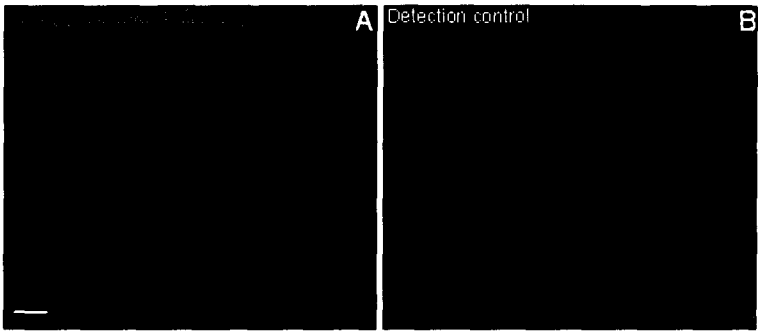

Figure 13. Proximity ligation detection between dystonin-a2 and MAP1B.
A. Positive signal was observed when protein specific probes for dystonin-a2 and MAP1B were applied to differentiated F11 cells, indicating that these proteins are in close proximity to each other *in situ.* **B.** Very little background staining was observed when detection was performed without the application of the protein probes. Scale bar: 5μm scale bar indicated in panel is applicable to panel B as well.

endogenous dystonin-a2 in differentiated F11 cells, a signal was detected, indicating that these proteins were within 40 nm of each other within the cell and therefore may be associated (Figure 13A). Controls showed minimal background signal (Figure 13B). This experiment was duplicated to ensure consistent signal detection.

MAP1B expression in vivo

In an effort to determine if there was any evidence that MAP1B expression was altered in *dt* mice as a result of its interaction with dystonin-a, an examination of MAP1B expression *in vivo* was performed. Figure 14 depicts a comparison of whole-brain MAP1B expression between phenotype stage (post-natal day14) $dt^{27J}$and age-matched wild-type control mice. Total MAP1B protein level was unaltered in the dt^{27J} mice. However, levels of phosphorylated MAP1B, measured by immunoblotting for SMI31 (Johnstone et al., 1997), were elevated in whole-brain lysate from phenotype stage (post-natal day14) dt^{27J}mice when compared to age-matched wild-type control animals (Figure 14). As elevated levels of phorsphorylated MAPs have been shown to play a role in several neurodegenerative diseases, this result provides possible insight into the progression of the *dt* pathology. Levels of phosphorylated GSK3β were also examined to determine whether the increase in phosphorylated MAP1B was due to an intrinsic regulation anomaly or the result of increased upstream activator. We observed no change in phosphorylated GSK3β levels.

Validation of clathrin heavy chain and dystonin-a interaction

Clathrin heavy chain co-immunoprecipitates with plakin domain of dystonin-a

The NtermLong, PlakinCH1 and Daxx constructs used for the MAP1B co-immunoprecipitation experiments were also used to perform clathrin heavy chain co-

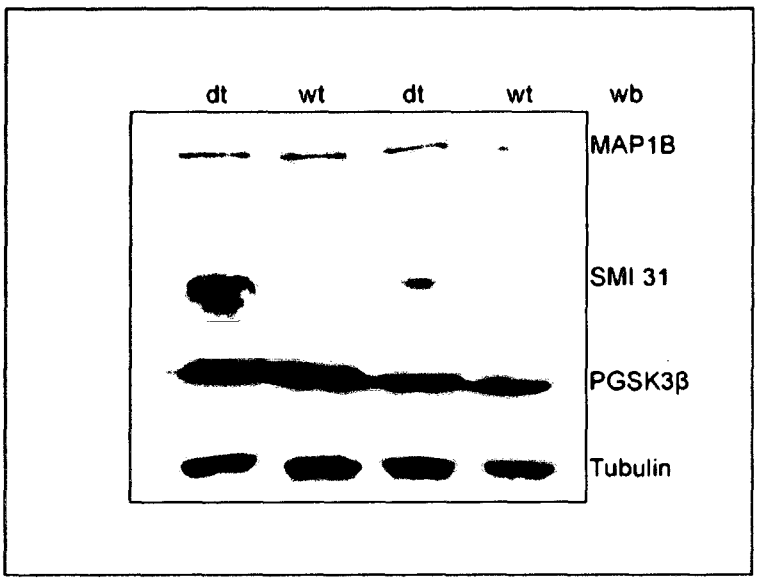

Figure 14. Western blot analysis of MAP1B and phosphorylated MAP1B protein levels *in vivo.*

MAP1B and phosphorylated MAP1B (SMI31) level was examined in whole-brain lysate from phenotype stage dt^{27J} and age-matched wild-type control mice. MAP1B expression was unaltered in phenotype stage dt^{27J} mice when compared to age-matched wild-type controls. SMI31, which is used as a marker for phosphorylated MAP1B expression, showed an elevated signal in phenotype stage (post-natal day 14) dt^{27J} mice. Phosphorylated GSKβ (PGSKβ) was also examined to determine if upstream regulation of MAP1B phosphorylation is also affected. β-tubulin (Tubulin) was used as a loading control. Blots were stripped and re-probed when necessary.

immunoprecipitation analysis. Clathrin heavy chain co-immunoprecipitated with NtermLong and PlakinCH1 but not with Daxx when using lysate from transiently transfected and differentiated PC12 cells (Figure 15B). Similarly, immunoprecipitation reactions performed on lysate from transiently transfected Cos-1 cells showed clathrin heavy chain co-immunoprecipitated with NtermLong but not with Daxx (Figure 15E). The validity of this is supported by the fact that despite comparatively higher levels of Daxx, clathrin heavy chain co-immunoprecipitated only with the plakin fusion proteins. Anti-flag immunoblot detected the flag epitope in the lysates from transiently transfected PC12 and Cos-1 cells. This indicates the successful expression and binding of the fusion constructs to the dynal magnetic protein G beads used for the immunoprecipitation reactions (Figure 15C and F). Clathrin heavy chain was successfully detected in the input lysate used for the immunoprecipitation reactions, ensuring its endogenous expression in the cell lines selected for the analyses (Figure 15D and G). The results depicted in Figure 15 indicate that the plakin domain of dystonin can interact with clathrin heavy chain in both neuronal and non-neuronal cells. The complete lack of clathrin heavy chain signal detection in the negative immunoprecipitation control as well as the ability of the plakin fusions to immunoprecipitate clathrin heavy chain in multiple cell types is indicative of the veracity of the interaction. Reciprocal immunoprecipitation reactions were attempted, however, plakin fusion constructs were unable to co-immunoprecipitate with clathrin heavy chain. Interestingly, these immunoprecipitation reactions were also unable to immunoprecipitate clathrin heavy chain itself. Unfortunately, according to the manufacturer, the clathrin heavy chain antibody used for these reciprocal immunoprecipitation reactions was not intended for this application, and as such its

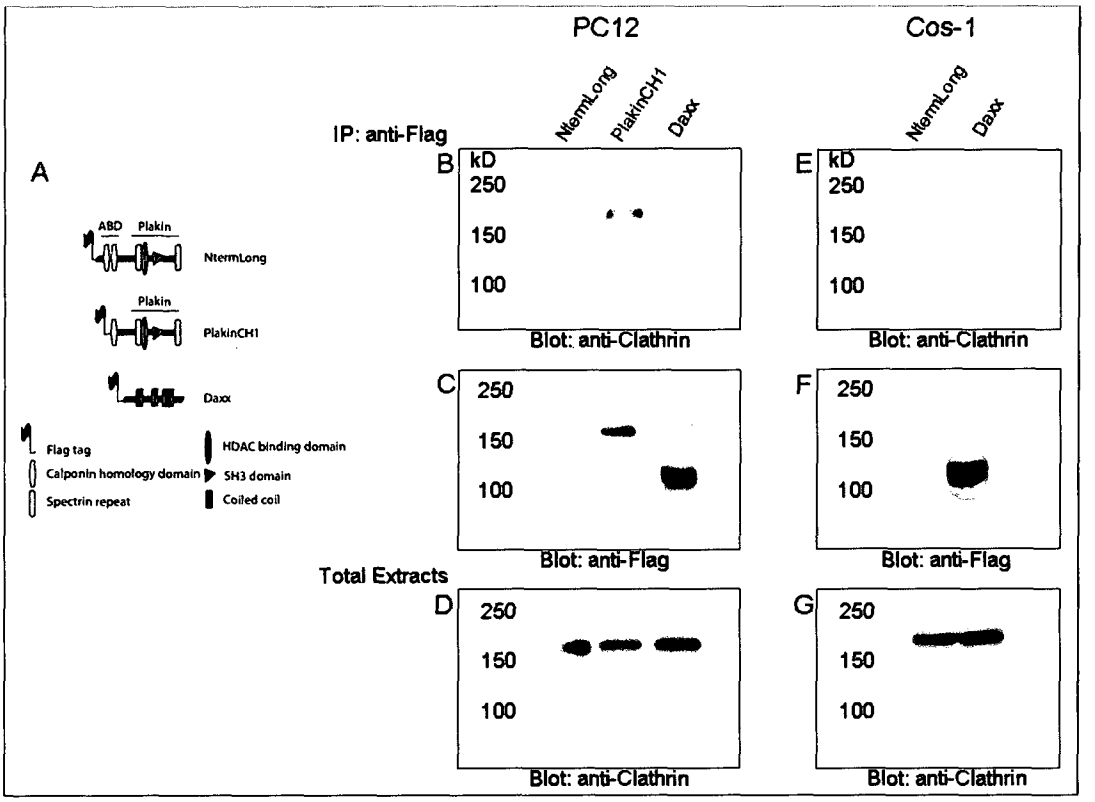

Figure 15. Clathrin heavy chain interacts with dystonin plakin domain. Co-immunoprecipitation of endogenous clathrin heavy chain (Clathrin) with flag epitope-tagged plakin fusion constructs from transiently transfected and differentiated PC12 cells as well as transiently transfected Cos-1 cells. **A.** Schematic diagrams of flag-tagged fusion constructs used for immunoprecipitation reactions are shown. Flag-tagged plakin domain with N-terminal region is referred to as NtermLong. Flag-tagged plakin domain with one calponin homology repeat is called PlakinCH1. A flag-tagged death associated protein construct called Daxx served as negative control. **B.** Immunoblot of clathrin following PAGE on eluates from immunoprecipitation reactions. Lysate from flag-fusion transiently transfected and differentiated PC12 cells was immunoblotted to detect for the successful co-immunoprecipitation of clathrin. Clathrin was successfully detected in lanes immunoprecipitated for flag from lysate containing NtermLong and PlakinCH1. Clathrin was not co-immunoprecipitated with Daxx. **C.** Anti-flag immunoblot of lysate from PC12 cells transiently transfected with the flag-tagged mammalian expression constructs shown in panel A and differentiated for 72 hours post-transfection. Detection of flag indicates successful transfection and expression of the fusion constructs. NtermLong was detected at 171 kD, PlakinCH1 was detected at 144 kD and Daxx was blotted at 110 kD. **D.** Immunoblot of clathrin demonstrated its endogenous expression within the lysate from PC12 cells used for the co-immunoprecipitation reactions. **E-G.** Co-immunoprecipitation of clathrin with NtermLong but not with Daxx when using lysate from transiently transfected Cos-1 cells.
efficacy in this respect could not be guaranteed.

Dystonin-a2 associates with clathrin heavy chain and alters its endogenous localization pattern

Co-immunofluorescence experiments were conducted to further validate the potential interaction of clathrin heavy chain with the plakin domain of dystonin-a. Cos-1 cells were transiently transfected with YFP-mini-a2 and co-immunofluorescence analysis with endogenous clathrin heavy chain was conducted. YFP-mini-a2 was found to transfect approximately 15% of the cells observed (plating density of 40,000 cells) (Figure 16A). Figure 16C depicts strong co-localization of YFP-mini-a2 and endogenous clathrin heavy chain. Over-expression of YFP-mini-a2 in the transfected Cos-1 cells resulted in a significant change in the pattern of endogenous clathrin heavy chain localization. The clathrin heavy chain signal is modified from a diffuse punctate pattern throughout the cell to one localized specifically to the over-expression pattern of YFP-mini-a2, consistent with what appears to be the MT cytoskeleton. This pattern of localization was observed in 40% of the transfected cells observed. The remaining transfected cells were observed to have very low endogenous clathrin heavy chain expression. The results from this co-immunofluorescence analysis were found to be highly reproducible as the experiment was performed in triplicate.

Expression of clathrin heavy chain in vivo

The co-immunoprecipitation and co-immunofluorescence data presented suggests that clathrin heavy chain is a novel binding partner of dystonin-a through its plakin domain. To further explore how this interaction may be having an influence in the *dt* pathology, *in vivo* immunofluorescence analyses were performed. Endogenous clathrin heavy chain

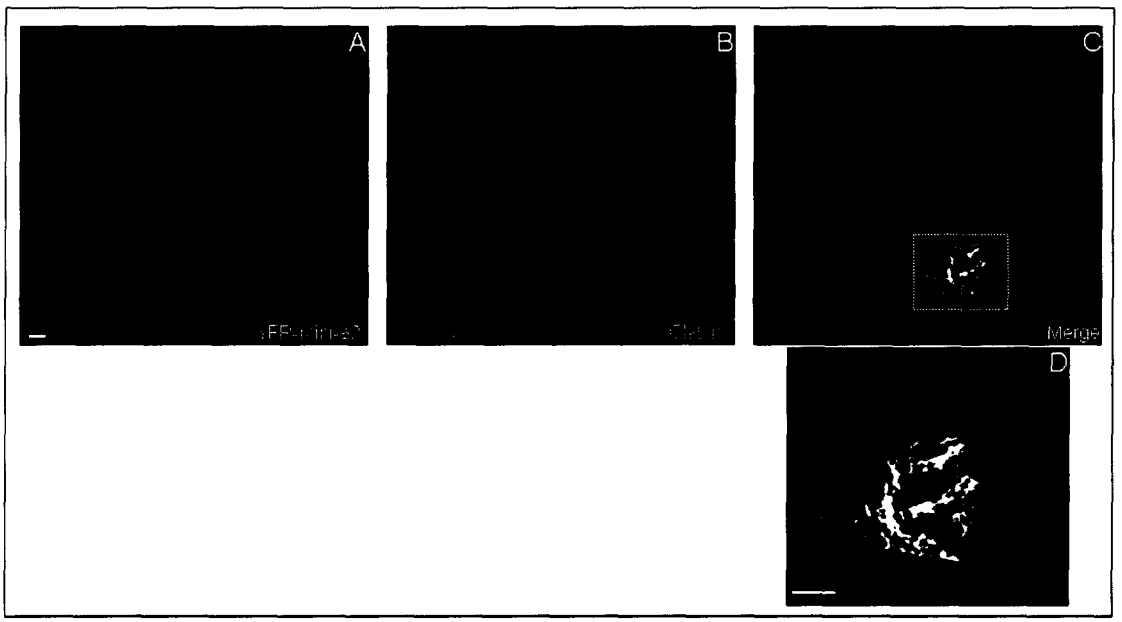

Figure 16. Endogenous clathrin heavy chain (Clathrin) and dystonin-a2 fusion protein expression in Cos-1 cells.
YFP-tagged-mini-dystonin-a2 (YFP-mini-a2) construct generated by Dr. Kevin Young encoding the structural components of the full-length dystonin-a2 with the spectrin repeat region shortened and YFP-tagged at the C-terminal end was transfected into Cos-1 cells. **A-C.** Confocal micrographs demonstrating the expression and co-localization of YFP-mini-a2 (green) and endogenous clathrin (red). In non-transfected cells, endogenous clathrin expression was punctate and diffuse throughout the cell body with some polarized aggregation around the nucleus. However, in YFP-mini-a2 transfected Cos-1 cells, the expression of clathrin was significantly altered. The clathrin signal strongly co-localized with the YFP-mini-a2 signal which appeared to be distributed along the MT cytoskeleton. **D.** Magnified merged image shown in panel C demonstrating robust co-distribution of transfected YFP-mini-a2 and clathrin in Cos-1 cells. Nuclei have been marked with DAPI nuclear stain and are visualized in blue. Scale bar: 5 uM scale bar indicated in panel A is applicable to panels B and C as well. 5 uM scale bar indicated in panel D.

expression was analysed *in vivo* using tissue from *dt* mice to identify any overt localization anomalies. Pattern of clathrin heavy chain in DRG cross-sections from phenotype stage (post-natal day 14) dt^{27J} mice and wild-type mice have been compared and contrasted and are depicted in Figure 17.

Clathrin heavy chain has partial localization with dystonin-b in C2C12 cells

As clathrin heavy chain is not found exclusively in nervous tissue, its localization with the muscle isoform of dystonin, dystonin-b, was also explored. For this purpose, the dystonin-b antibody was generated and characterized (Appendix I). Immunofluorescence analysis of endogenous clathrin heavy chain and endogenous dystonin-b in C2C12 myoblasts was performed. In approximately 25% of the cells, partial co-localization of the dystonin-b and clathrin heavy chain signals was observed (Figure 18A-C). Interestingly, in a majority of the cells, both clathrin heavy chain and dystonin-b aggregated in a polarized manner on one side of the nucleus (Figure 18D and E). The aggregated signal from each protein, however, did not always co-localize (Figure 18F). The aggregated clathrin heavy chain signal was most likely a result of its association with the trans-Golgi network. Characterization of the dystonin-b antibody revealed that it does not associate with the Golgi network (Appendix I).

Validation of myosin IIb interaction with dystonin-a

Myosin IIb co-immunoprecipitates with plakin domain of dystonin-a

Co-immunoprecipitation experiments were conducted in transiently transfected Cos-1 cells. The flag-epitope tagged fusion constructs employed to conduct the MAP1B co-immunoprecipitation analysis were used to perform myosin IIb co-immunoprecipitation

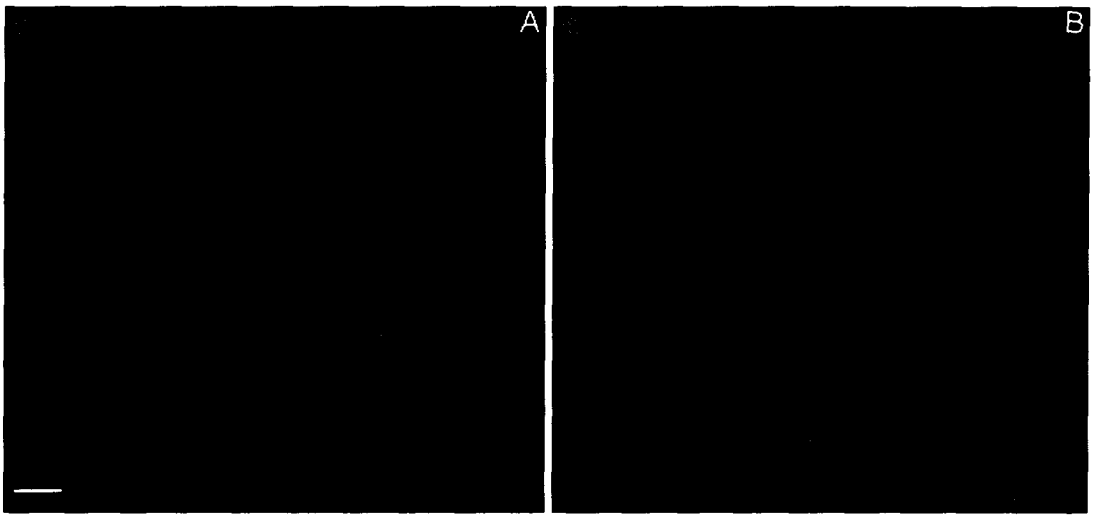

Figure 17. Clathrin heavy chain distribution *in vivo.*
Endogenous clathrin immunofluorescence was performed on dorsal root ganglia (DRG) cross sections from wild-type (wt) and phenotype-stage dt^{27J} (dt) mice. No differences between the two groups were observed. Scale bar: 20 μM scale bar indicated in panel A is applicable to panel B as well.

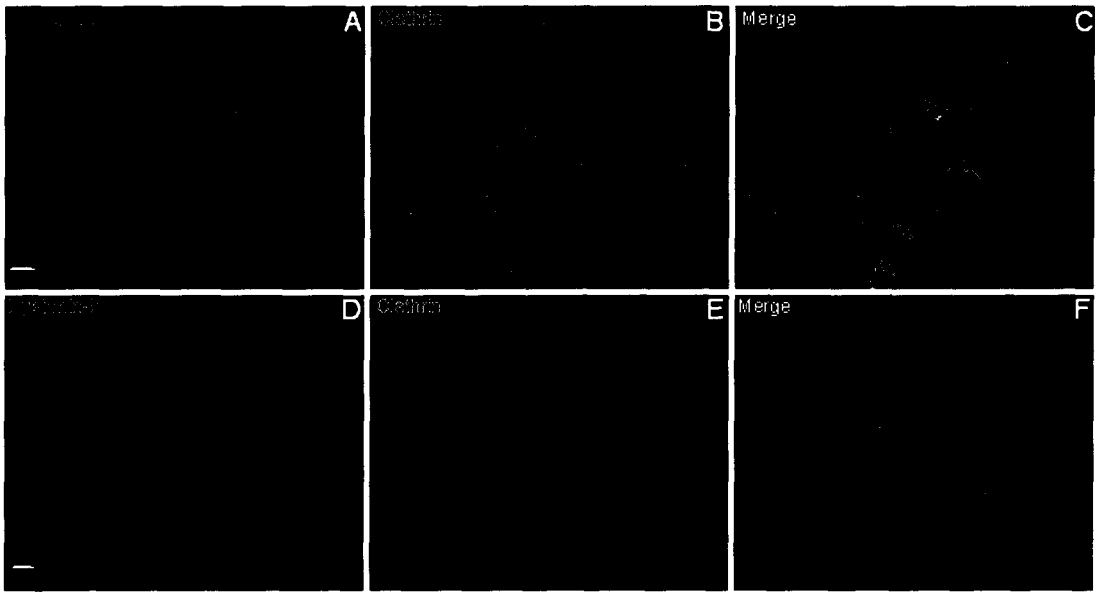

Figure 18. Endogenous dystonin-b and clathrin heavy chain co-immunofluorescence. **A-C.** Co-immunofluorescence of dystonin-b and clathrin heavy chain was performed on C2C12 myoblasts. Dystonin-b aggregated in a polarized manner to one side of the nucleus in addition to discretely spreading throughout the cell body. Partial co-loacalization was observed with clathrin heavy chain in approximately 25% of the cells (red arrows). **D-F.** Polarized aggregation of dystonin-b and clathrin heavy chain was observed around the nucleus in the majority of C2C12 cells with very little co-localization of the signals. Nuclei have been marked with DAPI nuclear stain and are visualized in blue. Scale bar: 5 uM scale bar indicated in panel A is applicable to panels B and C as well. 5 uM scale bar indicated in panel D is applicable to panels E and F.

experiments. Mysoin IIb was detected in the immunoprecipitation reactions using lysates from cells transfected with NtermLong (Figure 19B). Additionally, immunoprecipitation of Daxx did not result in the co-immunoprecipitation of myosin IIb despite the comparatively higher levels of Daxx in the input lysate (Figure 19B). Immunoblotting for flag detected the presence of the flag epitope in the immunoprecipitation eluates for all of the transfected fusion constructs, indicating the successful expression of the flag-tagged fusion proteins (Figure 19C). Figure 19 (D) illustrates the endogenous expression of myosin IIb in the lysate from the transiently transfected Cos-1 cells used as the input for the immunoprecipitation reactions. The co-immunoprecipitation data presented suggests that the plakin domain of dystonin-a is capable of an interaction with myosin IIb.

Myosin IIb does not localize with exogenously expressed dystonin-a2 in Cos-1

To determine if myosin IIb and dystonin-a associated *in situ*, Cos-1 cells were transiently transfected with YFP-mini-a2 and co-immunofluorescence analysis with endogenous myosin IIb was performed. YFP-mini-a2 was found to transfect approximately 15% of the cells observed (plating density of 40,000 cells). Figure 20 demonstrates that the YFP-mini-a2 signal did not co-localize with the endogenous myosin IIb staining pattern which was observed along the actin cytoskeleton. Over-expression of the YFP-mini-a2 construct led to a perturbation in the actin cytoskeleton and as a result also disrupted the normal localization pattern of myosin IIb (Figure 20D-F). The pattern of staining observed was found to be representative of nearly all of the transfected cells. Evidence from the co-immunoprecipitation experiment suggests that myosin IIb likely interacts with dystonin through its plakin domain; however, co-immunofluorescence observations indicate that this interaction in not likely with the

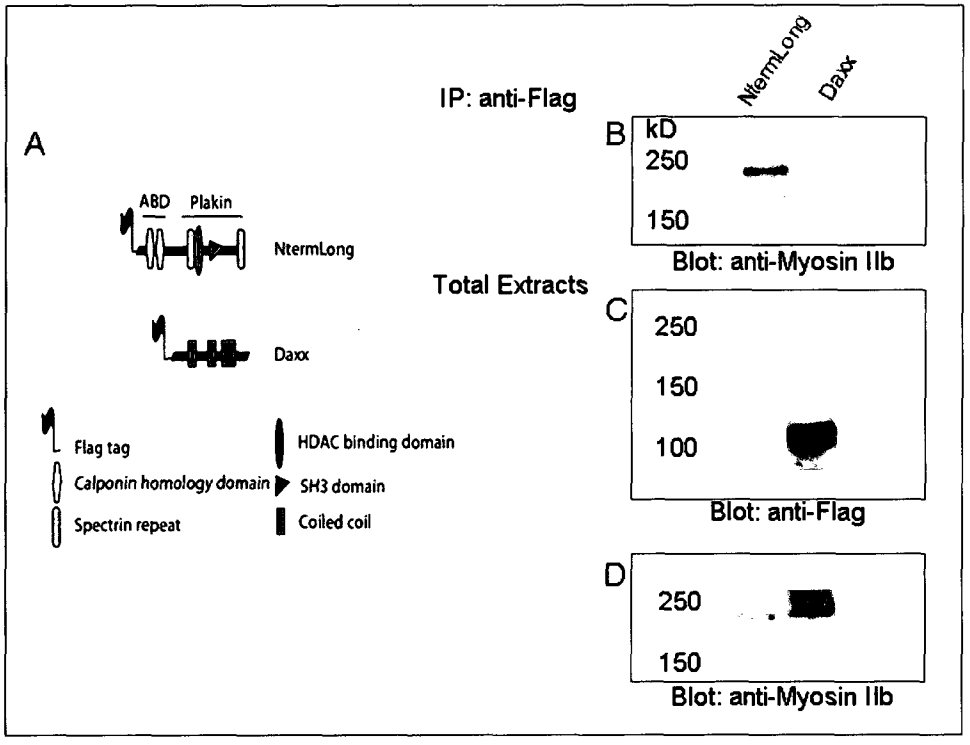

Figure 19. Myosin IIb interacts with plakin domain of dystonin.
Co-immunoprecipitation of endogenous myosin IIb with flag epitope-tagged plakin fusion constructs from transiently transfected Cos-1 cells. **A.** Schematics of flag-tagged fusion constructs used for immunoprecipitation reactions are shown. Flag-tagged plakin domain with N-terminal region is referred to as NtermLong. As a negative control for the co-immunoprecipitation assay, a flag-tagged Daxx construct was used. **B.** Immunoblot of myosin IIb following PAGE on eluates from immunoprecipitation reactions using lysate expressing flag-fusion constructs and containing endogenous myosin IIb from transiently transfected Cos-1 cells. Myosin IIb was detected in eluate which was immunoprecipitated for flag from lysate containing NtermLong from transiently transfected Cos-1 cells. Myosin IIb was not co-immunoprecipitated with Daxx. **C.** Anti-flag immunoblot of lysate from Cos-1 cells transiently transfected with the flag-tagged mammalian expression constructs shown in panel A. Detection of flag indicates successful transfection and expression of the fusion constructs. NtermLong was detected at 171 kD while Daxx was blotted at 110 kD. **D.** Immunoblot of myosin IIb demonstrates its endogenous expression within the lysate from the transiently transfected Cos-1 cells used for the co-immunoprecipitation reactions.

dystonin-a2 isoform. Further investigation will be required to determine which isoform of dystonin acts as a target for this non-muscle motor protein.

Validation of CRMP2 interaction with dystonin-a

CRMP2 does not co-immunoprecipitate with dystonin-a plakin domain

Co-immunoprecipitation experiments were conducted in transiently transfected and differentiated PC12 cells. The flag-epitope tagged fusion constructs employed to conduct the MAP1B co-immunoprecipitation analysis were also used for CRMP2 co-immunoprecipitation experiments. CRMP2 was not detected in the immunoprecipitation reactions using lysate from cells transfected with the flag-fusion constructs (Figure 21B). Immunoblotting for flag detected the presence of the flag epitope in the immunoprecipitation eluates from the lysate of cells transiently transfected with the fusion constructs.

The flag detection indicated successful expression and binding of the flag-tag fusion proteins to the dynal magnetic protein-G beads used for the reaction (Figure 21C). Figure 21 (D) illustrates the endogenous expression of CRMP2 in the lysate from the transiently transfected PC12 cells used as the input for the immunoprecipitation reactions. It is possible that CRMP2's potential interaction with dystonin is transient and mediated through post-translational modifications that may have been lost during the immunoprecipitation assay. MAP1B has been demonstrated to interact with CRMP2 primed through the semaphorin3A pathway and the activity of GSK-3β and JNK (Good et al., 2004).

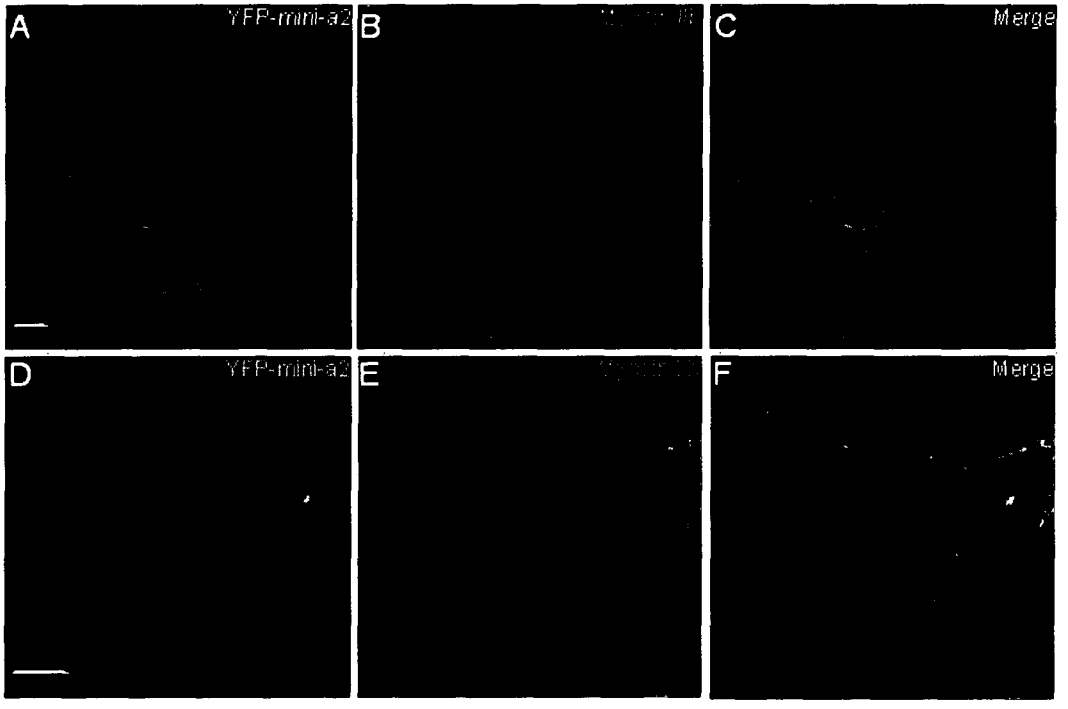

Figure 20. Endogenous myosin IIb and exogenous dystonin-a2 co-immunofluorescence in Cos-1 cells.
YFP-tagged-mini-dystonin-a2 (YFP-mini-a2) construct generated by Dr. Kevin Young encoding the structural components of full-length dystonin-a2 with the spectrin repeat region shortened and YFP-tagged at the C-terminal end was transfected into Cos-1 cells. **A-C.** Confocal micrographs demonstrating the expression of YFP-mini-a2 (green) and endogenous myosin IIb (red). No apparent co-localization of myosin IIb with YFP-mini-a2 was observed. **D-F.** Confocal micrographs demonstrating the expression of YFP-mini-a2 and endogenous myosin IIb. Cos-1 cells transfected with YFP-mini-a2 construct demonstrate aberrant endogenous myosin IIb localization patterns. Myosin IIb is no longer detected along the actin stress fibres in YFP-mini-a2 transfected cells, indicating a possible disruption of the actin cytoskeleton in these cells (panesl B and E). Nuclei have been marked with DAPI nuclear stain and are visualized in blue. Scale bar: 10 uM scale bar indicated in panel A is applicable to panels B and C as well. 10 uM scale bar indicated in panel D is applicable to panels E and F.

Dystonin-a2 localizes with CRMP2 and alters its localization in PC12 cells

PC12 cells were transfected with YFP-mini-a2 and differentiated preceding co-immunofluorescence analysis with endogenous CRMP2. YFP-mini-a2 was found to transfect approximately 10% of the cells observed (plating density of 35,000 cells). Figure 22 (C) depicts the co-localization of YFP-mini-a2 and endogenous CRMP2. Interestingly, the endogenous CRMP2 localization pattern was found to be altered in transfected PC12 cells. CRMP2 was no longer observed to be distributed evenly throughout the cell body; rather, it localized discretely with the YFP-mini-a2 signal. This pattern of immunofluorescence was representative of approximately 25% of the transfected cells. YFP-mini-a2 transfected PC12 cells also presented an aggregated YFP signal around the nucleus in 20% of the cells which was not shared by CRMP2 expression. The remaining transfected cells exhibited extremely low endogenous CRMP2 staining.

A summary of all of the validation experiments conducted for the novel interacting partners of the dystonin-a plakin domain have been presented in Table IV.

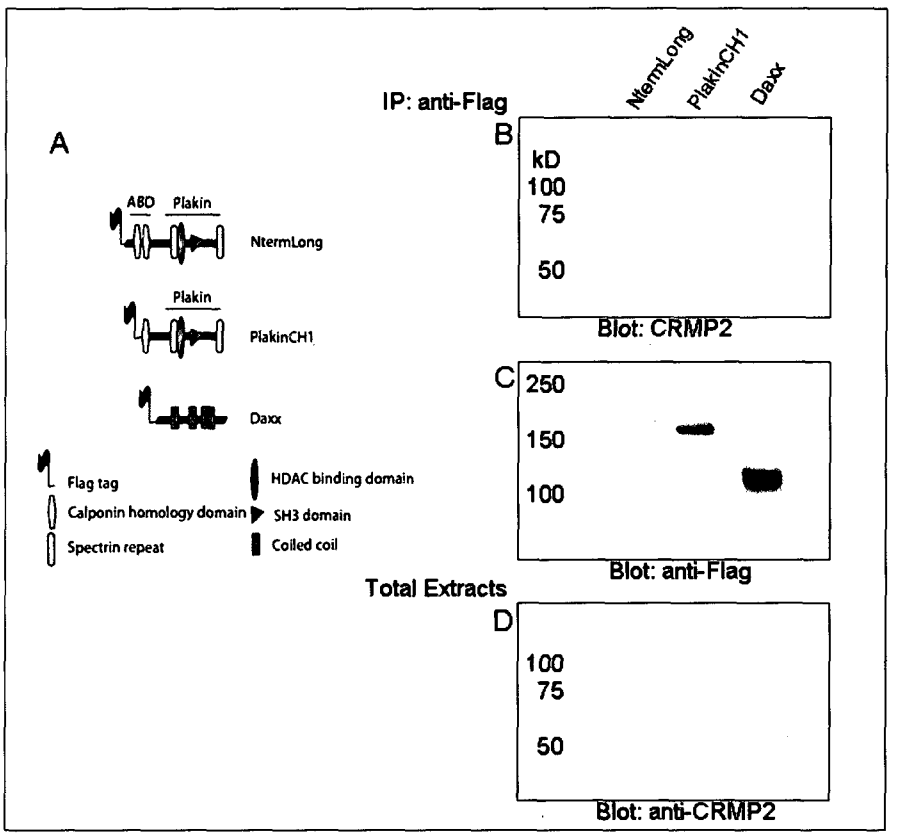

Figure 21. CRMP2 does not Co-immunoprecipitate with plakin domain of dystonin. Co-immunoprecipitation of endogenous CRMP2 with flag-tagged plakin fusion constructs from lysate of transiently transfected and differentiated PC12 cells. **A.** Schematics of flag-tagged fusion constructs used for immunoprecipitation reactions are shown. Flag-tagged plakin domain with N-terminal region is referred to as NtermLong. Flag-tagged plakin domain with one calponin homology repeat is named PlakinCH1. As a negative control for the co-immunoprecipitation assay, a flag-tagged Daxx construct was used. **B.** Immunoblot of CRMP2 following PAGE on eluates from immunoprecipitation reactions using lysate from PC12 cells transiently transfected with flag-fusion constructs, differentiated and, containing endogenous CRMP2. CRMP2 was not detected in any lanes containing eluates from the immunoprecipitation reactions of the flag-fusion constructs. **C.** Anti-flag immunoblot of lysate from PC12 cells transiently transfected with the flag-tagged mammalian expression constructs shown in panel A and differentiated for 72 hours post-transfection. Detection of flag indicates successful transfection and expression of the fusion constructs. NtermLong was detected at 171 kD, PlakinCH1 was detected at 144 kD and Daxx was blotted at 110 kD. **D.** Immunoblot of CRMP2 demonstrates its endogenous expression within the lysate used for the co-immunoprecipitation reactions from the transiently transfected and differentiated PC12 cells.

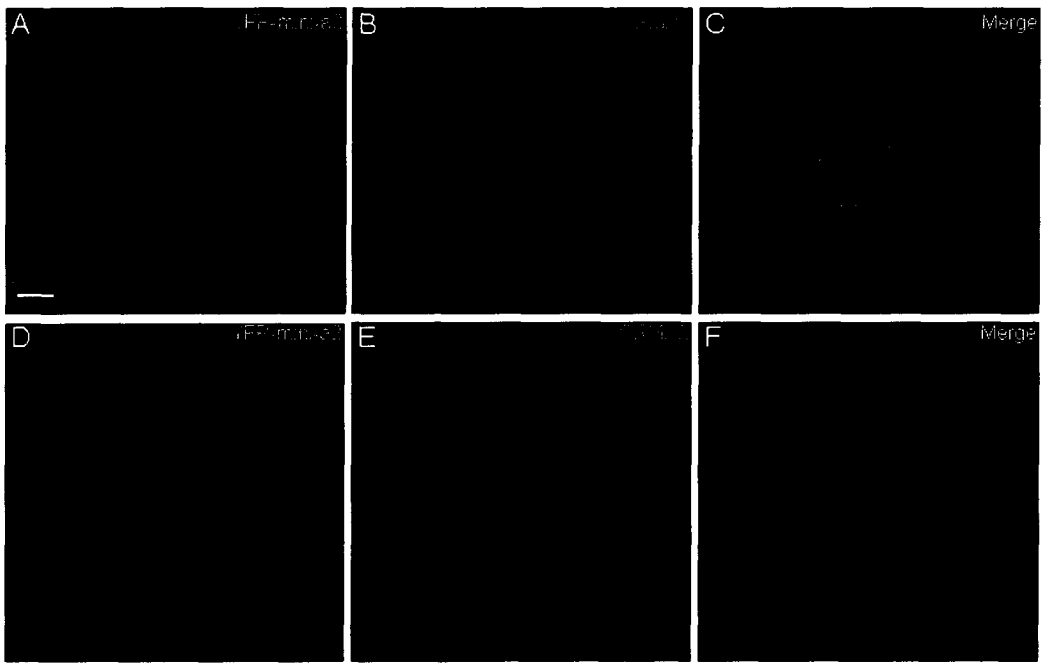

Figure 22. CRMP2 and dystonin-a2 expression in PC12 cells.
YFP-tagged-mini-dystonin-a2 (YFP-mini-a2) construct generated by Dr. Kevin Young encoding the structural components of the full-length dystonin-a2 with the spectrin repeat region shortened and YFP-tagged at the C-terminal end was transfected into PC12 cells, which were differentiated for 72 hours. **A-C.** Confocal micrographs demonstrating the expression and co-localization of endogenous CRMP2 and YFP-mini-a2 in transfected PC12 cells which were differentiated for 72 hours post-transfection. The co-localization pattern was found to occur throughout the cell body in 25% of the transfected cells. YFP-mini-a2 was also found to aggregate around the nucleus without CRMP2 in approximately 20% of the transfected cells. **D-F.** In approximately 25% of the PC12 cells transfected with YFP-mini-a2, endogenous CRMP2 expression was found to deviate from normal. CRMP2 was found to associate with YFP-mini-a2 in the perinuclear region as well as quite discretely throughout the cell. Nuclei have been marked with DAPI nuclear stain and are visualized in blue. Scale bar: 5 uM scale bar indicated in panel A is applicable to panels B-F as well.

Table IV. Summary of validation experiments

Validation / Interactor	Co-immunoprecipitation								Immunofluorescence Co-localization				Proximity ligation assay with exogenous dystonin isoform 3
	Normal IgG	Dystonin CH1	Flag/HA	Dys	Normal IgG	Dystonin CH1	Flag/HA	Dys	Normal IgG	Dystonin CH1	Flag/HA	Dys	Endogenous Dystonin-3	Transient Dystonin-3			
	F11				PC12				Cos-1				F11	F11	PC12	Cos-1	F11
MAP1B	√	√	√	X									√		√		√
Clathrin					√	√		X	√			X	N/A			√	N/A
Myosin IIb									√			X	N/A			X	N/A
CRMP2					X	X		X					N/A		√		N/A

√ = Positive; X = Negative; N/A = Not applicable due to reagant constraints

Discussion

The multi-domain structure of dystonin isoforms allow for their participation in numerous cell-type specific interactions. Previous characterization of the non-epithelial dystonin proteins has focussed on the alternatively spliced N-terminal ABD and the C-terminal MTBD. Interactions of the family-defining plakin domain of these proteins, however, have not been explored in detail. The purpose of the present study was to identify novel interacting partners of the plakin domain of the neuronal isoform of dystonin. To this end, pull-down interaction analyses were performed and several candidate interacting partners were identified. The legitimacy of the candidates was validated through co-immunoprecipitation, co-immunofluorescence and proximity ligation assays. MAP1B was one such candidate that demonstrated a strong interaction with neuronal dystonin. CRMP2 and myosin IIb were also identified as potential binding partners of the plakin domain of dystonin-a. These identified partner proteins show associations with components of the cytoskeleton, further supporting dystonin's role as a cytoskeletal linker protein. Additionally, the identification and validation of a strong interaction with clathrin heavy chain, the major component of the clathrin triskelion involved in intracellular transport and endocytosis, has raised possibilities for new, previously undiscovered roles for the dystonin protein.

Dystonin neuronal isoform-2 interacts with MAP1B

Dystonin and MAP1B

MAP1B is a major cytoskeletal protein and is necessary for neurite outgrowth. MAP1B has also been referred to as MAP1.2, MAP5 and MAP1x in the literature by several independent studies since its discovery (Greene et al., 1983; Bloom et al., 1985a, b;

Riederer et al., 1986). It is the earliest MAP expressed in the embryonic brain, found abundantly in developing axons (Matus and Riederer, 1986; Tucker et al., 1989). MAP1B is essential for neuritogenesis both in *in vivo* and *in vitro* model systems (Gonzalez-Billault et al., 2002a). As it is one of the earliest MAPs observed in the developing nervous system, its role in differentiation, growth of neuronal processes and MT assembly is imperative to normal development (Riederer et al., 1986; Brugg and Matus, 1988; Tucker et al., 1988; Pedrotti and Islam, 1995). Along with Tau and MAP2, MAP1B exhibits a synergistic role in neurite outgrowth. It is also essential for growth cone directionality and modulation of MT stability through its phosphorylation (Brugg and Matus, 1988; Mansfield et al., 1991; Mack et al., 2000; Takei et al., 2000; Garcia and Cleveland, 2001; Gonzalez-Billault et al., 2002b). Thus, MAP1B is an essential component of the cytoskeleton and is necessary for its proper functioning and regulation. However, for the cytoskeleton to function properly, regulation of MAP1B itself is also necessary. It is possible that such regulation of MAP1B is achieved by means of a cytolinker protein such as dystonin. The evidence presented in Figures 7-11 and 13 indicate that MAP1B interacts with dystonin-a through its plakin domain. The plakin region selected for the interaction analysis contains a putative SH3 domain, which demonstrates affinity for proline-rich peptide sequences (Li, 2005). As other MAP families (MAP2/Tau) possess proline rich peptide sequences, it is likely that a proline-rich region in MAP1B binds to dystonin through its SH3 domain.

The physiological functions of MAP1B

The importance of MAP1B is highlighted by the conditions that arise as a result of its aberrant function or absence. Although at times lethal (Gonzalez-Billault et al., 2000),

MAP1B null mice are able to survive, albeit with a delay in nervous system development (Takei et al., 1997), slower axonal growth rates, abnormal motor control, as well as morphological changes in Purkinje cells, olfactory bulb, and retina (Edelmann et al., 1996). These mice also possess poor axonal guidance in the peripheral nervous system. They also demonstrate the absence of a corpus callosum, accompanied by a reduction in large myelinated axons and improperly guided myelinated fibre bundles (Meixner et al., 2000). Interestingly, similar abnormalities in peripheral nervous system myelination have been observed in *dt* mice (Bernier et al., 1998). Some abnormalities of MAP1B can be compensated for by its redundancy with Tau and MAP2; thus, the full extent of the MAP1B loss in these animals cannot be entirely gauged (DiTella et al., 1996; Takei et al., 2000; Garcia and Cleveland, 2001; Bouquet et al., 2004). It is however clear that MAP1B is involved in a host of cellular processes necessary for proper functioning.

Phosphorylation and MAP1B activity

The phosphorylation of MAP1B is an essential post-translational modification that modulates its function and contributes to its diversity. Two types of MAP1B phosphorylations have been identified: Proline-dependant kinase or mode I, and casein kinase II or mode II (Riederer et al., 1990; Ulloa et al., 1994; Riederer, 1995; Ramon-Cueto and Avila, 1999; Mack et al., 2000). The phosphorylation of MAP1B through GSK3β and JNK has been examined. Interestingly, JNK1 null mice manifest with progressive loss of MTs in axons and dendrites, disruptions in the anterior commissure, and hyper-phosphorylation of MAP2 and MAP1B (Bush and Gordon-Weeks, 1994). GSK3β phosphorylation events are part of a larger signalling cascade involving semaphorins, amongst several other upstream regulators (Zhou and Snider, 2005). As

would be expected of such an integral protein, the aberrant functioning of MAP1B has been implicated in the manifestation of several neurodegenerative diseases. In addition to its role in giant axonal neuropathy and tuberous sclerosis (Yamanouchi et al., 1997; Ding et al., 2002), MAP1B (along with Tau) is proposed to contribute to early hippocampal neuropathy in Alzheimer's patients through its phosphorylation and potentially hyper-phosphorylation (Good et al., 2004).

MAP1B in dt mice

After the interaction between dystonin-a and MAP1B was validated, it was necessary to explore whether there was any evidence of anomalous MAP1B in *dt* mice. Levels of MAP1B in brain tissue from phenotype stage dt^{27J} mice were compared to age-matched wild-type controls. No difference was observed in the levels of MAP1B between these two groups (Figure 14). However, when phosphorylated MAP1B levels were compared amongst these groups using the SMI31 neurofilament antibody, which detects MAP1B phosphorylated by GSK3β (Johnstone et al., 1997), elevated levels were detected in the brains of dt^{27J} mice (Figure 14). Upon further investigation, no differences were observed in the levels of phosphorylated GSK3β between the brain tissue samples of the wild-type and *dt* mice at phenotype stage (Figure 14). Thus, the abnormal levels of phosphorylated MAP1B observed are not a result of anomalies in GSK3β regulation. An increase in phosphorylated MAP1B levels does raise the possibility that it may play a role in the neurodegeneration observed in *dt* mice. However, an analysis of protein levels from nervous tissue of *dt* mice pre-phenotype would be necessary to determine whether the elevated levels are a primary pathology of the condition, or a secondary characteristic resulting from the progression of the disease.

A possible mechanism for pathology

In light of the evidence presented, an understanding of the functional relevance of the MAP1B interaction with dystonin is essential. As mentioned above, regulation of MAP1B phosphorylation is necessary for it to carry out its functions. It may be possible that such regulation be provided through MAP1B's interaction with dystonin. Additionally, as a sensory neuropathy of the DRG is a hallmark of the *dt* pathology, it is interesting that DRGs are the only tissue that express MAP1B at relatively high levels after MAP1B's expression has significantly decreased in all other tissue (Ma et al., 1997). It is tempting to postulate that dystonin may act as a scaffolding protein for MAP1B, especially in DRGs, allowing for its post-translational modifications and facilitating its interactions with other substrates. As such, a deficiency in dystonin may result in the loss of MAP1B regulation resulting in the misregulation of its phosphorylation and contribute to the neuropathy observed.

Future directions for the dystonin-a and MAP1B interaction

To elucidate the functional relevance of this interaction, several avenues of analysis must be pursued. It will be necessary to determine whether there is altered expression and localization of MAP1B in *dt* mice. For this effort, primary DRGs harvested from *dt* and wild-type mice should be cultured, and localization and expression comparisons of MAP1B made. In addition, tyrosinated, detyrosinated and acetylated MTs should also be analyzed to determine whether there is any alteration in the stability of the MTs in *dt* mice. An increase in tyrosinated MTs (stabilized MTs) could suggest an increase in overall MAP1B activity (Goold et al., 1999). To further understand how dystonin may play a role in MT dynamics through its interaction with MAP1B, nocodazole treatment

could be performed. If the plakin domain of dystonin sequesters MAP1B the MTs in the DRGs from *dt* mice should be resistant to nocodazole depolymerization. Further, morphological analysis of DRGs from *dt* mice should reveal any aberrant localization of MAP1B in the absence of dystonin. Dystonin knockdown experiments in cultured DRGs could also help explore the possible scaffolding and regulatory roles dystonin may play for MAP1B. A loss of dystonin through knockdown would be expected to result in the upregulation of phosphorylated MAP1B, accompanied by morphological anomalies caused by neurodegeneration.

MAP1B associated pathology – implications for dystonin interactions with CRMP2

The improper regulation of post-translational modifications of MAP1B has also been implicated in the encephalopathy associated with Alzheimer's disease (Good et al., 2004). Good et al. (2004) suggest that elevated levels of phosphorylated MAP1B and Semaphorin 3A may be the primary pathology of the condition, as they precede the occurrence of characteristic neurofibrillary tangles associated with Alzheimer's disease. Interestingly, phosphorylated MAP1B along with CRMP2, which is a downstream substrate of Semaphorin 3A (Good et al., 2004), was found to be part of a complex identified in hippocampal tissue from Alzheimer's patients. Additionally, only CA1 hippocampal neurons were vulnerable to degeneration. Good et al. (2004) postulate that MAP1B is regulated through CRMP2 activity, and its absence from CA3 hippocampal neurons may result in a neuroprotective effect and confer resistance to degeneration associated with Alzheimer's disease in these neurons. Thus, our identification of CRMP2 as a potential dystonin interacting partner may be the result of an indirect interaction through MAP1B. Evidence presented (Figure 22) demonstrating partial co-localization of

CRMP2 with dystonin-a2 in PC12 cells appears to corroborate this hypothesis. The inability to co-immunoprecipitate CRMP2 with the plakin domain of dystonin suggests this potential complex interaction may be transient and possibly dependent upon phosphorylation events. Further analysis must be performed to fully understand what may be happening *in vivo.* An examination of Semaphorin 3A activity in *dt* mice would be essential to determine the relevance and role of CRMP2 in the neurodegeneration associated with these mice.

Dystonin plakin domain interacts with myosin IIb

Diverse roles for myosin

Myosins are generally composed of an N-terminal globular head and an α-helical coiled-coil C-terminal. Myosins function mainly to translocate actin filaments and contribute to the structural integrity of the cell (Conti and Adelstein, 2008). The translocation activity of the myosin family of motor proteins is a function of the globular motor domain and lever arm. The ability of myosins to act as motors within the cell redistributing material allows for cell polarity and therefore cell migration. The rod portion of the myosin structure enables these proteins to form filaments and to contribute to cyto-architecture. The myosin II family includes skeletal, cardiac and smooth muscle myosins, in addition to non-muscle myosin.

Myosin IIb interacts with the dystonin plakin domain

Myosin IIB is a non-muscle myosin encoded by the MYH10 gene (Conti and Adelstein, 2008). As with other myosins, myosin IIb has been implicated in cell polarization and cytoskeletal stabilization. Evidence presented in (Figures 7, 8 and 19) suggests that myosin IIb has the potential to interact with the plakin domain of dystonin; however, it

does not appear that this interaction occurs with dystonin-a2 (Figure 20). Myosin IIb was found to align, as expected, with the actin cytoskeleton along the periphery of the cells and the actin stress fibres (Conti and Adelstein, 2008). In contrast, over-expressed YFP-mini-a2 aligned with the MT cytoskeleton in most of the transfected Cos-1 cells observed. It should however be noted that the endogenous localization of dystonin-a2 is quite different from that observed in the YFP-mini-a2 over-expressed Cos-1 cells. It has been reported that dystonin-a2 is primarily localized in the perinuclear region and is associated with components of the nuclear envelope and endoplasmic reticulum (Young and Kothary, 2008). Over-expressed dystonin isoform 1 however, has been shown to co-align with the actin cytoskeleton and may therefore be a potential mysoin IIb interactor (Young et al., 2003).

Role for dystonin in myosin IIb functioning

Ablation of myosin IIb in mice results in neuronal and cardiac defects (Tullio et al., 1997; Tullio et al., 2001). Myosin IIb null mice experience lethality in later stages of embryonic development. The neuronal defects observed include severe hydrocephalus, as well as thinning of the ventricular and spinal cord lining (Tullio et al., 2001). Additionally, cultured neurons demonstrate reduced neurite extensions and abnormally narrow growth cones in comparison to age-matched wild type animals (Tullio et al., 2001). A structural role for myosin IIb can be ascertained when examining the defects observed in the neuronal tissue of myosin IIb deficient mice. The loss of myosin IIb in these tissues results in the collapse of the structural meshwork providing integrity to the tissue, resulting in blockage of spinal fluid and the subsequent hydrocephalus observed (Ma et al., 2007). The meshwork charged with maintaining the integrity is necessary for cell-cell

adhesion junctions, and is believed to act through the interactions of myosin IIb with the actin cytoskeleton, e-cadherin and β-catenin (Ma et al., 2007). Interestingly, β-catenin has been shown to interact with the plakin domain of MACF1 (Chen et al., 2006), and early evidence suggests that such an interaction may also be occurring with the plakin domain of dystonin-a/b (appendix 2). Thus, it may be possible that the plakin domain of MACF1 and/or dystonin acts as a scaffold, facilitating the myosin IIb interactions with the actin cytoskeleton and β-catenin.

In cardiac tissue myosin IIb has been implicated in double outlet right ventricle (DORV), a congenital condition resulting from the absence of cardiac myocyte migration due to lack of cell polarization (Tullio et al., 1997). The defects were unable to be rescued despite the introduction of other non-muscle myosins with strong homology (Bao et al., 2007). The investigators suggest that a defect in the polarization and transportation action of myosin IIb is likely responsible for the observed phenotype. Although no gross defects in cardiac muscle have been reported in *dt* mice, molecular level analysis reveals an upregulation of hypertrophic markers in the cardiac tissue of these animals, indicating early signs of cardiac distress (Boyer and Bodreau-Larivière, unpublished). It would be imperative to explore a potential interaction by examining myosin IIb in *dt* cardiac tissue. Aberrant localization would lend support to the proposed role for dystonin in the regulation of myosin IIb. The dystonin-b antibody generated (appendix I) would also prove to be an extremely useful tool to explore a dystonin-b interaction with myosin IIb.

Dystonin-a interacts with clathrin heavy chain

Clathrin mediated endo-exocytosis – a new role for dystonin?

The maintenance of a homeostatic state within a cell is dependent upon its ability to successfully internalize macromolecules from the extracellular matrix and distribute these internalized components throughout the cell. In eukaryotic cells, this essential function is performed primarily through the clathrin-mediated endocytic pathway. Once a cargo target has been identified through receptors on the cell's surface, clathrin coated pits invaginate and 'pinch off', allowing for the complete encapsulation of the cargo and formation of clathrin coated vesicles (Edeling et al., 2006). The inner membrane layer bound to the cargo and the outer clathrin coat are not in direct contact, but rather associate with each other through various adaptor proteins. The clathrin coat is formed by a three-dimensional array of triskelia, each composed of three clathrin heavy chains and three clathrin light chains. Each clathrin heavy chain appears as a three-legged structure with a globular N-terminal end possessing a seven-bladed β-propellar (Marsh and McMahon, 1999). The hub domain of the triskelion is centred at each vertex of the clathrin cage formed by the interlocking of the three-legged structures. Each leg thus contributes to two sides of a polygonal cell, resulting in a characteristic soccer ball shape (Marsh and McMahon, 1999).

Clathrin mediated endocytosis is a complex process relying on the interplay of numerous components. The clathrin coat along with dynamin and the actin cytoskeleton are the major components involved in the endocytic process (Schmid et al., 1998; Gaidarov et al., 1999; Yarar et al., 2005). This associated effort occurs at both the plasma membrane as well as during exocytosis of post-Golgi vesicles. The clathrin triskelia is

assembled at the plasma membrane through the actions of assembly polypeptides, which are also referred to as the adaptor proteins (Pearse, 1988). During trans-Golgi vesicle formation, this function is performed by adaptor protein-1 (AP1) (Edeling et al., 2006). The classical view of clathrin coated vesicle formation purports that when AP2 is recruited to the plasma membrane it triggers clathrin triskelion cage formation, which continually grow, invaginate and are finally released through the GTPase activity of dynamin with concurrent actin polymerization (Brodsky et al., 2001; Yarar et al., 2005). Dynamin, through its proline-rich domain, binds to the SH3 domain of the cytosolic protein amphiphysin (David et al., 1996). Subsequently, amphiphysin binds to AP2 (Wang et al., 1995), which links the components involved in endo-exocytosis, ultimately leading to the formation of the clathrin coated vesicle.

AP2, which is the predominant adaptor protein found in neuronal cells, plays a part in cargo sorting as it recognizes only specific motifs. When a target is bound, the clathrin coating cascade is triggered along with the internalization process (Chaudhuri et al., 2007; Doray et al., 2007). As dystonin-a isoforms are structurally similar to proteins that interact with AP2 and are associated with clathrin, it is tempting to speculate that dystonin plays an integral role in the endocytosis and trafficking processes. In addition to interacting with clathrin (Figures 7,8,15, and 16), dystonin proteins also possess putative SH3 domains, and are able to bind to F-actin and thus the actin cytoskeleton through their actin-binding domain (Young et al., 2003). Dystonin proteins also possess large spectrin repeat coiled-coil domains common amongst spectrin repeat family members that are often observed to play scaffolding roles (Jefferson et al., 2007; Sonnenberg and Liem, 2007). Thus, dystonin may play a significant role in providing the necessary scaffolding

for all of the components involved in clathrin coat formation. The plakin domain of dystonin-a may serve as a docking region for clathrin heavy chain, as well as other components involved in coat formation such as dynamin. As the actin cytoskeleton generates the necessary force to internalize the newly forming clathrin coated vesicle, it may relay this force through dystonin (Figure 23). Interestingly, just as with MAP1B, the sequence of events that ultimately lead to the formation of a clathrin coated vesicle are believed to be a result of sequential phosphorylation activity (Marsh and McMahon, 1999; Edeling et al., 2006). It may be possible that this cascade of phosphorylation could be taking place within the plakin domain.

Although AP1 and AP2 have been shown to perform similar functions, these adaptors localize to different regions of the cell and therefore demonstrate non-redundancy in their functions. AP1 is involved in trafficking between the trans-Golgi network and endosomes, however the direction in which this trafficking occurs has not been fully determined (Robinson, 2004; Traub, 2005; Bonifacino and Rojas, 2006). Although the classical view of clathrin mediated trafficking highlighted only two adaptor protein complexes necessary for its recruitment, recent evidence has proposed the existence of several alternative adaptors whose function and role may be cargo specific. Numerous regulating proteins necessary for coat formation, vesicle fission, and coating removal have also been identified (Traub, 2005). Interestingly, AP1 adaptors have been shown to interact with MTs via scaffolding proteins, namely MAPs at the trans-Golgi network (Orzech et al., 2001). As dystonin-a2 has been shown to localize to the NE/ER (Young and Kothary, 2008) and associate around the Golgi complex (Young et al., 2006) in addition to possessing the capacity to bind to MTs as well as other cytoskeletal

components, it is tempting to postulate that dystonin may be playing a role in the trafficking of vesicles from the trans-Golgi to endosomes.

Clathrin and axonal transport associated neurodegeneration

As clathrin is a required component of endocytosis, and *dt* is a sensory neuropathy, it is necessary to examine how dystonin could be playing a part in the endocytic modulation and functioning of clathrin in the nervous system. In neurons, clathrin is transported down the axon to the synapse where clathrin-mediated endocytosis is believed to be the predominant form of synaptic vesicle recycling (Augustine et al., 2006). Transportation down the axon is achieved through fast and slow means (Okabe and Hirokawa, 1989). Slow axonal transport has been demonstrated to fall into two categories, namely slow component-a (SCa) and slow component-b (SCb). SCa is mainly responsible for the transportation of proteins that form cytoskeletal components such as MTs and neurofilaments. SCb is composed of numerous components including cytoskeletal aspects such as actin and tubulin, as well as various enzymes, calmodulin and clathrin (Oblinger et al., 1987; Siegel, 1999). SCa has been shown to be the main form of slow transport in large motor neurons, however its contribution in smaller sensory axons such as the optic nerve is much less where SCb appears to be the dominant form of axonal transport (Oblinger et al., 1987; Siegel, 1999). The rate of transport for these cellular components varies depending upon the load of material required by the neuron for axonal growth and regeneration (Siegel, 1999). As such rates of slow transport have been shown to increase in axons subjected to lesions; this suggests a critical role for slow axonal transport in the regeneration and repair process within the neuron (Siegel, 1999). With the indispensible

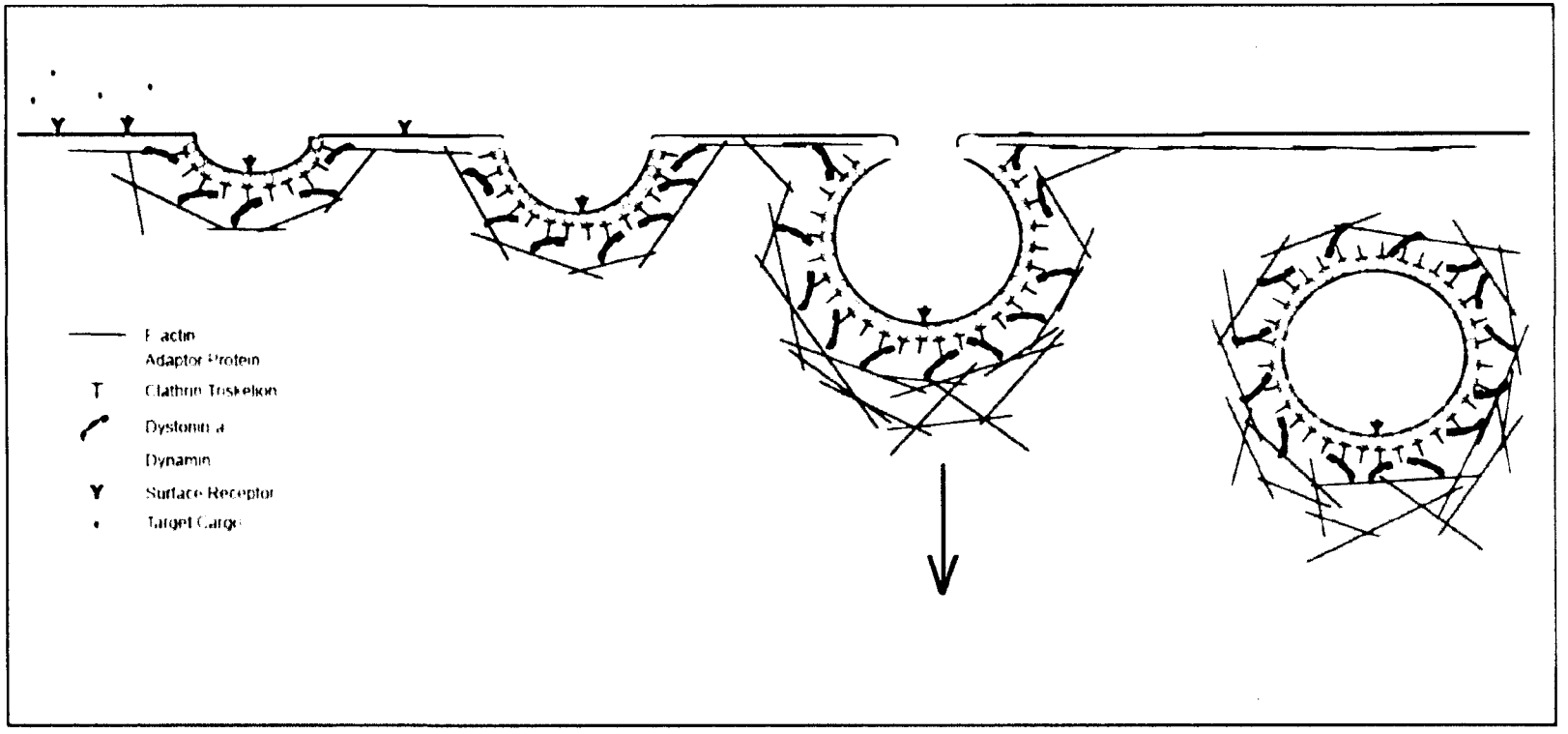

Figure 24. Role for dystonin in clathrin mediated endo-exocytosis.
Target cargo is identified by surface receptors that associate with adaptor proteins. Once a cargo has been accepted by its complementary receptor, the adaptor proteins begin recruiting clathrin triskelia to for a polygonal coat around the invaginating membrane. The force for the invagination is provided by the actin cytoskeleton which may associate with the clathrin coat through dystonin. After sufficient invagination by the membrane, dynamin forms a collar around the top of the budding vesicle and through a GTPase dependent process 'pinches off' the newly formed clathrin coated vesicle which is released into the cytosol.

role played by axonal transport in the maintenance and functioning of the neuron it is not surprising that disruptions in its mechanism have been implicated in a host of neurodegenerative disorders including Alzheimer's disease, Charcot-Marie-Tooth neuropathies, ALS and Huntington's chorea (Roy et al., 2005; De Vos et al., 2008). Finding evidence of the involvement of axonal transport in the *dt* condition has therefore always been a logical pursuit.

The *dt* pathology has long been associated with MT network abnormalities, neurofilament disorganization, and axonal swellings comprising accumulated membranous organelles (Duchen and Strich, 1964; Janota, 1972). De Repentigny et al. (2003) have demonstrated axonal transportation defects in *dt* mice by evaluating fast transport after ligature in sciatic nerve. Transport defects were also proposed to be a primary aetiology of the *dt* condition when an interaction of neuronal dystonin with the dynein/dynactin motor complex was demonstrated (Liu et al., 2003). Interestingly, Liu et al. (2003) also showed an accumulation of vesicles and mitochondria in the sciatic nerve of *dt* mice using ligature techniques. It is worth mentioning however, that defects in trafficking of macromolecules and mitochondria were not observed in cultured *dt* DRG neurons (Pool et al., 2006). Additionally, in short-term sensory neuron cultures, Pool et al. (2006) did not observe defects in MT organization, and as such suggest that dystonin may not be essential to the dynien/dynactin motor complex. However, this investigation was performed on cultured DRG neurons that were not subjected to polarization events and thus may not have necessarily been able to replicate the conditions found *in vivo*.

Dystonin-a interaction with clathrin - implications for dt pathology

An association with a trafficked non-cytoskeletal cellular component such as clathrin, which is involved in endocytosis and synaptic vesicle recycling, once again raises the possibility of the involvement of a dystonin neuronal isoform in axonal trafficking. It is tempting to speculate how a neuronal dystonin isoform may be participating in this trafficking activity. Based on the role of clathrin in endocytosis and synaptic vesicle recycling, and given the significant role of the actin cytoskeleton in mediating clathrin's activity, the dystonin protein may play a pivotal role in associating these cellular components. A lack of a neuronal dystonin isoform could then be postulated to cause an exhaustion of synaptic vesicles, ultimately leading to synaptic dysfunction. As dorsal root sensory neurons possess comparatively lower levels of proteins such as MACF1 that can compensate for the loss of dystonin (Sonnenberg and Liem, 2007), these neurons become the primary site for dysfunctions associated with the *dt* condition. The possible synaptic dysfunction may then trigger an increase in slow axonal transport as part of repair and regeneration response in these sensory neurons. SCb would be the likely form of slow transport in these sensory neurons. An increase in SCb transport in sensory neurons that do not possess dystonin may then result in a disrupted transport process that ultimately fails and leads to an accumulation of material resulting in the characteristic axonal swellings. Through a 'dying back' phenomenon, the axonal defects could ultimately lead to neuronal death and present the overt *dt* phenotype. Ventral motor neurons which are largely unaffected by the *dt* pathology may be able to stave off excessive degeneration due to a reliance on the SCa mode slow transport. An investigation into the form of transport dystonin associates with would be necessary to validate this hypothesis.

Neurodegeneration associated with loss of endocytic components

Intriguingly, a phenotype reminiscent of *dt* mice is observed in homozygous recessive dynamin knockout mice (Ferguson et al., 2007). Ferguson et al. (2007) found that mice null for dynamin-1 formed normal, functional synapses; however, under high synaptic activity an increase in clathrin-coated invaginations occurred in these synapses. At birth these knockout mice were indistinguishable from their wild type littermates, but soon after, these animals displayed limb incoordination and were unable to survive past 2 weeks post-partum. It would be extremely beneficial to explore an interaction between dynamin, necessary for vesicle budding, and dystonin-a. Such an interaction would support the notion that dystonin-a acts as a scaffold for the endocytic process mediating clathrin's activity. To validate a scaffolding role for dystonin-a, it would be necessary to conduct live cell imaging experiments whereby a fluorophore-tagged clathrin construct could be followed in cultured sensory neurons from *dt* and wild-type mice. It should be noted, however, that the presence of a neuronal isoform of dystonin at the synapse has not yet been observed. Our analysis has revealed that clathrin strongly associates with the plakin domain of dystonin-a. Rearrangement of the endogenous clathrin expression pattern to one that is associated with over-expressed YFP-mini-a2 (Figure 16) supports the notion that such an interaction is occurring with dystonin-a2. However, as the plakin domain is common amongst all of the neuronal dystonin isoforms, this interaction could be occurring with other dystonin-a isoforms.

The existence of several neuronal dystonin isoforms suggests its involvement in numerous cellular activities. The association of dystonin-a2 with the endoplasmic reticulum and components of the nuclear envelope has supported the notion that

disruption in dystonin functioning may result in protein processing anomalies contributing to the neuropathy of the *dt* condition (Young and Kothary, 2008). An association with a coat protein such as clathrin has helped support such a hypothesis. Interactions with COP-I and II, which are involved in cis-Golgi transport (Robinson, 2004), should be explored to further investigate this possibility. As trans-Golgi transport is performed through the actions of clathrin and its associated proteins, a role for dystonin in trafficking along the axon can also be proposed. Loss of a dystonin neuronal isoform (dystonin-a1?) along the axon may disrupt axonal transport and further compound potential processing defects at the endoplasmic reticulum, ultimately leading to the debilitating *dt* phenotype.

TorsinA dystonia and synaptic vesicle trafficking

Defects in synaptic vesicle trafficking have been implicated as a primary aetiology in neuropathologies such as Alzheimer's disease (Yuyama and Yanagisawa, 2009) and human torsinA dystonia (Granata et al., 2008). TorsinA, the mutant form of which is believed to result in human dystonia, has been shown to interact with snapin, a SNARE complex associated protein. The SNARE complex is involved in synaptic vesicle maturation and exocytosis (Horikawa et al., 1993). TorsinA has also been shown to associate with the nuclear envelope and endoplasmic reticulum in fibroblasts from torsinA dystonia patients, where it is believed to act as a chaperone protein (Hewett et al., 2003; Naismith et al., 2004). It has recently been shown to associate with nesprin-3, a kash domain protein, and is believed to link the nuclear envelope to the cytoskeleton through plectin (Nery et al., 2008).

Interestingly, Granata et al. (2008) demonstrate an accumulation of torsinA at the synapse of PC12 and neuroblastoma cells, where it is associated with snapin and dense core granules. However, mutant torsinA associates with the endoplasmic reticulum and was not found at the terminal ends of the axon. Further examination revealed the involvement of torsinA in synaptic vesicle modulation and recycling, leading to the postulation that it mediates dopamine function (Granata et al., 2008). Human dystonia has a similar phenotype to the *dt* condition in mice; however, no overt neurodegeneration has been reported. Still, dopamine regulation abnormalities are strongly implicated in the condition (Balcioglu et al., 2007). An examination of neurotransmitter activity in *dt* mice has not yet been reported and would be an extremely interesting avenue to pursue for further elucidation of the role of dystonin in the *dt* neuropathy. For this effort it would be insightful to perform endo-exocytosis assays in *dt* and wild-type cultured sensory neurons. Interestingly, the antibody for the intravesicular domain of SytI is internalized into the pre-synaptic zone when synaptic vesicles fuse to the pre-synaptic membrane (Granata et al., 2008). Incubation of cultured neurons with this antibody in resting state and depolarizing conditions, followed by incubation with, and imaging of a fluorophore tagged secondary antibody, would determine if there are any synaptic vesicle modulation abnormalities. To further examine any possible dysfunction, the dye FM1-43 that selectively binds organelles undergoing endo-exocytosis in living cells (Brumback et al., 2004; Granata et al., 2008) could be monitored in differential polarizing conditions, and an evaluation could be made in living *dt* and wild type cultured sensory neurons.

Conclusion

The multi-domain structure of dystonin renders it a likely candidate for interactions with various components of the cell. Previous characterization of this giant spectraplakin has highlighted interactions with the major components of the cytoskeleton. The goal of the present study was to identify novel interacting partners of the plakin domain of neuronal dystonin isoform. The initial pull-down screen identified several interesting candidates that warranted further analysis. Of the candidates identified, the cytoskeletal supporting protein MAP1B has helped further establish dystonin's potential role in modulating the cytoskeleton and link its various components. This interaction has also raised possible insight into the pathological progression of the *dt* condition through the modulation of phosphorylation events. Further investigation into dystonin's role in the functioning of MAP1B will advance our understanding of the biological relevance of this newly identified interaction and will help shed light on the *dt* condition. Interestingly, the interaction screen also revealed a novel non-cytoskeletal dystonin interacting partner in the form of clathrin heavy chain. In addition to facilitating our understanding of the diverse roles played by dystonin in the cell, this interaction has also raised numerous questions that suggest dystonin's involvement in both endocytosis and the late secretory pathway. Such an involvement brings to light a new, previously unknown role for dystonin that may eventually help elucidate the aetiology of the *dt* pathology as well as better our understanding of cytoskeletal and trafficking dynamics.

The novel interactions identified in this study have provided new avenues of investigation to further our understanding of dystonin. These interactions have also highlighted the importance, and necessity, of understanding how cellular components can

modulate each other's functions and must be viewed in a global perspective with respect to the cell. Although this work has brought us closer to understanding the functions of dystonin, much remains to be done to fully comprehend the role of this diverse protein in the proper functioning of a cell.

References

al-Ali SY, al-Zuhair AG (1989) Fine structural study of the spinal cord and spinal ganglia in mice afflicted with a hereditary sensory neuropathy, dystonia musculorum. J Submicrosc Cytol Pathol 21:737-748.

Alberts B (2002) Molecular biology of the cell, 4th Edition. New York: Garland Science.

Augustine GJ, Morgan JR, Villalba-Galea CA, Jin S, Prasad K, Lafer EM (2006) Clathrin and synaptic vesicle endocytosis: studies at the squid giant synapse. Biochem Soc Trans 34:68-72.

Balcioglu A, Kim MO, Sharma N, Cha JH, Breakefield XO, Standaert DG (2007) Dopamine release is impaired in a mouse model of DYT1 dystonia. J Neurochem 102:783-788.

Bao J, Ma X, Liu C, Adelstein RS (2007) Replacement of nonmuscle myosin II-B with II-A rescues brain but not cardiac defects in mice. J Biol Chem 282:22102-22111.

Bernier G, Kothary R (1998) Prenatal onset of axonopathy in Dystonia musculorum mice. Dev Genet 22:160-168.

Bernier G, De Repentigny Y, Mathieu M, David S, Kothary R (1998) Dystonin is an essential component of the Schwann cell cytoskeleton at the time of myelination. Development 125:2135-2148.

Bernier G, Brown A, Dalpe G, De Repentigny Y, Mathieu M, Kothary R (1995) Dystonin expression in the developing nervous system predominates in the neurons that degenerate in dystonia musculorum mutant mice. Mol Cell Neurosci 6:509-520.

Bernier G, Pool M, Kilcup M, Alfoldi J, De Repentigny Y, Kothary R (2000) Acf7 (MACF) is an actin and microtubule linker protein whose expression predominates in neural, muscle, and lung development. Dev Dyn 219:216-225.

Bloom GS, Luca FC, Vallee RB (1985a) Identification of high molecular weight microtubule-associated proteins in anterior pituitary tissue and cells using taxol-dependent purification combined with microtubule-associated protein specific antibodies. Biochemistry 24:4185-4191.

Bloom GS, Luca FC, Vallee RB (1985b) Microtubule-associated protein 1B: identification of a major component of the neuronal cytoskeleton. Proc Natl Acad Sci U S A 82:5404-5408.

Bonifacino JS, Rojas R (2006) Retrograde transport from endosomes to the trans-Golgi network. Nat Rev Mol Cell Biol 7:568-579.

Bouquet C, Soares S, von Boxberg Y, Ravaille-Veron M, Propst F, Nothias F (2004) Microtubule-associated protein 1B controls directionality of growth cone migration and axonal branching in regeneration of adult dorsal root ganglia neurons. J Neurosci 24:7204-7213.

Bradford MM (1976) A rapid and sensitive method for the quantitation of microgram quantities of protein utilizing the principle of protein-dye binding. Anal Biochem 72:248-254.

Brodsky FM, Chen CY, Knuehl C, Towler MC, Wakeham DE (2001) Biological basket weaving: formation and function of clathrin-coated vesicles. Annu Rev Cell Dev Biol 17:517-568.

Brown A, Dalpe G, Mathieu M, Kothary R (1995a) Cloning and characterization of the neural isoforms of human dystonin. Genomics 29:777-780.

Brown A, Bernier G, Mathieu M, Rossant J, Kothary R (1995b) The mouse dystonia musculorum gene is a neural isoform of bullous pemphigoid antigen 1. Nat Genet 10:301-306.

Brown A, Copeland NG, Gilbert DJ, Jenkins NA, Rossant J, Kothary R (1994) The genomic structure of an insertional mutation in the dystonia musculorum locus. Genomics 20:371-376.

Brugg B, Matus A (1988) PC12 cells express juvenile microtubule-associated proteins during nerve growth factor-induced neurite outgrowth. J Cell Biol 107:643-650.

Brumback AC, Lieber JL, Angleson JK, Betz WJ (2004) Using FM1-43 to study neuropeptide granule dynamics and exocytosis. Methods 33:287-294.

Buck KB, Zheng JQ (2002) Growth cone turning induced by direct local modification of microtubule dynamics. J Neurosci 22:9358-9367.

Bush MS, Gordon-Weeks PR (1994) Distribution and expression of developmentally regulated phosphorylation epitopes on MAP 1B and neurofilament proteins in the developing rat spinal cord. J Neurocytol 23:682-698.

Cairns NJ, Lee VM, Trojanowski JQ (2004) The cytoskeleton in neurodegenerative diseases. J Pathol 204:438-449.

Capetanaki Y, Milner DJ, Weitzer G (1997) Desmin in muscle formation and maintenance: knockouts and consequences. Cell Struct Funct 22:103-116.

Chaudhuri R, Lindwasser OW, Smith WJ, Hurley JH, Bonifacino JS (2007) Downregulation of CD4 by human immunodeficiency virus type 1 Nef is dependent on clathrin and involves direct interaction of Nef with the AP2 clathrin adaptor. J Virol 81:3877-3890.

Chen HJ, Lin CM, Lin CS, Perez-Olle R, Leung CL, Liem RK (2006) The role of microtubule actin cross-linking factor 1 (MACF1) in the Wnt signaling pathway. Genes Dev 20:1933-1945.

Conti MA, Adelstein RS (2008) Nonmuscle myosin II moves in new directions. J Cell Sci 121:11-18.

Copeland NG, Gilbert DJ, Li K, Sawamura D, Giudice GJ, Chu ML, Jenkins NA, Uitto J (1993) Chromosomal localization of mouse bullous pemphigoid antigens. BPAG1 and BPAG2: identification of a new region of homology between mouse and human chromosomes. Genomics 15:180-181.

Dalpé G, Leclerc N, Vallee A, Messer A, Mathieu M, De Repentigny Y, Kothary R (1998) Dystonin is essential for maintaining neuronal cytoskeleton organization. Mol Cell Neurosci 10:243-257.

David C, McPherson PS, Mundigl O, de Camilli P (1996) A role of amphiphysin in synaptic vesicle endocytosis suggested by its binding to dynamin in nerve terminals. Proc Natl Acad Sci U S A 93:331-335.

De Repentigny Y, Deschenes-Furry J, Jasmin BJ, Kothary R (2003) Impaired fast axonal transport in neurons of the sciatic nerves from dystonia musculorum mice. J Neurochem 86:564-571.

De Vos KJ, Grierson AJ, Ackerley S, Miller CC (2008) Role of axonal transport in neurodegenerative diseases. Annu Rev Neurosci 31:151-173.

Ding J, Liu JJ, Kowal AS, Nardine T, Bhattacharya P, Lee A, Yang Y (2002) Microtubule-associated protein 1B: a neuronal binding partner for gigaxonin. J Cell Biol 158:427-433.

DiTella MC, Feiguin F, Carri N, Kosik KS, Caceres A (1996) MAP-1B/TAU functional redundancy during laminin-enhanced axonal growth. J Cell Sci 109 (Pt 2):467-477.

Djinovic-Carugo K, Gautel M, Ylanne J, Young P (2002) The spectrin repeat: a structural platform for cytoskeletal protein assemblies. FEBS Lett 513:119-123.

Doray B, Lee I, Knisely J, Bu G, Kornfeld S (2007) The gamma/sigma1 and alpha/sigma2 hemicomplexes of clathrin adaptors AP-1 and AP-2 harbor the dileucine recognition site. Mol Biol Cell 18:1887-1896.

Dowling J, Yang Y, Wollmann R, Reichardt LF, Fuchs E (1997) Developmental expression of BPAG1-n: insights into the spastic ataxia and gross neurologic degeneration in dystonia musculorum mice. Dev Biol 187:131-142.

Duchen LW (1976) Dystonia musculorum--an inherited disease of the nervous system in the mouse. Adv Neurol 14:353-365.

Duchen LW, Strich SJ (1964) Clinical and pathological studies of an hereditary neuropathy in mice. Brain 87:367-378.

Duchen LW, Falconer DS, Strich SJ (1963) Dystonia Musculorum. A hereditary neuropathy of mice affecting mainly sensory pathways. J Physiol 165:7-9.

Edeling MA, Smith C, Owen D (2006) Life of a clathrin coat: insights from clathrin and AP structures. Nat Rev Mol Cell Biol 7:32-44.

Edelmann W, Zervas M, Costello P, Roback L, Fischer I, Hammarback JA, Cowan N, Davies P, Wainer B, Kucherlapati R (1996) Neuronal abnormalities in microtubule-associated protein 1B mutant mice. Proc Natl Acad Sci U S A 93:1270-1275.

Ferguson SM, Brasnjo G, Hayashi M, Wolfel M, Collesi C, Giovedi S, Raimondi A, Gong LW, Ariel P, Paradise S, O'Toole E, Flavell R, Cremona O, Miesenbock G, Ryan TA, De Camilli P (2007) A selective activity-dependent requirement for dynamin 1 in synaptic vesicle endocytosis. Science 316:570-574.

Foisner R, Wiche G (1987) Structure and hydrodynamic properties of plectin molecules. J Mol Biol 198:515-531.

Fuchs E, Karakesisoglou I (2001) Bridging cytoskeletal intersections. Genes Dev 15:1-14.

Gaidarov I, Santini F, Warren RA, Keen JH (1999) Spatial control of coated-pit dynamics in living cells. Nat Cell Biol 1:1-7.

Garcia ML, Cleveland DW (2001) Going new places using an old MAP: tau, microtubules and human neurodegenerative disease. Curr Opin Cell Biol 13:41-48.

Getsios S, Huen AC, Green KJ (2004) Working out the strength and flexibility of desmosomes. Nat Rev Mol Cell Biol 5:271-281.

Giorda R, Cerritello A, Bonaglia MC, Bova S, Lanzi G, Repetti E, Giglio S, Baschirotto C, Pramparo T, Avolio L, Bragheri R, Maraschio P, Zuffardi O (2004) Selective disruption of muscle and brain-specific BPAG1 isoforms in a girl with a 6;15

translocation, cognitive and motor delay, and tracheo-oesophageal atresia. J Med Genet 41:e71.

Gonzalez-Billault C, Owen R, Gordon-Weeks PR, Avila J (2002a) Microtubule-associated protein 1B is involved in the initial stages of axonogenesis in peripheral nervous system cultured neurons. Brain Res 943:56-67.

Gonzalez-Billault C, Engelke M, Jimenez-Mateos EM, Wandosell F, Caceres A, Avila J (2002b) Participation of structural microtubule-associated proteins (MAPs) in the development of neuronal polarity. J Neurosci Res 67:713-719.

Gonzalez-Billault C, Demandt E, Wandosell F, Torres M, Bonaldo P, Stoykova A, Chowdhury K, Gruss P, Avila J, Sanchez MP (2000) Perinatal lethality of microtubule-associated protein 1B-deficient mice expressing alternative isoforms of the protein at low levels. Mol Cell Neurosci 16:408-421.

Good PF, Alapat D, Hsu A, Chu C, Perl D, Wen X, Burstein DE, Kohtz DS (2004) A role for semaphorin 3A signaling in the degeneration of hippocampal neurons during Alzheimer's disease. J Neurochem 91:716-736.

Goold RG, Owen R, Gordon-Weeks PR (1999) Glycogen synthase kinase 3beta phosphorylation of microtubule-associated protein 1B regulates the stability of microtubules in growth cones. J Cell Sci 112 (Pt 19):3373-3384.

Granata A, Watson R, Collinson LM, Schiavo G, Warner TT (2008) The dystonia-associated protein torsinA modulates synaptic vesicle recycling. J Biol Chem 283:7568-7579.

Greene LA, Liem RK, Shelanski ML (1983) Regulation of a high molecular weight microtubule-associated protein in PC12 cells by nerve growth factor. J Cell Biol 96:76-83.

Guo L, Degenstein L, Dowling J, Yu QC, Wollmann R, Perman B, Fuchs E (1995) Gene targeting of BPAG1: abnormalities in mechanical strength and cell migration in stratified epithelia and neurologic degeneration. Cell 81:233-243.

Hewett J, Ziefer P, Bergeron D, Naismith T, Boston H, Slater D, Wilbur J, Schuback D, Kamm C, Smith N, Camp S, Ozelius LJ, Ramesh V, Hanson PI, Breakefield XO (2003) TorsinA in PC12 cells: localization in the endoplasmic reticulum and response to stress. J Neurosci Res 72:158-168.

Hisahara S, Chiba S, Matsumoto H, Horio Y (2005) Transcriptional regulation of neuronal genes and its effect on neural functions: NAD-dependent histone deacetylase SIRT1 (Sir2alpha). J Pharmacol Sci 98:200-204.

Horikawa HP, Saisu H, Ishizuka T, Sekine Y, Tsugita A, Odani S, Abe T (1993) A complex of rab3A, SNAP-25, VAMP/synaptobrevin-2 and syntaxins in brain presynaptic terminals. FEBS Lett 330:236-240.

Janmey PA (1991) Mechanical properties of cytoskeletal polymers. Curr Opin Cell Biol 3:4-11.

Janota I (1972) Ultrastructural studies of an hereditary sensory neuropathy in mice (dystonia musculorum). Brain 95:529-536.

Jefferson JJ, Leung CL, Liem RK (2004) Plakins: goliaths that link cell junctions and the cytoskeleton. Nat Rev Mol Cell Biol 5:542-553.

Jefferson JJ, Leung CL, Liem RK (2006) Dissecting the sequence specific functions of alternative N-terminal isoforms of mouse bullous pemphigoid antigen 1. Exp Cell Res 312:2712-2725.

Jefferson JJ, Ciatto C, Shapiro L, Liem RK (2007) Structural analysis of the plakin domain of bullous pemphigoid antigen1 (BPAG1) suggests that plakins are members of the spectrin superfamily. J Mol Biol 366:244-257.

Johnstone M, Goold RG, Bei D, Fischer I, Gordon-Weeks PR (1997) Localisation of microtubule-associated protein 1B phosphorylation sites recognised by monoclonal antibody SMI-31. J Neurochem 69:1417-1424.

Khaitlina SY (2001) Functional specificity of actin isoforms. Int Rev Cytol 202:35-98.

Koster J, Geerts D, Favre B, Borradori L, Sonnenberg A (2003) Analysis of the interactions between BP180, BP230, plectin and the integrin alpha6beta4 important for hemidesmosome assembly. J Cell Sci 116:387-399.

Kothary R, Clapoff S, Brown A, Campbell R, Peterson A, Rossant J (1988) A transgene containing lacZ inserted into the dystonia locus is expressed in neural tube. Nature 335:435-437.

Leung CL, Green KJ, Liem RK (2002) Plakins: a family of versatile cytolinker proteins. Trends Cell Biol 12:37-45.

Leung CL, Zheng M, Prater SM, Liem RK (2001) The BPAG1 locus: Alternative splicing produces multiple isoforms with distinct cytoskeletal linker domains, including predominant isoforms in neurons and muscles. J Cell Biol 154:691-697.

Levavasseur F, Zhu Q, Julien JP (1999) No requirement of alpha-internexin for nervous system development and for radial growth of axons. Brain Res Mol Brain Res 69:104-112.

Li K, Guidice GJ, Tamai K, Do HC, Sawamura D, Diaz LA, Uitto J (1992) Cloning of partial cDNA for mouse 180-kDa bullous pemphigoid antigen (BPAG2), a highly conserved collagenous protein of the cutaneous basement membrane zone. J Invest Dermatol 99:258-263.

Li SS (2005) Specificity and versatility of SH3 and other proline-recognition domains: structural basis and implications for cellular signal transduction. Biochem J 390:641-653.

Liu JJ, Ding J, Wu C, Bhagavatula P, Cui B, Chu S, Mobley WC, Yang Y (2007) Retrolinkin, a membrane protein, plays an important role in retrograde axonal transport. Proc Natl Acad Sci U S A 104:2223-2228.

Liu JJ, Ding J, Kowal AS, Nardine T, Allen E, Delcroix JD, Wu C, Mobley W, Fuchs E, Yang Y (2003) BPAG1n4 is essential for retrograde axonal transport in sensory neurons. J Cell Biol 163:223-229.

Ma D, Nothias F, Boyne LJ, Fischer I (1997) Differential regulation of microtubule-associated protein 1B (MAP1B) in rat CNS and PNS during development. J Neurosci Res 49:319-332.

Ma X, Bao J, Adelstein RS (2007) Loss of cell adhesion causes hydrocephalus in nonmuscle myosin II-B-ablated and mutated mice. Mol Biol Cell 18:2305-2312.

Mack TG, Koester MP, Pollerberg GE (2000) The microtubule-associated protein MAP1B is involved in local stabilization of turning growth cones. Mol Cell Neurosci 15:51-65.

Mansfield SG, Diaz-Nido J, Gordon-Weeks PR, Avila J (1991) The distribution and phosphorylation of the microtubule-associated protein MAP 1B in growth cones. J Neurocytol 20:1007-1022.

Marsh M, McMahon HT (1999) The structural era of endocytosis. Science 285:215-220.

Matus A, Riederer B (1986) Microtubule-associated proteins in the developing brain. Ann N Y Acad Sci 466:167-179.

Meixner A, Haverkamp S, Wassle H, Fuhrer S, Thalhammer J, Kropf N, Bittner RE, Lassmann H, Wiche G, Propst F (2000) MAP1B is required for axon guidance and Is involved in the development of the central and peripheral nervous system. J Cell Biol 151:1169-1178.

Mitchison TJ, Maddox P, Gaetz J, Groen A, Shirasu M, Desai A, Salmon ED, Kapoor TM (2005) Roles of polymerization dynamics, opposed motors, and a tensile element in governing the length of Xenopus extract meiotic spindles. Mol Biol Cell 16:3064-3076.

Naismith TV, Heuser JE, Breakefield XO, Hanson PI (2004) TorsinA in the nuclear envelope. Proc Natl Acad Sci U S A 101:7612-7617.

Nery FC, Zeng J, Niland BP, Hewett J, Farley J, Irimia D, Li Y, Wiche G, Sonnenberg A, Breakefield XO (2008) TorsinA binds the KASH domain of nesprins and participates in linkage between nuclear envelope and cytoskeleton. J Cell Sci 121:3476-3486.

Oblinger MM, Brady ST, McQuarrie IG, Lasek RJ (1987) Cytotypic differences in the protein composition of the axonally transported cytoskeleton in mammalian neurons. J Neurosci 7:453-462.

Okabe S, Hirokawa N (1989) Axonal transport. Curr Opin Cell Biol 1:91-97.

Orzech E, Livshits L, Leyt J, Okhrimenko H, Reich V, Cohen S, Weiss A, Melamed-Book N, Lebendiker M, Altschuler Y, Aroeti B (2001) Interactions between adaptor protein-1 of the clathrin coat and microtubules via type 1a microtubule-associated proteins. J Biol Chem 276:31340-31348.

Pearse BM (1988) Receptors compete for adaptors found in plasma membrane coated pits. EMBO J 7:3331-3336.

Pedrotti B, Islam K (1995) Microtubule associated protein 1B (MAP1B) promotes efficient tubulin polymerisation in vitro. FEBS Lett 371:29-31.

Percipalle P, Visa N (2006) Molecular functions of nuclear actin in transcription. J Cell Biol 172:967-971.

Pool M, Rippstein P, McBride H, Kothary R (2006) Trafficking of macromolecules and organelles in cultured Dystonia musculorum sensory neurons is normal. J Comp Neurol 494:549-558.

Pool M, Boudreau Lariviere C, Bernier G, Young KG, Kothary R (2005) Genetic alterations at the Bpag1 locus in dt mice and their impact on transcript expression. Mamm Genome 16:909-917.

Ramon-Cueto A, Avila J (1999) Two modes of microtubule-associated protein 1B phosphorylation are differentially regulated during peripheral nerve regeneration. Brain Res 815:213-226.

Reichelt J, Bussow H, Grund C, Magin TM (2001) Formation of a normal epidermis supported by increased stability of keratins 5 and 14 in keratin 10 null mice. Mol Biol Cell 12:1557-1568.

Riederer B, Cohen R, Matus A (1986) MAP5: a novel brain microtubule-associated protein under strong developmental regulation. J Neurocytol 15:763-775.

Riederer BM (1995) Differential phosphorylation of MAP1b during postnatal development of the cat brain. J Neurocytol 24:45-54.

Riederer BM, Guadano-Ferraz A, Innocenti GM (1990) Difference in distribution of microtubule-associated proteins 5a and 5b during the development of cerebral cortex and corpus callosum in cats: dependence on phosphorylation. Brain Res Dev Brain Res 56:235-243.

Robinson MS (2004) Adaptable adaptors for coated vesicles. Trends Cell Biol 14:167-174.

Roper K, Gregory SL, Brown NH (2002) The 'Spectraplakins': cytoskeletal giants with characteristics of both spectrin and plakin families. J Cell Sci 115:4215-4225.

Roy S, Zhang B, Lee VM, Trojanowski JQ (2005) Axonal transport defects: a common theme in neurodegenerative diseases. Acta Neuropathol 109:5-13.

Ruhrberg C, Watt FM (1997) The plakin family: versatile organizers of cytoskeletal architecture. Curr Opin Genet Dev 7:392-397.

Saulnier R, De Repentigny Y, Yong VW, Kothary R (2002) Alterations in myelination in the central nervous system of dystonia musculorum mice. J Neurosci Res 69:233-242.

Sawamura D, Li K, Chu ML, Uitto J (1991) Human bullous pemphigoid antigen (BPAG1). Amino acid sequences deduced from cloned cDNAs predict biologically important peptide segments and protein domains. J Biol Chem 266:17784-17790.

Schmid SL, McNiven MA, De Camilli P (1998) Dynamin and its partners: a progress report. Curr Opin Cell Biol 10:504-512.

Schulze SR, Curio-Penny B, Li Y, Imani RA, Rydberg L, Geyer PK, Wallrath LL (2005) Molecular genetic analysis of the nested Drosophila melanogaster lamin C gene. Genetics 171:185-196.

Shimada Y, Suzuki H, Konno A (1997) Dynamics of actin in cardiac myofibrils and fibroblast stress fibers. Cell Struct Funct 22:59-64.

Siegel GJ (1999) Basic neurochemistry : molecular, cellular, and medical aspects, 6th Edition. Philadelphia: Lippincott, Williams & Wilkins.

Sonnenberg A, Liem RK (2007) Plakins in development and disease. Exp Cell Res 313:2189-2203.

Sotelo C, Guenet JL (1988) Pathologic changes in the CNS of dystonia musculorum mutant mouse: an animal model for human spinocerebellar ataxia. Neuroscience 27:403-424.

Strelkov SV, Herrmann H, Aebi U (2003) Molecular architecture of intermediate filaments. Bioessays 25:243-251.

Takei Y, Teng J, Harada A, Hirokawa N (2000) Defects in axonal elongation and neuronal migration in mice with disrupted tau and map1b genes. J Cell Biol 150:989-1000.

Takei Y, Kondo S, Harada A, Inomata S, Noda T, Hirokawa N (1997) Delayed development of nervous system in mice homozygous for disrupted microtubule-associated protein 1B (MAP1B) gene. J Cell Biol 137:1615-1626.

Tang HY, Chaffotte AF, Thacher SM (1996) Structural analysis of the predicted coiled-coil rod domain of the cytoplasmic bullous pemphigoid antigen (BPAG1). Empirical localization of the N-terminal globular domain-rod boundary. J Biol Chem 271:9716-9722.

Traub LM (2005) Common principles in clathrin-mediated sorting at the Golgi and the plasma membrane. Biochim Biophys Acta 1744:415-437.

Tucker RP, Binder LI, Matus AI (1988) Neuronal microtubule-associated proteins in the embryonic avian spinal cord. J Comp Neurol 271:44-55.

Tucker RP, Garner CC, Matus A (1989) In situ localization of microtubule-associated protein mRNA in the developing and adult rat brain. Neuron 2:1245-1256.

Tullio AN, Bridgman PC, Tresser NJ, Chan CC, Conti MA, Adelstein RS, Hara Y (2001) Structural abnormalities develop in the brain after ablation of the gene encoding nonmuscle myosin II-B heavy chain. J Comp Neurol 433:62-74.

Tullio AN, Accili D, Ferrans VJ, Yu ZX, Takeda K, Grinberg A, Westphal H, Preston YA, Adelstein RS (1997) Nonmuscle myosin II-B is required for normal development of the mouse heart. Proc Natl Acad Sci U S A 94:12407-12412.

Ulloa L, Ibarrola N, Avila J, Diez-Guerra FJ (1994) Microtubule-associated protein 1B (MAP1B) is present in glial cells phosphorylated different than in neurones. Glia 10:266-275.

Wang LH, Sudhof TC, Anderson RG (1995) The appendage domain of alpha-adaptin is a high affinity binding site for dynamin. J Biol Chem 270:10079-10083.

Wilm M, Shevchenko A, Houthaeve T, Breit S, Schweigerer L, Fotsis T, Mann M (1996) Femtomole sequencing of proteins from polyacrylamide gels by nano-electrospray mass spectrometry. Nature 379:466-469.

Woods CM, Lazarides E (1986) Spectrin assembly in avian erythroid development is determined by competing reactions of subunit homo- and hetero-oligomerization. Nature 321:85-89.

Yamanouchi H, Jay V, Rutka JT, Takashima S, Becker LE (1997) Evidence of abnormal differentiation in giant cells of tuberous sclerosis. Pediatr Neurol 17:49-53.

Yang Y, Dowling J, Yu QC, Kouklis P, Cleveland DW, Fuchs E (1996) An essential cytoskeletal linker protein connecting actin microfilaments to intermediate filaments. Cell 86:655-665.

Yang Y, Bauer C, Strasser G, Wollman R, Julien JP, Fuchs E (1999) Integrators of the cytoskeleton that stabilize microtubules. Cell 98:229-238.

Yarar D, Waterman-Storer CM, Schmid SL (2005) A dynamic actin cytoskeleton functions at multiple stages of clathrin-mediated endocytosis. Mol Biol Cell 16:964-975.

Young KG, Kothary R (2005) Spectrin repeat proteins in the nucleus. Bioessays 27:144-152.

Young KG, Kothary R (2007) Dystonin/Bpag1--a link to what? Cell Motil Cytoskeleton 64:897-905.

Young KG, Kothary R (2008) Dystonin/Bpag1 is a necessary endoplasmic reticulum/nuclear envelope protein in sensory neurons. Exp Cell Res 314:2750-2761.

Young KG, Pool M, Kothary R (2003) Bpag1 localization to actin filaments and to the nucleus is regulated by its N-terminus. J Cell Sci 116:4543-4555.

Young KG, Pinheiro B, Kothary R (2006) A Bpag1 isoform involved in cytoskeletal organization surrounding the nucleus. Exp Cell Res 312:121-134.

Yuyama K, Yanagisawa K (2009) Late endocytic dysfunction as a putative cause of amyloid fibril formation in Alzheimer's disease. J Neurochem 109:1250-1260.

Zhou FQ, Snider WD (2005) CELL BIOLOGY: GSK-3beta and Microtubule Assembly in Axons. Science 308:211-214.

Zhu Q, Couillard-Despres S, Julien JP (1997) Delayed maturation of regenerating myelinated axons in mice lacking neurofilaments. Exp Neurol 148:299-316.

Zhu Q, Lindenbaum M, Levavasseur F, Jacomy H, Julien JP (1998) Disruption of the NF-H gene increases axonal microtubule content and velocity of neurofilament transport: relief of axonopathy resulting from the toxin beta,beta'-iminodipropionitrile. J Cell Biol 143:183-193.

Appendix I

Generation of an antibody specific to the muscle isoform of dystonin

To generate an antibody specific to the muscle isoform of dystonin, a pET30a plasmid expressing 6x his-tags at both the N-terminal and C-terminal end of a short fragment encoding a region from the dystonin isoform-b was used. The fusion coded for the intermediate filament-binding domain 2 (bp 6980 – bp 8142 GenBank Accession NM134448.2) of an isoform b specific region just downstream of the plakin domain. The his-tagged IFBD2 construct (his-IFBD) (previously generated) was produced in soluble form using the bacterial protein expression protocol described. A gradient pump (Bio-Rad) was used to pass 50 ml of the soluble fraction from bacterial lysate containing the his-tagged construct through a high-flow his-trap column (GE healthcare) as per the manufacturer's protocol. The eluate obtained was concentrated by placing it in dialysis tubing (porosity for MW 8000) and immersing the tube in an Erlenmeyer flask containing a solution of poly-ethylene-glycol (MW 15000) (Sigma) for 3 hours at 4°C under gentle agitation. A total of 4 mg of concentrated protein was sent to Cedarlane Laboratories (Ontario, Canada) and was used to inoculate 2 chickens. Serum containing the antibody was received and used for biochemical analyses to determine specificity and efficacy of the final product.

Dystonin-b antibody characterization

Immunoblot and immunofluorescence analyses were performed to determine the antibody specificity against the IFBD2 region of dystonin-b. A western blot was performed on protein from a bacterially expressed fusion of his-IFBD. Anti-his immunoblot detected the expression of the his-tag (Figure A1). A similarly sized band

was detected in an immunoblot using the dystonin-b antibody (Figure A1). To ensure that the antibody was not targeting the his-epitope used in its generation, Cos-1 cells were transfected with a flag-epitope tagged IFBD2 mammalian expression fusion. Indeed, the dystonin-b antibody co-localized with the anti-flag antibody used to identify transfected cells (Figure A2). We characterized the localization pattern of the antibody in C2C12 myoblast cells. A distinct staining pattern was observed with polarized perinuclear aggregation of the signal to one side of the nucleus (Figure A3).

Co-immunofluorescence using various cell structure and organellar markers was employed to determine the targeting site of the antibody. Co-staining with anti-golgi marker (GM130) and the IF, vimentin, revealed that the dystonin-b antibody did not localize to either of these cellular components (Figure A4A-F). However, partial co-localization of dystonin-b with protein disulfide isomerase, an endoplasmic reticulum marker, was observed (Figure A4G-I).

Dystonin-b antibody staining was performed on tibialis anterior skeletal muscle cross-sections from both dt^{27J} and age-matched wild-type mice in an effort to determine its localization and efficacy *in vivo*. It is evident from the confocal micrographs presented in Figure A5A that the dystonin-b antibody localizes to what appears to be the sarcolemma in the wild-type sections. As expected, minimal staining, at background levels, was observed in the dt^{27J} sections (Figure A5B). Figure A6 depicts dystonin-b and desmin co-immunofluorescence in longitudinal sections of cardiac muscle tissue from wild-type mice. Dystonin-b appears localized to a banding pattern aligning with the striated desmin bands located at the Z-disc, however, we do not observe co-localization between the two signals. It should be noted that desmin localization is not altered in *dt*

mice, therefore a direct interaction between desmin and dystonin-b may not be likely (Figure A6).

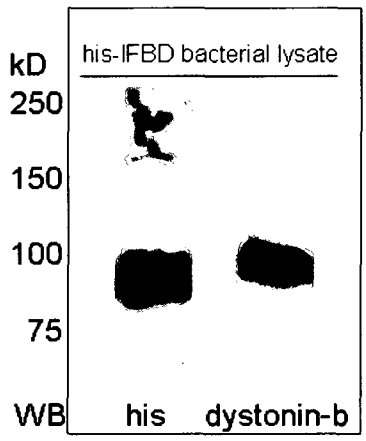

Figure A1. Detection of his-IFBD fusion with dystonin-b antibody. Immunodetection analysis was performed on bacterial lysate expressing the his-IFBD construct used as the antigen for the generation of the dystonin-b antibody. Lane 1 illustrates the detection of the his-tag in the lysate with an anti-his antibody (~90kD). Lane 2 demonstrates the successful detection of a similar band with the dystonin-b antibody.

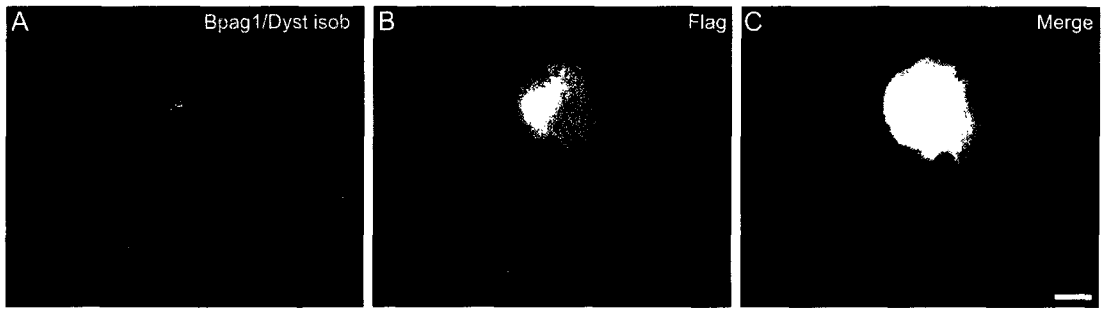

Figure A2. Co-localization of flag-tagged IFBD2 and dystonin-b antibody.
Cos-1 cells were transiently transfected with a flag-tagged IFBD2 construct and immunofluorescence analysis was performed. **A.** Micrograph illustrating the detection of the flag epitope in the Cos-1 cells transiently transfected with the flag-tagged IFBD2 construct. **B.** A micrograph of dystonin-b antibody targeting the IFBD2 region of the flag-tagged IFBD2 construct in transiently transfected Cos-1 cells. **C.** Strong co-localization of the flag and dystonin-b signal indicating successful targeting of the dystonin-b antibody. Nuclei have been stained with DAPI nuclear marker and are visualized in blue. Scale bar: 5 μM scale bar indicated in panel C is applicable to panels A and B as well.

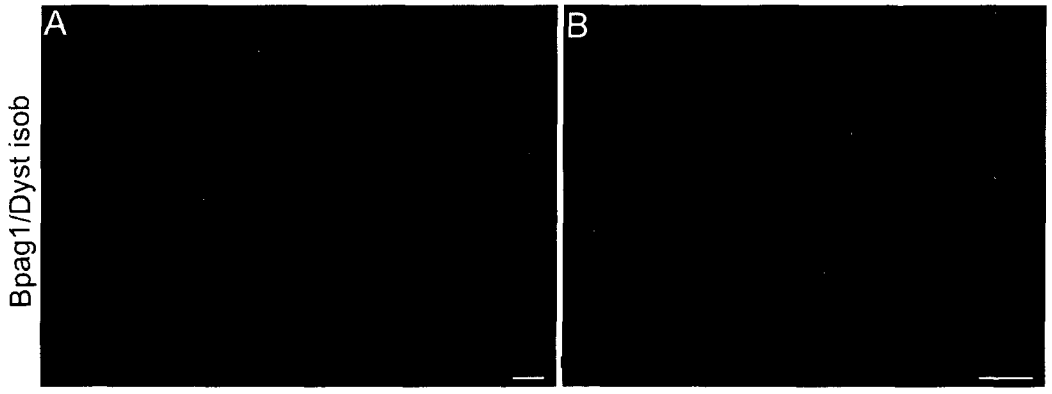

Figure A3. Confocal micrograph of dystonin-b antibody in C2C12 myoblasts. Endogenous detection of dystonin-b in C2C12 myoblasts with dystonin-b antibody. A. The dystonin-b antibody (red) appears to stain the perinuclear region in C2C12 myoblasts with signal aggregation to one side of the nucleus (blue). B. A magnified image illustrating the strong polarized localization of dystonin-b observed in C2C12 myoblasts. Nuclei have been stained with DAPI nuclear marker and are visualized in blue. Scale bar: 5 μM scale bar as indicated.

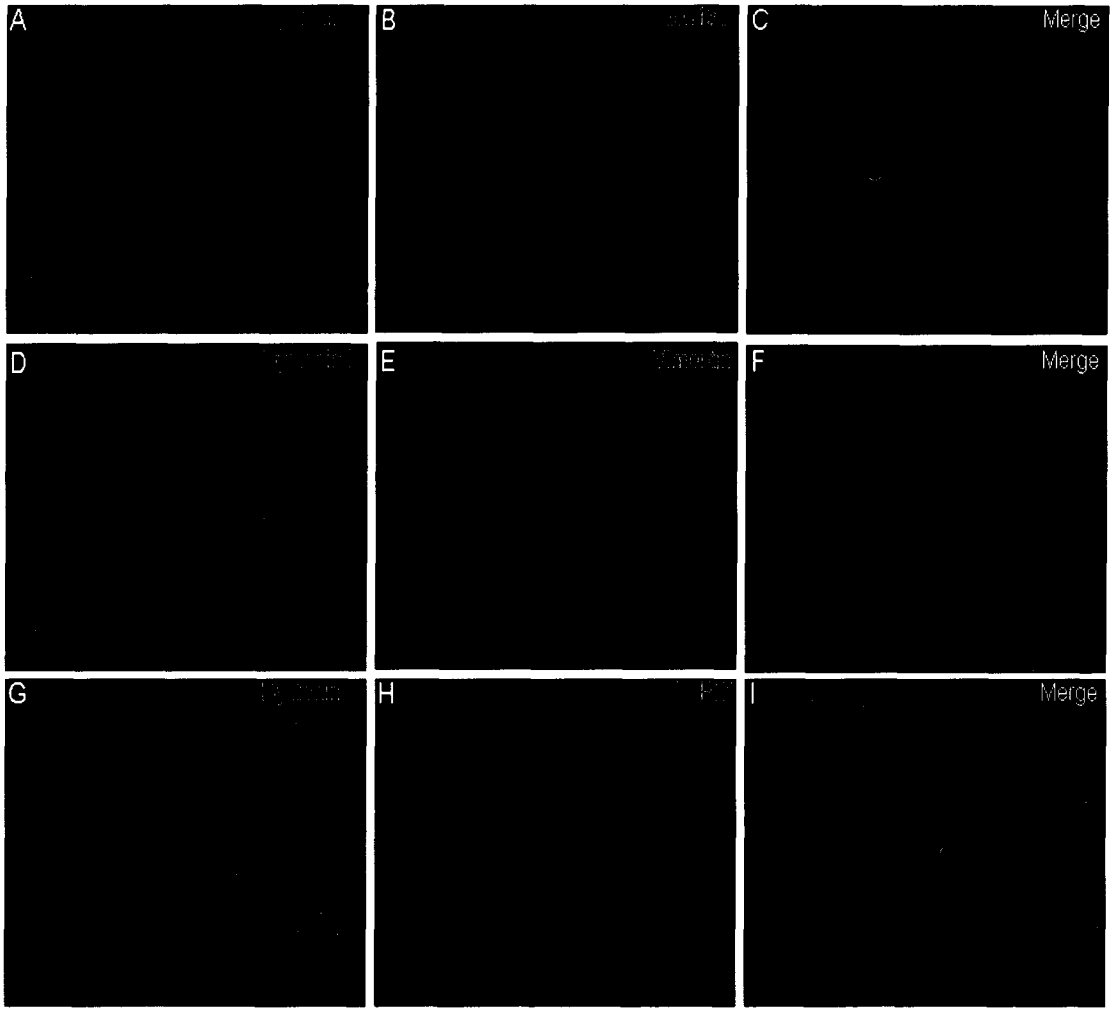

Figure A4. Co-staining of dystonin-b and various cellular components in C2C12 myoblasts.
A-C. Co-staining of dystonin-b and GM130, a golgi-marker. Polarized peri-nuclear staining of dystonin-b (red) does not appear to co-localize with the polarized golgi (green) stain in C2C12 myoblasts. **D-F.** Vimentin (green), an intermediate filament, does not appear to co-localize with dystonin-b (red) in C2C12 myoblasts. **G-I.** Partial co-localization (arrows) of dystonin-b (red) and protein disulfide isomerase (green), an ER marker was observed in C2C12 myoblasts. Nuclei have been stained with DAPI nuclear marker and are visualized in blue.

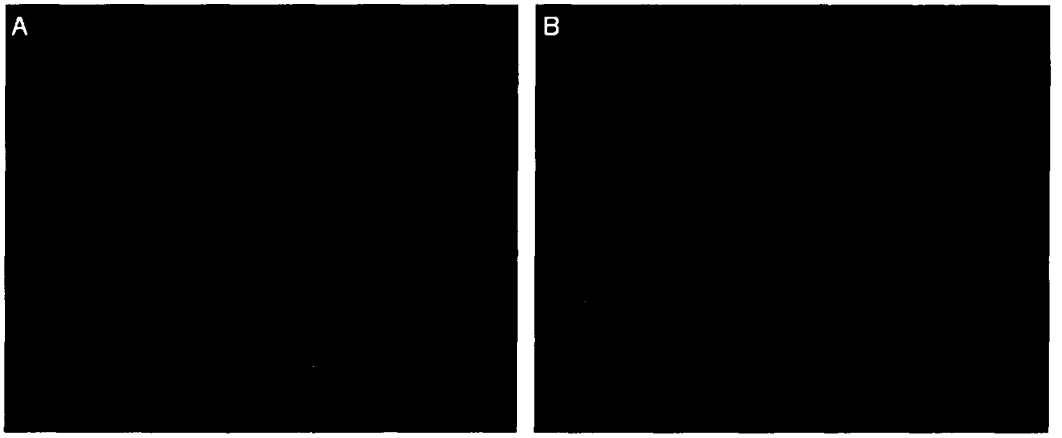

Figure A5. Dystonin-b antibody staining *in vivo.*

Cross sections of the tibialis muscle from dt^{27J} (dt) and age-matched wild-type (wt) mice were immunostained with the dystonin-b antibody. **A.** Confocal micrographs depicts staining of wt tibialis cross-section with dystonin-b antibody and reveals what appears to be sarcolemmic localization. **B.** dt^{27J} tibialis cross-section staining shows negligible, background levels of staining.

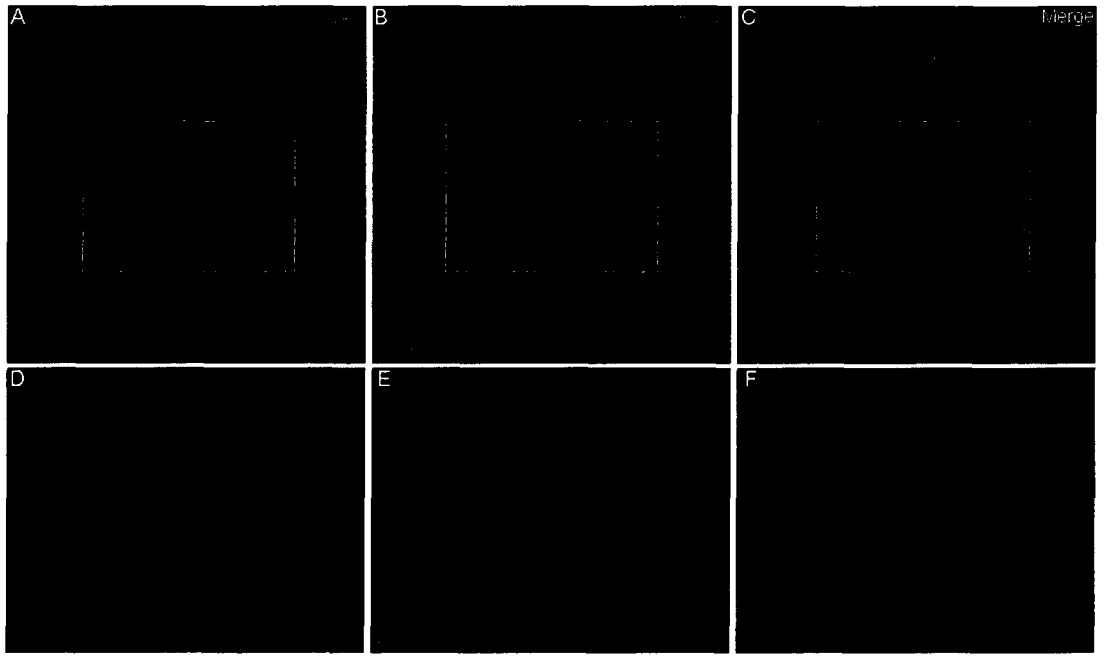

Figure A6. Dystonin-b antibody staining cardiac muscle.
Longitudinal cardiac muscle sections from wild-type (wt) mice were immunostained with the dystonin-b antibody as well as an antibody for the intermediate filament, desmin. **A-C.** Confocal micrographs depict staining of wt longitudinal cardiac sections with dystonin-b antibody. Dystonin-b appears to present a striated pattern aligning with desmin. **D-F.** Magnified view of images presented in panels A-C. Dystonin-b exhibits a striated pattern similar to desmin.

Appendix II

A role for plakins in Wnt signalling

The MACF1 null condition results in embryonic lethality presenting with headless trunk morphology. Interestingly, these embryos are characteristically similar to Wnt-3 null embryos (Chen et al., 2006). This observation has led to an understanding of the role MACF1 plays in the early canonical Wnt signaling pathway. MACF1 is associated with the core canonical Wnt protein complex composed of β-catenin, axin, GSK3β and APC (Chen et al., 2006). The role for MACF1 in the Wnt signaling pathway has raised the possibility that dystonin may also be engaging in a similar function. As β-catenin interacts with MACF1 through its plakin domain, specifically through its SH3 region, we investigated whether a similar interaction was occurring with dystonin-a through its plakin domain.

A pull-down approach was utilized to explore this potential interaction. For this purpose we used a his-tagged dystonin plakin domain plasmid (his-plakin) as well as a GST-tagged β-catenin plasmid (GST-β-catenin).

Generation of GST-β-catenin

RT-PCR was performed to generate the β-catenin plasmid. cDNA was obtained from mouse (CD-1) brain RNA (200 ng) which was incubated with 5 μM poly(dN) and heated to 65°C for 5 minutes followed by 5 minutes on ice. Then, 5X RT buffer (Gibco) and 10X dNTPs were then added to the reaction tube along with MuLV reverse transcriptase (Gibco) and RNAse inhibitor (Gibco). The reaction was incubated for 1 hour at 37°C and inactivated by heating at 95°C for 5 minutes. The cDNA generated was either used

immediately or stored at -20°C later processing. The TA-cloning kit (Invitrogen) was used in the generation of the desired β-catenin plasmid.

β-catenin forward (5' GCTACTCAAGCTGACCTGATG 3') and reverse (5'TTACAGGTCAGTATCAAACCAG 3') primers were added to the cDNA generated with 10X PCR buffer (Gibco), platinum Taq polymerase (Invitrogen) and $MgCl_2$. The reaction was incubated in a thermocycler (Eppendorf) for 25 cycles. The 3'A overhangs generated were used to clone the β-catenin sequence (bp 216 – bp 2555 GenBank Accession NM007614.2) into a PCR2.1 vector (Invitrogen). Blue-white screening was employed to identify successful insertion of β-catenin coding sequence. Restriction digests were performed to ensure appropriate orientation of cloning products was obtained. Using restriction enzymes BamHI and XhoI, the β-catenin coding sequence was removed from the PCR2.1 vector and inserted into the pGex4t1 vector (GE Healthcare), which contained an N-terminal GST-tag under the T7 promoter.

Plakin domain of dystonin-a interacts with β-catenin

His-plakin and GST-β-catenin were expressed in bacterial cultures (previously described) and used for the pull-down interaction analysis. His-plakin (500 μg) was purified using a his-bind kit (Novagen). Purified his-plakin still bound to the purification beads was incubated with soluble GST-β-catenin (500 μg) from bacterial culture for 3 hours at 4°C; following which a wash protocol using PBS was performed. His-desmin was used as a negative control for the interaction analysis. After the final wash protocol was performed, the his-plakin (and his-desmin) was eluted off of the his-bind beads with elution buffer (500 mM imidazole). SDS-PAGE was performed on the eluates. After transfer to a PVDF membrane, β-catenin was probed. β-catenin was successfully pulled-down with his-

plakin (Figure A7). Minimal background detection of β-catenin was observed in the his-desmin lane (Figure A7). These preliminary results indicate that β-catenin may in fact be a dystonin interacting partner.

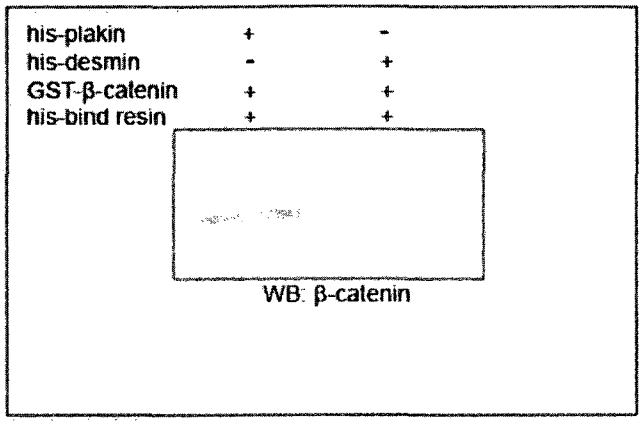

Figure A7. Immunoblot of GST-β-catenin pulled-down by his-plakin.
Bacterially expressed GST-tagged β-catenin (GST-β-catenin) fusion is pulled-down by bacterial expressed his-tagged plakin domain fusion protein (his-plakin). Detection of β-catenin signal in lane 1 depicts the successful pull-down of GST-β-catenin by his-plakin. Minimal detection of β-catenin in lane 2 indicates that GST-β-catenin is not pulled-down with his-desmin. This suggests that the potential β-catenin and dystonin plakin domain interaction observed is not an artifact.